eLIFE elifesciences.org

RESEARCH ARTICLE

Crumbs organizes the transport machinery by regulating apical levels of PI(4,5)P_2 in *Drosophila*

Johanna Lattner[1], Weihua Leng[1], Elisabeth Knust[1], Marko Brankatschk[2]*, David Flores-Benitez[1]*

[1]Max-Planck Institute of Molecular Cell Biology and Genetics (MPI-CBG), Dresden, Germany; [2]The Biotechnological Center of the TU Dresden (BIOTEC), Dresden, Germany

Abstract An efficient vectorial intracellular transport machinery depends on a well-established apico-basal polarity and is a prerequisite for the function of secretory epithelia. Despite extensive knowledge on individual trafficking pathways, little is known about the mechanisms coordinating their temporal and spatial regulation. Here, we report that the polarity protein Crumbs is essential for apical plasma membrane phospholipid-homeostasis and efficient apical secretion. Through recruiting β_{Heavy}-Spectrin and MyosinV to the apical membrane, Crumbs maintains the Rab6-, Rab11- and Rab30-dependent trafficking and regulates the lipid phosphatases Pten and Ocrl. Crumbs knock-down results in increased apical levels of PI(4,5)P_2 and formation of a novel, Moesin- and PI(4,5)P_2-enriched apical membrane sac containing microvilli-like structures. Our results identify Crumbs as an essential hub required to maintain the organization of the apical membrane and the physiological activity of the larval salivary gland.

***For correspondence:** marko.brankatschk@tu-dresden.de (MB); flores@mpi-cbg.de (DF-B)

Competing interest: See page 35

Funding: See page 36

Received: 06 August 2019
Accepted: 25 October 2019
Published: 07 November 2019

Reviewing editor: Utpal Banerjee, University of California, Los Angeles, United States

Introduction

Epithelia can organize as layers or tubes, which form barriers and thus separate internal biological compartments from the environment. Many epithelia are specialized for absorption or secretion by performing selective and directional transport of nutrients, enzymes and waste products, which is essential for metazoan life (***Cereijido et al., 2004***; ***Rodriguez-Boulan and Macara, 2014***; ***Lemaitre and Miguel-Aliaga, 2013***). To perform these functions, epithelial cells are highly polarized: plasma membrane proteins and lipids are distributed asymmetrically into an apical domain facing the environment or a lumen, and a basolateral domain that contacts the neighboring cell and/or a basal lamina. In addition, polarity is manifested by uneven distribution of organelles, asymmetric cytoskeleton organization and directed trafficking (***Rodriguez-Boulan and Macara, 2014***; ***Knust and Bossinger, 2002***; ***Eaton and Martin-Belmonte, 2014***). The latter is particularly obvious in secretory epithelia, for example the salivary glands, which produce vast amounts of material that is secreted into the gland lumen (***Blasky et al., 2015***; ***Iruela-Arispe and Beitel, 2013***; ***Eaton and Martin-Belmonte, 2014***; ***Chung et al., 2014***; ***Miguel-Aliaga et al., 2018***).

Several evolutionarily conserved proteins regulate epithelial cell polarity. These include members of the apical Crumbs- and PAR-complexes, and the basolateral Scrib-Dlg-Lgl module (reviewed in ***Flores-Benitez and Knust, 2016***; ***Román-Fernández and Bryant, 2016***). The Crumbs (Crb) protein has a large extracellular domain (>2000 aa), and a small intracellular domain (37 aa) (***Tepass et al., 1990***; ***Wodarz et al., 1993***), which harbors two protein-protein interaction motifs, a C-terminal PDZ (**P**ostsynaptic density/**D**iscs large/**Z**O-1)-domain binding motif (PBM) and a juxtamembrane FERM (protein **4**.1/**e**zrin/**r**adixin/**m**oesin)-domain binding motif (FBM). The PBM is important for cell polarity and can bind Stardust (Sdt) and Par-6 (***Li et al., 2014***; ***Roh et al., 2002***; ***Bulgakova et al., 2008***;

Bachmann et al., 2001; *Hong et al., 2001*; *Kempkens et al., 2006*; *Ivanova et al., 2015*). The FBM can directly interact with Yurt (Yrt), Expanded (Ex) and Moesin (Moe) (*Klebes and Knust, 2000*; *Laprise et al., 2006*; *Ling et al., 2010*; *Wei et al., 2015*), FERM-proteins that act as adaptors between membrane proteins and the actin cytoskeleton (*Bennett and Baines, 2001*; *Lemmon et al., 2002*; *McClatchey, 2014*; *Sauvanet et al., 2015*). The FBM of Crb is also important for β_{Heavy}-Spectrin (β_H-Spec) recruitment to the apical plasma membrane, and thereby supports the polarized organization of the membrane-associated cytoskeleton (cytocortex) (*Wodarz et al., 1995*; *Richard et al., 2009*; *Pellikka et al., 2002*; *Lee et al., 2010*; *Lee and Thomas, 2011*; *Médina et al., 2002b*).

Several epithelia of *crb* or *sdt* mutant *Drosophila* embryos show severe polarity defects, disruption of cell-cell adhesion and loss of tissue integrity. On the other hand, over-expression of Crb in the embryonic epidermis increases the size of the apical membrane (*Tepass and Knust, 1993*; *Grawe et al., 1996*; *Tepass et al., 1990*; *Das and Knust, 2018*; *Tepaß and Knust, 1990*). Similar phenotypes have been reported in mouse embryos mutant for *Crb2* or *Crb3* (*Charrier et al., 2016*; *Szymaniak et al., 2015*; *Whiteman et al., 2014*; *Xiao et al., 2011*; *Ramkumar et al., 2016*). In addition, *Drosophila* Crb has been associated with other functions, which are independent of its roles in epithelial integrity, such as regulation of tissue growth via the Hippo pathway, regulation of Notch signaling (*Das and Knust, 2018*; *Nemetschke and Knust, 2016*; *Perez-Mockus et al., 2017*; *Herranz et al., 2006*), as well as photoreceptor morphogenesis and survival under light stress (reviewed in *Pocha and Knust, 2013*; *Bulgakova and Knust, 2009*; *Genevet and Tapon, 2011*).

Apico-basal polarity is also essential for polarized membrane traffic. Directed trafficking depends on the phosphoinositide composition of the plasma membrane, the cytocortex and various Rab (**Ra**s-related in **b**rain) proteins. All of these are closely interconnected to organize and maintain the identity of apical and basolateral membranes (*Weisz and Rodriguez-Boulan, 2009*; *Eaton and Martin-Belmonte, 2014*; *Blasky et al., 2015*; *Rodriguez-Boulan et al., 2005*; *Croisé et al., 2014*). Epithelial cell polarity and polarized membrane traffic require differential enrichment of phosphatidylinositol 4,5-bisphosphate (PI(4,5)P_2) and phosphatidylinositol 3,4,5-trisphosphate (PI(3,4,5)P_3) in the apical and basolateral membranes, respectively (*Di Paolo and De Camilli, 2006*; *Martin-Belmonte and Mostov, 2007*). PI(4,5)P_2 levels are controlled by Pten (Phosphatase and tensin homolog deleted on chromosome ten), which converts PI(3,4,5)P_3 into PI(4,5)P_2, by the type I phosphatidylinositol 4-phosphate 5-kinase Skittles (Sktl), which produces PI(4,5)P_2 from phosphatidylinositol 4-phosphate (PI4P), and by Ocrl (Oculocerebrorenal syndrome of Lowe), which dephosphorylates PI(4,5)P_2 into PI4P (*de Renzis et al., 2002*; *Knirr et al., 1997*; *Maehama et al., 2004*; *Claret et al., 2014*; *Gervais et al., 2008*; *Worby and Dixon, 2014*; *Balakrishnan et al., 2015*; *Weixel et al., 2005*). Pten activity is antagonistic to that of the type IA phosphatidylinositol three kinase (Pi3K), which is enriched at basolateral membranes and converts PI(4,5)P_2 into PI(3,4,5)P_3 (*Gassama-Diagne et al., 2006*; *Peng et al., 2015*; *Balakrishnan et al., 2015*; *Gao et al., 2000*; *Goberdhan et al., 1999*; *Huang et al., 1999*). PI(4,5)P_2 can bind to pleckstrin homology (PH)-domains of FERM proteins and β-Spectrins (*Yoon et al., 1994*; *Harlan et al., 1995*), thereby linking the plasma membrane to the cytocortex and to the trafficking machinery (*Barroso-González et al., 2009*; *Ramel et al., 2013*; *Beck and Nelson, 1998*; *Holleran and Holzbaur, 1998*; *Kang et al., 2009*). Moreover, PI(4,5)P_2 is directly implicated in the regulation of exocytosis (*Milosevic et al., 2005*; *Gong et al., 2005*; *Massarwa et al., 2009*; *Rousso et al., 2013*) and in all forms of endocytosis (*Antonescu et al., 2011*; *Mayinger, 2012*; *Jost et al., 1998*).

Here, we studied the functions of Crb in a differentiated, highly polarized secretory epithelium, namely the salivary gland (SG) of the *Drosophila* larva, to decipher its possible role in polarized trafficking. We identified Crb as a novel regulator of apical secretion and maintenance of the apical microvilli in SG cells. We show that loss of Crb in SGs disrupts the apical cytocortex, apical secretion and the apical trafficking machinery, including the organization of Rab6-, Rab11- and Rab30-positive apical compartments, and the localization of their effector Myosin V (MyoV) (*Lindsay et al., 2013*). Our results show that Crb controls the apical secretion machinery via regulation of phosphoinositide metabolism. Loss of Crb increases apical levels of PI(4,5)P_2, a phenotype that requires the activity of Pten, and impairs the function of the apical secretory machinery. These defects are accompanied by the formation of a novel apical membrane compartment, which emerges as a solitary intracellular sac of PI(4,5)P_2- and phospho-Moe-enriched apical membrane containing microvilli. This compartment is reminiscent to intracellular vacuolar structures found in patients with MVID (microvillus

inclusion disease), a fatal genetic disease characterized by lack of microvilli on the surface of enterocytes (www.omim.org/entry/251850). We conclude that Crb acts as an apical hub to couple phospholipid metabolism and cytoskeleton scaffolds with apical membrane traffic. Our work sheds light on the mechanism behind the determination of the apical membrane by Crb and its possible implications in different pathologies.

Results

The Crb complex is dispensable for maintenance of apico-basal polarity in larval salivary glands (SGs)

To investigate the role of the Crb protein complex in a differentiated secretory epithelium, we silenced Crb or its binding partner Sdt in the larval SG by RNAi-mediated knock-down (KD) using the SG-specific driver *fkh*-GAL4 (***Zhou et al., 2001***). We took advantage of the fact that this strategy does not affect embryonic development (data not shown). The larval SG consists of two tubes composed of columnar epithelial cells, each with a central lumen (***Figure 1A***). Strikingly, although the KD of Crb effectively reduces apical levels of Crb, Sdt and *D*Patj (***Figure 1B–C'*** and ***Figure 1—figure supplement 1C,D,Q***), it does not affect the overall morphology of SGs, as determined by phalloidin staining (***Figure 1—figure supplement 1A,B***). Yet, the SGs lacking Crb are shorter when compared to their control counterparts (***Figure 1—figure supplement 1R***, ***Figure 1—figure supplement 1—source data 1***). Similar results were observed upon RNAi-mediated KD of Sdt (***Figure 1—figure supplement 1R–X***). Interestingly, KD of Crb or Sdt does not alter the polarized distribution of any canonical apical or basolateral polarity marker tested, including Bazooka (Baz, ***Figure 1D,E***), aPKC (***Figure 1—figure supplement 1E,F***), Par-6 (***Figure 1—figure supplement 1G,H and Y,Z***), Disc large (Dlg, ***Figure 1F,G*** and ***Figure 1—figure supplement 1AA, BB***), Yurt (Yrt) (***Figure 1—figure supplement 1I,J***) and Coracle (Cora, ***Figure 1—figure supplement 1K,L***). Taken together, these results show that the Crb protein complex is dispensable for maintenance of tissue integrity and overall epithelial cell polarity of larval SGs.

The Crb protein complex is required for proper apical secretion in larval SGs

Because depletion of the Crb protein complex does not affect the overall polarity or integrity of the larval SGs, we analyzed whether it plays any role in maintaining their physiological functions. SGs of feeding larvae produce saliva required to digest food, whereas in later stages they produce and secrete predominantly glue proteins required to attach the pupae to surfaces (***Thomopoulos, 1988***; ***Chung et al., 2014***; ***Maruyama and Andrew, 2012***; ***Csizmadia et al., 2018***; ***Gregg et al., 1990***; ***Fraenkel and Brookes, 1953***). Thus, we speculated that any defect in saliva secretion could result in less food intake and hence delayed larval development. In fact, when compared to control larvae, the time necessary to reach the pupal stage is prolonged upon depletion of Crb (***Figure 1H***, ***Figure 1—source data 1***) or Sdt (***Figure 1—figure supplement 1KK***, ***Figure 1—figure supplement 1—source data 2***).

To test whether the delay in pupation correlates with defects in apical membrane transport, we analyzed the localization of Cadherin99C (Cad99C), an apical transmembrane protein involved in regulation of microvillar length (***Chung and Andrew, 2014***), and CD8-RFP, a heterologous transmembrane protein normally targeted to the apical membrane (***Xu et al., 2002***; ***Lee and Luo, 1999***). We found that upon silencing of Crb or Sdt, Cad99C and CD8-RFP do not localize properly at the apical membrane but instead localize in intracellular vesicles (***Figure 1I,J*** and ***Figure 1—figure supplement 1CC,DD,M,N and EE,FF***).

To evaluate apical secretion, we analyzed the expression of Sgs3-GFP. However, the glue proteins are not expressed at the feeding stage we study here (beginning of the 3rd instar) but almost 2 days later (***Tran and Ten Hagen, 2017***). Indeed, at the stage of glue secretion, vesicle delivery appears normal in Crb-deficient SGs (***Videos 1*** and ***2***) (***Tran et al., 2015***). Furthermore, several proteins that are known to be apically secreted in other tubular epithelia, like Piopio, Vermiform and UAS-driven secreted proteins (cherry-sec, GFP-tagged wheat germ agglutinin) (***Jaźwińska et al., 2003***; ***Luschnig et al., 2006***; ***Brankatschk and Eaton, 2010***) were not suitable for our studies since they could not be detected in the lumen of wild-type feeding larval SGs (not shown). Therefore, we

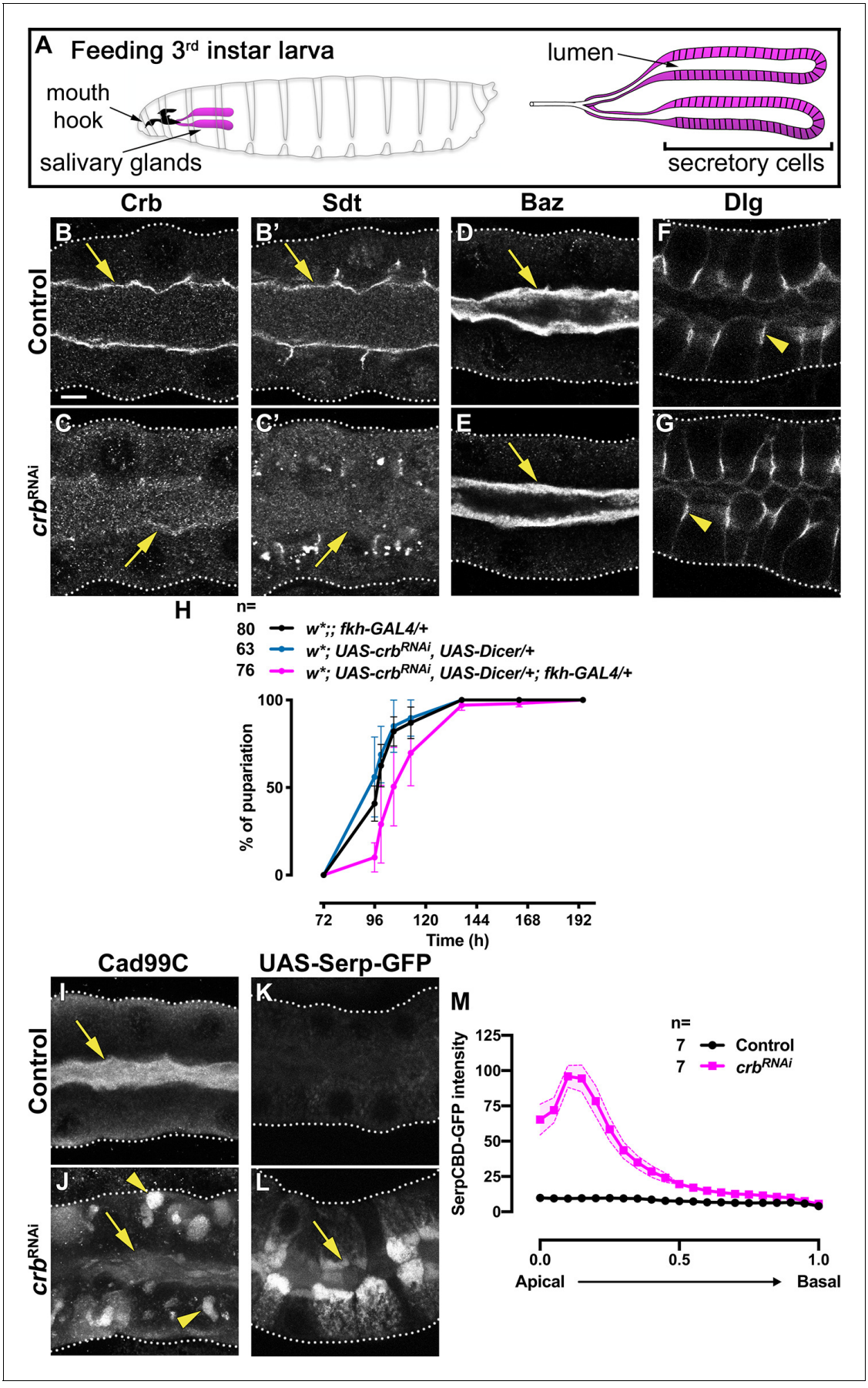
A
Feeding 3rd instar larva
mouth hook
salivary glands
lumen
secretory cells
Crb
Sdt
Baz
Dlg
Control
crbRNAi
B
B'
D
F
C
C'
E
G
H
n=
80 w*;; fkh-GAL4/+
63 w*; UAS-crbRNAi, UAS-Dicer/+
76 w*; UAS-crbRNAi, UAS-Dicer/+; fkh-GAL4/+
% of pupariation
100
50
0
72
96
120
144
168
192
Time (h)
Cad99C
UAS-Serp-GFP
I
K
J
L
M
SerpCBD-GFP intensity
125
100
75
50
25
0
n=
7 Control
7 crbRNAi
0.0
0.5
1.0
Apical
Basal

Figure 1. Crb is required for efficient apical secretion in SG cells. (**A**) Scheme indicating the anatomic location of the SG in the larval stage. (**B-G**) Localization of Crb (**B,C**), Sdt (**B',C'**), Baz (**D,E**) and Dlg (**F,G**) in control (**B,B',D,F**, *fkh>/+*) and Crb KD (**C,C',E,G**, *fkh >UAS crb^{RNAi}*) animals. H. Pupariation efficiency of controls (black and blue) and larvae with reduced levels of Crb (magenta) at 29 ˚C. Error bars indicate the standard error of the mean, n indicates number of traced individual larvae of the corresponding genotypes in three independent experiments. (**I,J**) Localization of the apical transmembrane protein Cadherin99C in SGs from control (**I**) and Crb KD (**J**) animals. (**K,L**) Localization of the secreted apical cargo SerpCBD-GFP in live SGs of control (**K**, *fkh >UAS* SerpCBD-GFP) and Crb KD (**L**, *fkh >UAS crb^{RNAi}; UAS-SerpCBD-GFP*) animals. Arrows indicate the apical plasma membrane. Arrowheads mark the lateral plasma domain. Dotted lines indicate the basal membrane. Scale bar in A indicates10 μm applies to all panels. (**M, M**) Plotted is the fluorescence intensity (arbitrary units) of SerpCBD-GFP along the apical-to-basal direction in live SGs of control (black, *fkh >UAS* SerpCBD-GFP) and Crb KD (magenta, *fkh >UAS crb^{RNAi}; UAS-SerpCBD-GFP*). Error bars indicate the standard error of the mean, n indicates number of glands from the corresponding genotypes.

The online version of this article includes the following source data and figure supplement(s) for figure 1:

Source data 1. Dataset for tracking of larval development.
Source data 2. Dataset for SerpCBD-GFP fluorescence intensity in control glands.
Source data 3. Dataset for SerpCBD-GFP fluorescence intensity in Crb KD glands.
Figure supplement 1. Knock-down of the Crb protein complex in larval SGs disrupts apical secretion.
Figure supplement 1—source data 1. Dataset for salivary gland lengths.
Figure supplement 1—source data 2. Dataset for tracking of larval development.
Figure supplement 1—source data 3. Dataset for SerpCBD-GFP fluorescence intensity in control glands (note is the same dataset for ***Figure 1M*** control).
Figure supplement 1—source data 4. Dataset for SerpCBD-GFP fluorescence intensity in Sdt KD glands.
Figure supplement 2. The Crb protein complex is dispensable for maintenance of cell-cell junctions in larval SGs.

used the chitin-binding domain of Serpentine tagged with GFP (UAS-SerpCBD-GFP), a well-established marker to evaluate apical secretion (***Luschnig et al., 2006***; ***Kakihara et al., 2008***; ***Förster et al., 2010***; ***Petkau et al., 2012***; ***Dong et al., 2013***; ***Dong et al., 2014***; ***Bätz et al., 2014***). Notably, while SerpCBD-GFP is barely detectable upon overexpression in control glands, loss of Crb or Sdt results in an obvious intracellular retention of SerpCBD-GFP at the apical aspect (***Figure 1K–M***, ***Figure 1—source data 2*** and ***3***; and ***Figure 1—figure supplement 1 GG, HH, and LL***, ***Figure 1—figure supplement 1—source data 3*** and ***4***). In support of the idea that Crb is necessary for efficient apical secretion, we also found that glycoprotein secretion is impaired upon loss of Crb or Sdt, as revealed by intracellular retention of peanut-agglutinin-GFP (PNA-GFP, ***Figure 1—figure supplement 1O,P and II,JJ***), which can bind to glycoproteins produced by the SGs (***Korayem et al., 2004***; ***Theopold et al., 2001***; ***Tian and Ten Hagen, 2007***). Taken together, these results show that the Crb protein complex is required for proper apical membrane protein delivery and protein secretion in SGs of feeding larvae.

The Crb protein complex is dispensable for maintenance of cell-cell junctions in larval SGs

Impaired apical secretion after KD of Crb could be related to defects in cell-cell junctions. In particular, the pleated septate junctions (pSJs) are involved in apical secretion in the embryonic tracheae (***Wang et al., 2006***; ***Laprise et al., 2010***; ***Nelson et al., 2010***). Therefore, we examined the SGs by transmission electron microscopy (TEM). We did not find any abnormalities in the localization of the *zonula adherens* (ZA) of Crb-deficient SG cells (***Figure 1—figure supplement 2A',C'*** arrowheads).

In contrast to ZA, pSJs are morphologically abnormal in SGs of Crb KD animals, showing many interruptions (***Figure 1—figure supplement 2C***, green highlight) and disorganized regions (***Figure 1—figure supplement 2D***). In contrast, control SG cells, pSJs run uniformly along the lateral membrane with few interruptions (***Figure 1—figure supplement 2A,B***). Defects in pSJs were corroborated by reduced immunostaining of some pSJ components, including Sinuous (Sinu, ***Figure 1—figure supplement 2E,F***), Kune-kune (Kune, ***Figure 1—figure supplement 2G,H***), while others, such as Fasciclin3 (Fas3, ***Figure 1—figure supplement 2I,J***), Dlg (***Figure 1F,G***), Lachesin-GFP and Nervana2-GFP (not shown) were not affected. Given the defects observed in pSJs, we analyzed their permeability by monitoring any luminal appearance of fluorescently labeled 10 kDa-Dextran ex vivo (***Lamb et al., 1998***). Interestingly, KD of Crb does not increase dye penetration into the lumen when compared to control glands (***Figure 1—figure supplement 2K–L'***), suggesting that the epithelium is tight. In contrast, KD of Fas3-GFP, used as a positive control, enhances the diffusion of 10 kDa-Dextran into the gland lumen (***Figure 1—figure supplement 2M,M'***).

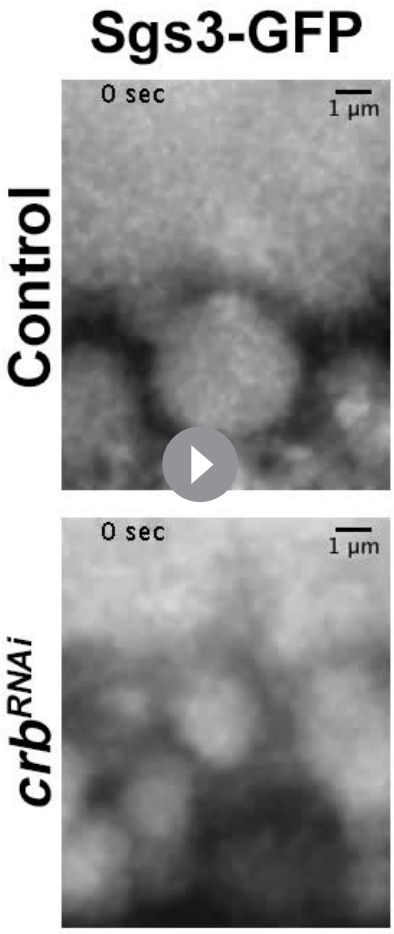

Video 1. Fusion of a glue vesicle followed by expulsion of the cargo Sgs3-GFP into the lumen SG lumen of control (*fkh>+*, top) and Crb KD (*fkh >UAS crb^{RNAi}*, bottom) animals.
https://elifesciences.org/articles/50900#video1

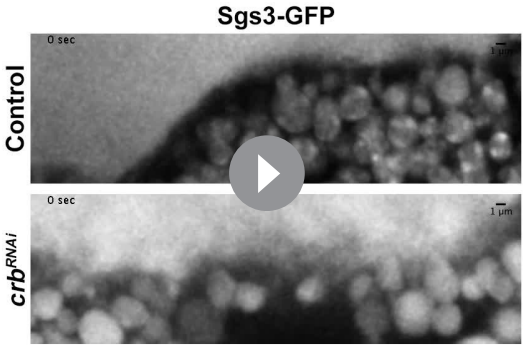

Video 2. Overview showing the fusion of glue vesicles followed by expulsion of Sgs3-GFP into the SG lumen of control (*fkh>+*, top) and Crb KD (*fkh >UAS crb^{RNAi}*, bottom) animals. Note that the increase of fluorescence in the vesicle occurs when they open to the lumen.
https://elifesciences.org/articles/50900#video2

Taken together, these results suggest that loss of Crb does not affect adherens junctions or the epithelial barrier function of SGs.

Crb regulates apical membrane organization via the apical cytocortex

Crb recruits Moesin (Moe) and β_H-Spectrin (β_H-Spec, encoded by the gene *karst -kst*) to the apical membrane (***Richard et al., 2009***; ***Lee et al., 2010***; ***Lee and Thomas, 2011***; ***Médina et al., 2002b***; ***Kerman et al., 2008***), where they mediate interactions between transmembrane proteins and the apical cytocortex (reviewed in ***Fehon et al., 2010***; ***Baines et al., 2014***). Therefore, we analyzed whether Crb KD affects the organization of the apical cytocortex in SG cells, and if so, whether this relates to the defects in apical secretion.

We found that KD of Crb decreases apical levels of F-actin (***Figure 2A–C***, ***Figure 2—source data 1***) and β_H-Spec (***Figure 2D–F***, ***Figure 2—source data 2***). Similarly, silencing a knock-in Crb tagged with GFP on the extracellular domain, Crb-GFP-A (***Huang et al., 2009***), using *fkh >gfp^{RNAi}* as an alternative approach for the KD of the Crb protein complex (***Figure 2—figure supplement 1A–D***) also decreases apical levels of F-actin (***Figure 2—figure supplement 1E,F***). Moreover, KD of Crb-GFP-A induces accumulation of Moe, as well as its active form phospho-Moe, into a single sac per cell localized right below the apical domain (***Figure 2G,H***, arrows, ***Video 3*** and not shown). These sacs are also positive for the apical transmembrane protein Stranded at second tagged with YFP (***Firmino et al., 2013***) (Sas-YFP, ***Figure 2I,J***) suggesting that they have an apical plasma membrane identity. On the other hand, KD of Crb has no evident effects on the organization of α-Tubulin or α-Spectrin (***Figure 2—figure supplement 1G–J***). These results show that Crb is required to maintain the organization of the apical cytocortex and the morphology of the apical membrane in larval SGs.

To examine in more detail the morphology of the apical aspect of Crb-deficient cells, we prepared SGs for TEM analysis by employing the high-pressure freezing technique. This technique immobilizes complex macromolecular assemblies in their native state and helps to preserve cytoskeleton-rich structures like microvilli (***Studer et al., 2008***). Strikingly, cells from Crb-depleted SGs display intracellular vesicles containing microvilli (***Figure 2L'***, arrowheads and ***Figure 2—figure***

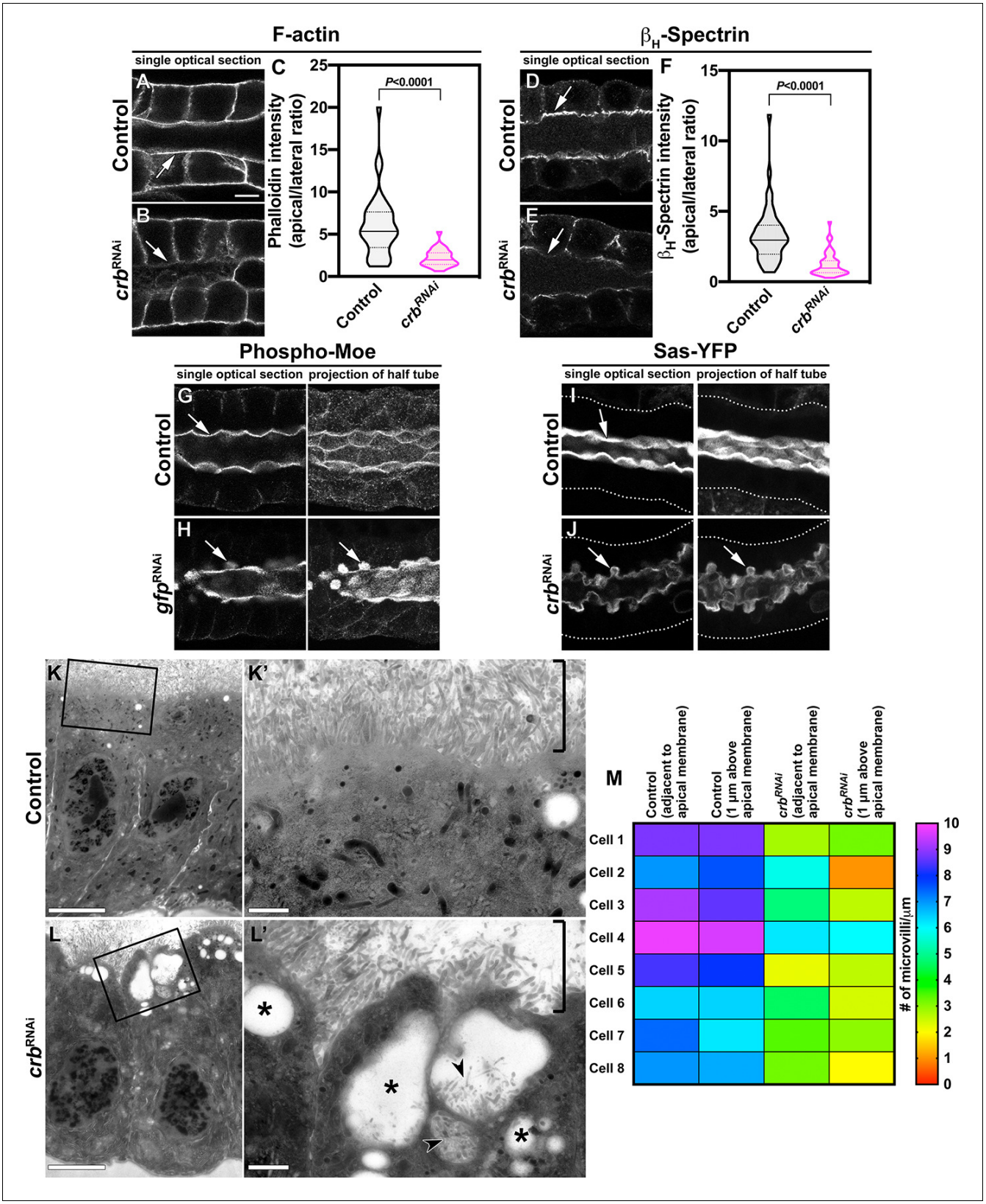

Figure 2. Crb is necessary to specifically maintain the apical cytoskeleton and the morphology of the apical membrane. (**A-F**) Localization and quantification of F-actin (phalloidin staining, **A-C**) and β_H-Spec (**D-F**) in control (**A,D**, *fkh>/+*) and Crb KD (**B,E**, *fkh >UAS crb^{RNAi}*) SGs. Violin graphs (**C,F**) show the fluorescence intensity (apical vs lateral ratio) indicating the mean and quartiles for F-actin (**C**, n = 36 cells for control and 28 cells for Crb KD)

Figure 2 continued on next page

Figure 2 continued

and β_H-Spec (**F**, n = 44 cells for control and 40 cells for Crb KD). Statistical significance was analyzed in an unpaired two-tailed *t*-test. (**G-H**) Localization of phospho-Moe in control (**G**, *Crb-GFP, fkh>/+*) and Crb KD (**H**, *Crb-GFP, fkh >UAS gfp^{RNAi}*) SGs. (**I,J**) Localization of the apical protein Stranded at second (Sas-YFP) in live SGs of control (**I**, *fkh>/+*) and Crb KD (**J**, *Crb-GFP, fkh >UAS gfp^{RNAi}*) animals. Shown are single optical slices and maximal projections of half of the z-stack (half SG-tube). Arrows point to the apical domain of the cell. Dotted lines indicate the basal membrane. Scale bar in (**A**) displays 10 µm and applies to panes (**A-J**). (**K-L'**) TEM images of SGs prepared using the high-pressure freezing technique, visualizing the apical aspect of SG cells of control (**K,K'**, *fkh>/+*) and Crb KD (**L,L'**, *fkh >UAS crb^{RNAi}*) animals. The brackets in **K,L'** indicate the apical microvilli. Asterisks in (**L'**) mark large intracellular vesicles found in Crb-deficient glands. Arrowheads in L' indicate microvilli found inside vesicles. Scale bars in (**K,L**) indicate 5 µm and in (**K',L'**) indicate 1 µm. (**M, M**) Mean number of microvilli following along the apical membrane over a distance of 1 µm, adjacent to the membrane and 1 µm above the apical membrane in SG cells of control (*fkh>/+*) and Crb KD (*fkh >UAS crb^{RNAi}*) animals. The heatmap indicates the scale bar for the number of microvilli/µm.

The online version of this article includes the following source data and figure supplement(s) for figure 2:

Source data 1. Dataset for phalloidin fluorescence intensity.
Source data 2. Dataset for β_H-Spec fluorescence intensity.
Source data 3. Dataset for microvilli quantifications.
Figure supplement 1. Crb is necessary to specifically maintain the apical membrane organization.
Figure supplement 2. TEM images of intracellular extensions of apical membrane in Crb-deficient glands.
Figure supplement 3. Increased lysosomal activity in Crb and Sdt deficient glands.
Figure supplement 4. KD of β_H-Spec induces the formation of PAMS.

supplement 2), which seem to correspond to the Sas-YFP positive sacs described above (***Figure 2J***). In fact, we also observed cases of intracellular sacs whose membrane were continuous with the apical membrane (***Figure 2—figure supplement 2A,A'***). Moreover, in Crb-deficient SGs, the density of apical microvilli is dramatically reduced (***Figure 2K',L'***, brackets, and M, ***Figure 2—source data 3***). The number of microvilli per micron adjacent to the apical plasma membrane is 8.0 ± 1.219 in control vs. 4.125 ± 1.446 in Crb-deficient cells (mean ± SD, p<0.0001, n = 8). This difference is even bigger when measured at 1 µm above the plasma membrane, 7.75 ± 1.222 in control vs. 2.850 ± 1.441 in Crb-deficient cells (mean ± SD, p<0.0001, n = 8), indicating that microvilli are also shorter in Crb-deficient cells. In addition, Crb-deficient SG cells exhibit large intracellular vesicles not present in control SGs, which probably correspond to enlarged lysosomes (asterisks in ***Figure 2L'*** and in ***Figure 2—figure supplement 2B'C'***; see also ***Figure 1—figure supplement 2C*** blue highlight). Indeed, live imaging of SGs incubated with Lysotracker showed that KD of Crb or Sdt increases lysosomal activity (***Figure 2—figure supplement 3***). This suggests that lysosomal activity increases due to impaired secretion upon loss of Crb.

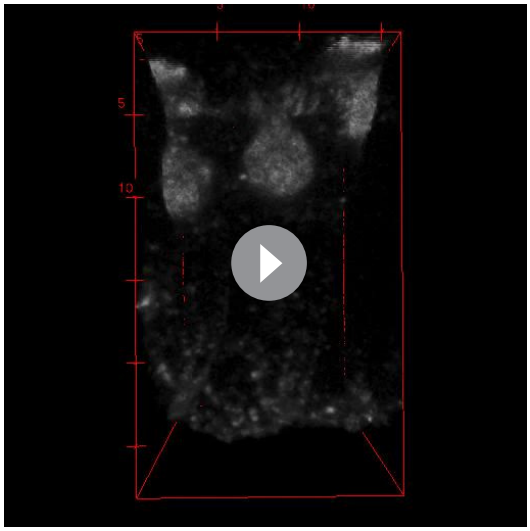

Video 3. 3D rendering of a SG from a Crb KD animal (*fkh >UAS crb^{RNAi}*) probed for phospho-Moesin. The extraction focuses on one cell to appreciate the accumulation of phospho-Moesin at the apical membrane. Apical is up.
https://elifesciences.org/articles/50900#video3

Since these apical membrane invaginations are enriched in PI(4,5)P_2 (described below), we refer to them as PAMS: **p**hospho-Moe and PI(4,5)P_2-enriched **a**pical **m**embrane **s**acs. Given that silencing of Crb reduces apical β_H-Spec, we analyzed the effect of β_H-Spec KD on PAMS formation. Indeed, loss of β_H-Spec (***Figure 2—figure supplement 4A,B***) prompts formation of PAMS marked by phospho-Moe (***Figure 2—figure supplement 4C,D***). Moreover, in SGs deficient in β_H-Spec, Crb remains apical and additionally localizes to the PAMS (***Figure 2—figure supplement 4E,F***). These results indicate that Crb localizes to the apical domain independently of β_H-Spec while β_H-Spec requires Crb to be organized at the apical cytocortex.

Taken together, these results indicate that Crb is essential to maintain the proper amount and

organization of the apical membrane by stabilizing the apical cytocortex.

Crb regulates the apical membrane organization via MyosinV

The PAMS described above are reminiscent to microvilli-containing vesicles found in samples from MVID (microvillus inclusion disease) patients, which is linked to mutations in the *MYO5b* gene (**Müller et al., 2008**). Similar inclusions are found in animal models of MVID (**Sidhaye et al., 2016**). MyosinV (MyoV) is a processive motor that transports cargos along F-actin (**Reck-Peterson et al., 2000**) and is a component of the apical secretory machinery in epithelia (**Massarwa et al., 2009**; **Reck-Peterson et al., 2000**; **Li et al., 2007**; **Pocha et al., 2011a**). Moreover, in photoreceptor cells, Crb regulates apical transport of Rhodopsin-1 by interacting with MyoV (encoded by the gene *didum*) (**Pocha et al., 2011a**). Therefore, we analyzed whether Crb regulates MyoV in the SGs. Indeed, the KD of Crb decreases apical MyoV (**Figure 3A,B,D**, **Figure 3—source data 1** and **2**). Importantly, overexpression of MyoV-GFP in Crb-deficient glands does not rescue its apical localization (**Figure 3—figure supplement 1A–C**, **Figure 3—figure supplement 1—source data 1** and **2**). Furthermore, KD of β_H-Spec also decreases apical MyoV (**Figure 3A,C,D**, **Figure 3—source data 1** and **3**) as well as apical secretion as revealed by the apical retention of SerpCBD-GFP (**Figure 3—figure supplement 2A–C**, **Figure 3—figure supplement 2—source data 1** and **2**). This suggests that β_H-Spec acts downstream of Crb to maintain apical MyoV.

To examine the role of MyoV in apical secretion and PAMS formation, we silenced MyoV expression in the SGs using a specific RNAi (*didum*^{RNAi}). Analysis of Crb, phospho-Moe and Sas-YFP in MyoV-deficient SGs shows that while these proteins localize apically, they are also found in PAMS (**Figure 3E–J**). Additionally, live imaging of SGs expressing Sas-YFP shows large vesicles inside the cell (**Figure 3J**, arrowhead), which resemble similar structures seen in an organoid model for MVID established from mouse intestinal cells with impaired apical transport (**Mosa et al., 2018**). Indeed, we found that MyoV KD impairs secretion of SerpCBD-GFP, which in turn accumulates at the apical aspect of MyoV-deficient SG cells (**Figure 3K–M**, **Figure 3—source data 4** and **5**). These results suggest that formation of PAMS can be a consequence of defects in the apical secretory machinery.

Together, our results indicate that loss of Crb disrupts the apical β_H-Spec cytocortex. As a consequence, the apical localization of MyoV is reduced, apical secretion is impaired, and apical membrane morphology is defective, resulting in PAMS formation.

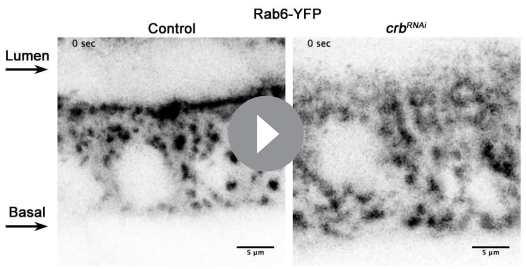

Video 4. Live imaging of endogenously expressed Rab6-YFP in SGs of control (left, *Rab6-YFP, fkh>/+*) and Crb KD (right, *Rab6-YFP, fkh >UAS crb*^{RNAi}). 5 min recording, time lapse 5 s.
https://elifesciences.org/articles/50900#video4

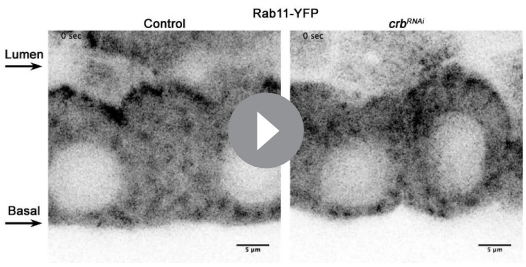

Video 5. Live imaging of endogenously expressed Rab11-YFP in SGs of control (left, *Rab11-YFP, fkh>/+*) and Crb KD (right, *Rab11-YFP, fkh >UAS crb*^{RNAi}). 5 min recording, time lapse 5 s.
https://elifesciences.org/articles/50900#video5

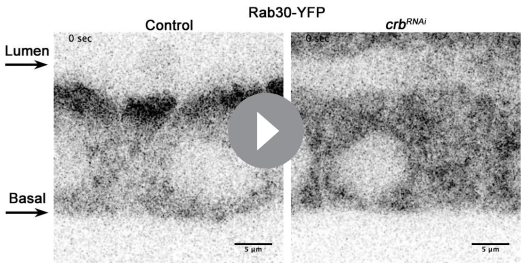

Video 6. Live imaging of endogenously expressed Rab30-YFP in SGs of control (left, *Rab30-YFP, fkh>/+*) and Crb KD (right, *Rab30-YFP, fkh >UAS crb*^{RNAi}). 5 min recording, time lapse 5 s.
https://elifesciences.org/articles/50900#video6

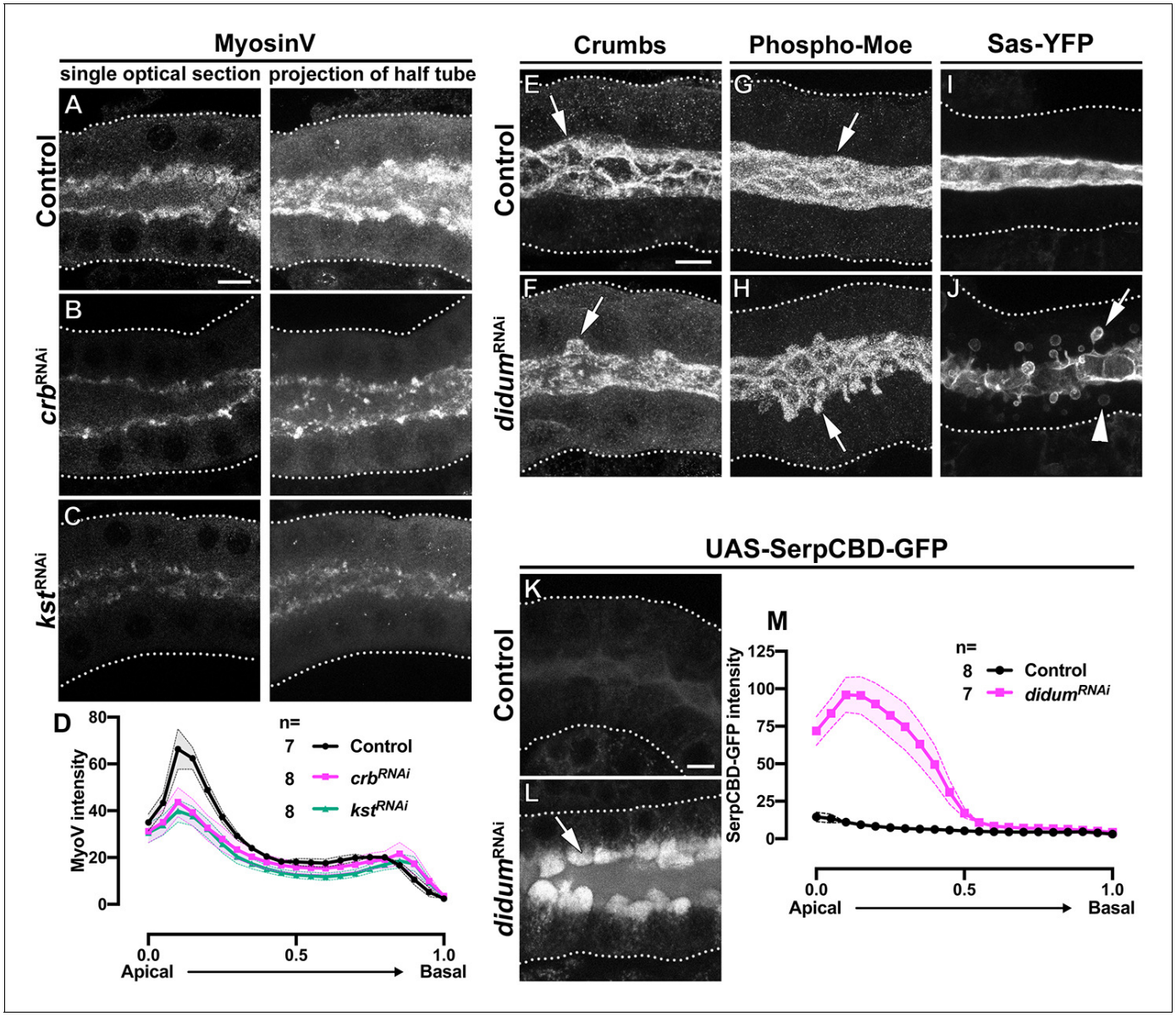

Figure 3. MyoV KD induces the intracellular extension of the apical membrane and disrupts apical secretion. (**A-C**) Single optical slices and maximal projection of half of the z-stack (half SG-tube) showing the localization of MyoV in fixed SGs of control (**A**, *fkh>/+*), Crb KD (**B**, *fkh >UAS crb^{RNAi}*) and β_H-Spec KD (**C**, *fkh >UAS kst^{RNAi}*) animals. (**D, D**) Plotted is the intensity (arbitrary units) of MyoV detected by immunofluorescence along the apical-to-basal direction in SGs of control (black, *fkh>/+*), Crb KD (magenta, *fkh >UAS crb^{RNAi}*) and β_H-Spec (green, *fkh >UAS kst^{RNAi}*) animals. Error bars indicate the standard error of the mean, n indicates number of glands from the corresponding genotypes. (**E-J**) Maximal projection of half of the z-stack (half SG-tube) showing the localization of Crb (**E,F**), Phospho-Moe (**G,H**) and Sas-YFP in SGs of control (**E,G,I**, *fkh>/+*) and MyoV KD (**F,H,J**, *fkh >UAS didum^{RNAi}*) animals. (**K,L**) Localization of SerpCBD-GFP in live SGs of control (**K**, *fkh >UAS* SerpCBD-GFP) and MyoV KD (**L**, *fkh >UAS didum^{RNAi}; UAS-SerpCBD-GFP*) animals. Arrows point to the apical and dotted lines indicate the basal membrane. Scale bars in (**A,E,K**) indicate 10 μm. (**M, M**) Plotted is the fluorescence intensity (arbitrary units) of SerpCBD-GFP along the apical-to-basal direction in live SGs of control (black, *fkh >UAS* SerpCBD-GFP), and MyoV KD (magenta, *fkh >UAS didum^{RNAi}; UAS-SerpCBD-GFP*) animals. Error bars indicate the standard error of the mean, n indicates number of glands from the corresponding genotypes.

The online version of this article includes the following source data and figure supplement(s) for figure 3:

Source data 1. Dataset for MyosinV fluorescence intensity in control glands.
Source data 2. Dataset for MyosinV fluorescence intensity in Crb KD glands.
Source data 3. Dataset for MyosinV fluorescence intensity in βH-Spec KD glands.
Source data 4. Dataset for SerpCBD-GFP fluorescence intensity in control glands.
Source data 5. Dataset for SerpCBD-GFP fluorescence intensity in MyoV KD glands.
Figure supplement 1. Proper apical localization of MyoV requires Crb.

Figure 3 continued on next page

Figure 3 continued

Figure supplement 1—source data 1. Dataset for MyosinV-GFP fluorescence intensity in control glands.
Figure supplement 1—source data 2. Dataset for MyosinV-GFP fluorescence intensity in Crb KD glands.
Figure supplement 2. β_H-Spec is required for proper apical secretion.
Figure supplement 2—source data 1. Dataset for SerpCBD-GFP fluorescence intensity in control glands.
Figure supplement 2—source data 2. Dataset for SerpCBD-GFP fluorescence intensity in βH-Spec KD glands.

Crb is a novel regulator of the apical Rab machinery in larval SGs

Other works have provided genetic evidence that links the presence of microvilli-containing inclusions to defects in the apical Rab trafficking machinery (***Feng et al., 2017***; ***Knowles et al., 2015***; ***Knowles et al., 2014***; ***Sato et al., 2007***). The Rab protein family is a major regulator of intracellular membrane traffic routes (***Wandinger-Ness and Zerial, 2014***; ***Pfeffer, 2013***) and MyoV is known to interact with Rab6 and Rab11 (***Lindsay et al., 2013***; ***Li et al., 2007***; ***Iwanami et al., 2016***), which play an important role in apical membrane trafficking and recycling (***Khanal et al., 2016***; ***Iwanami et al., 2016***; ***Chung and Andrew, 2014***; ***Li et al., 2007***; ***Satoh et al., 2005***; ***Pelissier et al., 2003***). Therefore, to evaluate the effects of Crb depletion on the Rab machinery, we took advantage of the recently published library of Rab proteins endogenously tagged with YFP (***Dunst et al., 2015***). We knocked-down Crb in larval SG cells and systematically screened the expression of all Rab proteins (***Figure 4—figure supplement 1***). Strikingly, we found that loss of Crb affects the localization of a subset of Rab proteins, namely Rab6-YFP, Rab11-YFP and Rab30-YFP. Specifically, the apically localized pools of these Rab proteins are reduced (***Figure 4A–F'***, and ***Videos 4–6***), while the basal pools are not affected significantly. The effects on this subset of Rab proteins are specific, as Crb KD does not alter the organization of other Rab proteins, like Rab1-YFP (***Figure 4G–H'***, ***Video 7***, and ***Figure 4—figure supplement 1***). Similar results were obtained in Sdt KD glands (data not shown). Importantly, total protein levels of these Rab proteins do not change significantly upon Crb KD (***Figure 4I***).

As shown above, KD of β_H-Spec affects MyoV localization and apical secretion similarly to Crb KD. Therefore, we tested the effects of β_H-Spec KD on the localization of Rab6-YFP, Rab11-YFP, Rab30-YFP and Rab1-YFP. Strikingly, KD of β_H-Spec only removes the apical pools of Rab6-YFP and Rab11-YFP (***Figure 4—figure supplement 2A–D***), while the apical Rab30-YFP and the intracellular Rab1-YFP compartments are not affected (***Figure 4—figure supplement 2E–H***). Thus, the apical localization of Rab6 and Rab11 require a functional apical cytocortex.

To examine whether the reduction in Rab6-YFP or Rab11-YFP relates to the formation of PAMS, we silenced them individually using a gfp^{RNAi} and analyzed CD8-RFP localization. CD8-RFP accumulates intracellularly and localizes to the PAMS in Crb- and Sdt-deficient SGs (***Figure 1—figure supplement 1M,N*** and EE,FF, and not shown). We found that KD of Rab6-YFP severely affects the morphology of the SGs and produces intracellular accumulation of CD8-RFP in large vesicles (***Figure 4—figure supplement 3A–B''***), which agrees with the general requirement of Rab6 in secretion (***Homma et al., 2019***). KD of Rab11-YFP also affects the morphology of the SGs, although a single lumen is still patent (***Figure 4—figure supplement 3D'***, asterisk). More importantly, loss of Rab11 results in formation of PAMS in larval SG cells (***Figure 4—figure supplement 3D''***, arrows). Hence, defects in the apical secretory machinery can induce the formation of PAMS.

Together, our results show that Crb is a novel regulator of apically localized Rab6-YFP, Rab11-YFP and Rab30-YFP. Moreover, β_H-Spec acts downstream of Crb to organize the apical localization of Rab6-YFP and Rab11-YFP. Therefore, the stabilization of β_H-Spec by Crb is essential to organize aspects of the apical Rab machinery for efficient apical secretion in larval SGs.

Crb regulates apical membrane levels of PI(4,5)P_2

As we describe above, depletion of Crb, Sdt, β_H-Spec or MyoV induces accumulation of phospho-Moe in a subapical structure that we termed PAMS. Phospho-Moe can bind to PI(4,5)P_2 via its PH-domain (***Yonemura et al., 2002***; ***Fiévet et al., 2007***; ***Fehon et al., 2010***; ***Roch et al., 2010***) and the phosphoinositide composition of a membrane regulates Rab protein activity, as well as the localization of cytoskeleton proteins (***Wandinger-Ness and Zerial, 2014***; ***Tan et al., 2015***; ***Mayinger, 2012***; ***Liem, 2016***; ***Bennett and Healy, 2009***; ***Fehon et al., 2010***). Therefore, we explored whether loss of

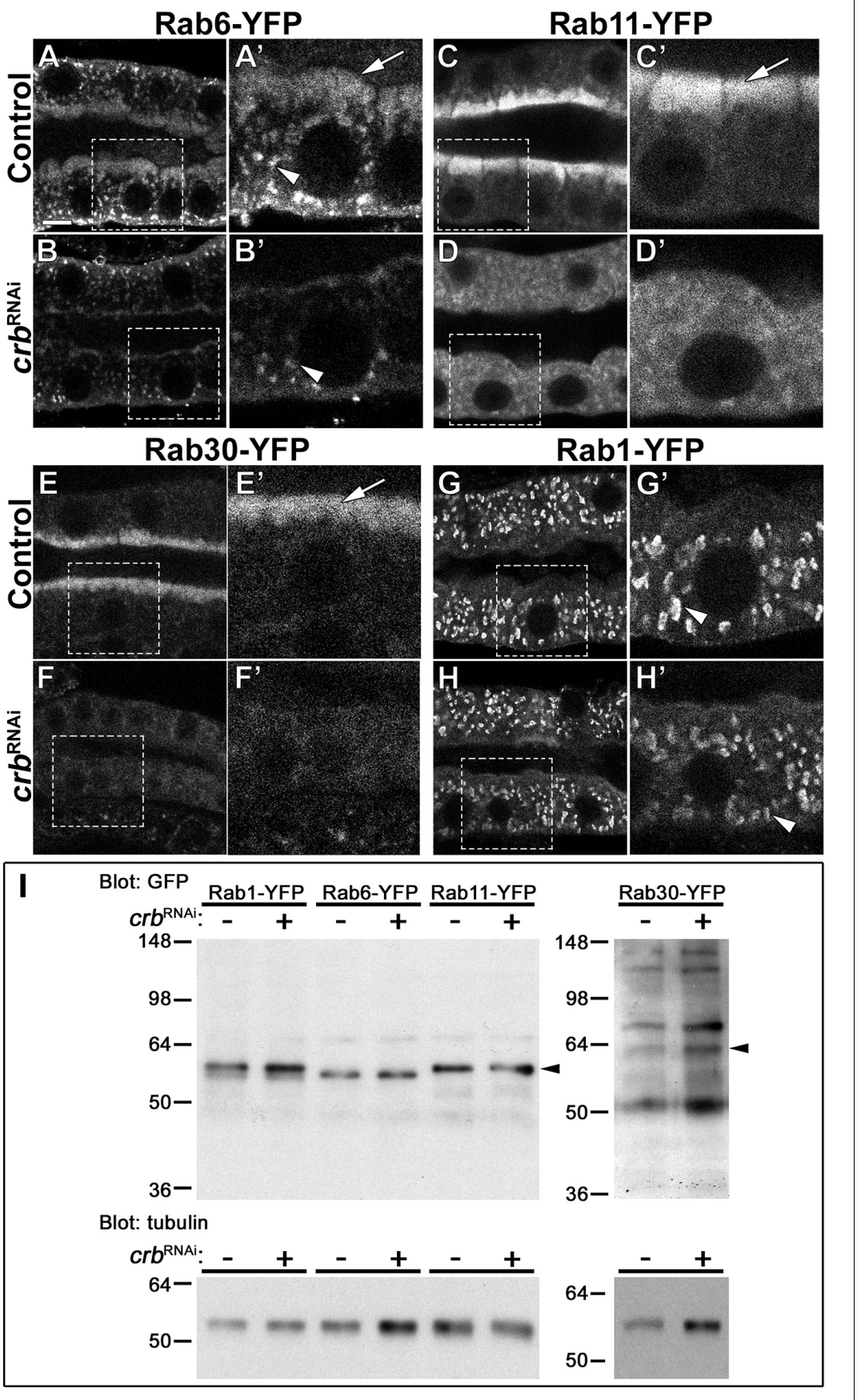
Rab6-YFP
Rab11-YFP
Control
crbRNAi
A
A'
B
B'
C
C'
D
D'
Rab30-YFP
Rab1-YFP
E
E'
F
F'
G
G'
H
H'
I
Blot: GFP
Rab1-YFP
Rab6-YFP
Rab11-YFP
Rab30-YFP
crbRNAi: - + - + - + - +
148
98
64
50
36
Blot: tubulin
64
50

Figure 4. Crb organizes the apical Rab machinery in larval SG cells. (**A-H'**) Confocal images of SGs to localize endogenously expressed Rab-YFP proteins. Rab6-YFP (**A-B'**), Rab11-YFP (**C-D'**), Rab30-YFP (**E-F'**) and Rab1-YFP (**G-H'**) in control (**A,C,E,G**, *fkh>/+*) and Crb KD (**B,D,F,H,** *fkh >UAS crb^{RNAi}*) SGs. Dotted-line squares in A-H indicate the area blown-up to the right of the respective panel (**A'-H'**). Arrows point to the apical pool of Rab6-YFP (**A'**), Rab11-YFP (**C'**) and Rab30-YFP (**E'**). Arrowheads mark the intracellular vesicular localization of Rab6-YFP (**A',B'**) and Rab1-YFP (**G',H'**). Scale bar (**A**) indicates 10 µm. (**I, I**) Western blot of endogenously expressed Rab-YFP proteins. Rab1-YFP, Rab6-YFP, Rab11-YFP, and Rab30-YFP in control (*fkh>/+*) and Crb KD (*fkh >UAS crb^{RNAi}*) SGs, indicated as *crb^{RNAi}* – or +, respectively. Membranes were probed for tubulin (loading control) and for GFP; arrowheads point to Rab-YFP proteins.

The online version of this article includes the following figure supplement(s) for figure 4:

Figure supplement 1. Localization of Rab-YFP proteins after KD of Crb in larval SGs.

Figure supplement 2. The apical cytocortex is necessary for the organization of apical Rab6 and Rab11 trafficking machinery.

Figure supplement 3. Loss of Rab11 in larval SG induces the formation of PAMS.

Crb modulates the phosphoinositide composition of the apical membrane. For this, we monitored PI(4,5)P_2 localization by employing a well-established reporter containing the PI(4,5)P_2-specific PH-domain of phospholipase Cδ fused to GFP (PLCδ-PH-EGFP) (***Gervais et al., 2008***; ***Rousso et al., 2013***; ***Balla et al., 1998***; ***Várnai and Balla, 1998***; ***Rescher et al., 2004***).

Live imaging of larval SGs shows that PI(4,5)P_2 is enriched in the apical membrane (***Figure 5B,H***, ***Figure 5—source data 1***), as previously observed in late 3rd instar SGs (***Rousso et al., 2013***). Importantly, quantification of PLCδ-PH-EGFP fluorescence intensity of Crb-deficient SGs shows an increase in apical levels of PI(4,5)P_2 (***Figure 5C,H***, ***Figure 5—source data 2***). Additionally, PI(4,5)P_2 localizes in the PAMS (***Figure 5C***), which are also positive for phospho-Moe (***Video 8***). Similar results were observed in Sdt KD glands (***Figure 5—figure supplement 1A,B***).

To analyze whether β_H-Spec or MyoV participate in the accumulation of PI(4,5)P_2, we analyzed the distribution of PLCδ-PH-EGFP upon β_H-Spec or MyoV depletion. Indeed, KD of β_H-Spec or MyoV induces accumulation of PI(4,5)P_2 in the PAMS (***Figure 5—figure supplement 1C,D***), suggesting that loss of β_H-Spec and MyoV facilitates the increase of apical PI(4,5)P_2 levels and formation of PAMS.

We noted that PAMS are very heterogenous structures that are poorly preserved during fixation for immunohistochemistry. Therefore, we made use of live imaging to assess the frequency and morphology of the PAMS in the different genetic backgrounds. We used the signal from PLCδ-PH-EGFP and *D*E-cadherin-mTomato to measure the apical membrane area and volume (see Materials and methods). Our measurements show that KD of Crb, β_H-Spec or MyoV do not significantly change the amount of apical membrane surface or its volume, except for Crb-deficient cells, which have a slightly increased volume (***Figure 5—figure supplement 1E***, ***Figure 5—figure supplement 1—source data 1***). We found that, when PAMS appear (% of cells with PAMS: 0% in control n = 322 cells; 46.7% in Crb KD n = 417 cells, 49.3% in β_H-Spec KD n = 503 cells; and 41,9% in MyoV KD n = 393 cells), there is a single sac per cell, which localizes toward the center of the apical domain. The PAMS diameter varies between 1.737 µm to 11.52 µm (mean ± SD: 5.325 ± 1.552 µm in Crb KD, 4.718 ± 1.382 µm in β_H-Spec KD, 5.012 ± 1.544 µm in MyoV KD; ***Figure 5—source data 12***), suggesting that they could be dynamic. However, following up on single sacs by live imaging for 20 min revealed that these structures are rather steady (***Video 9***). Nevertheless, PAMS are not present in late 3rd instar SGs of wandering larvae (***Figure 5—figure supplement 1F,G***). Taken together these results indicate that Crb is essential to control the levels of PI(4,5)P_2 at the apical membrane. Moreover, our results suggest that at least part of this control is exerted by organizing β_H-Spec and MyoV at the apical aspect.

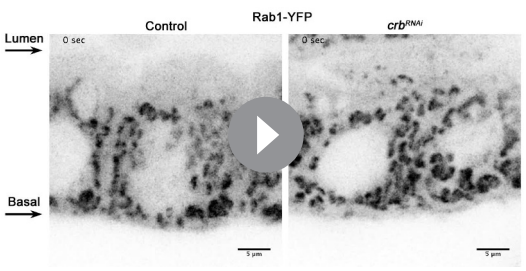

Video 7. Live imaging of endogenously expressed Rab1-YFP in SGs of control (left, *Rab1-YFP, fkh>/+*) and Crb KD (right, *Rab1-YFP, fkh >UAS crb^{RNAi}*). 5 min recording, time lapse 5 s.
https://elifesciences.org/articles/50900#video7

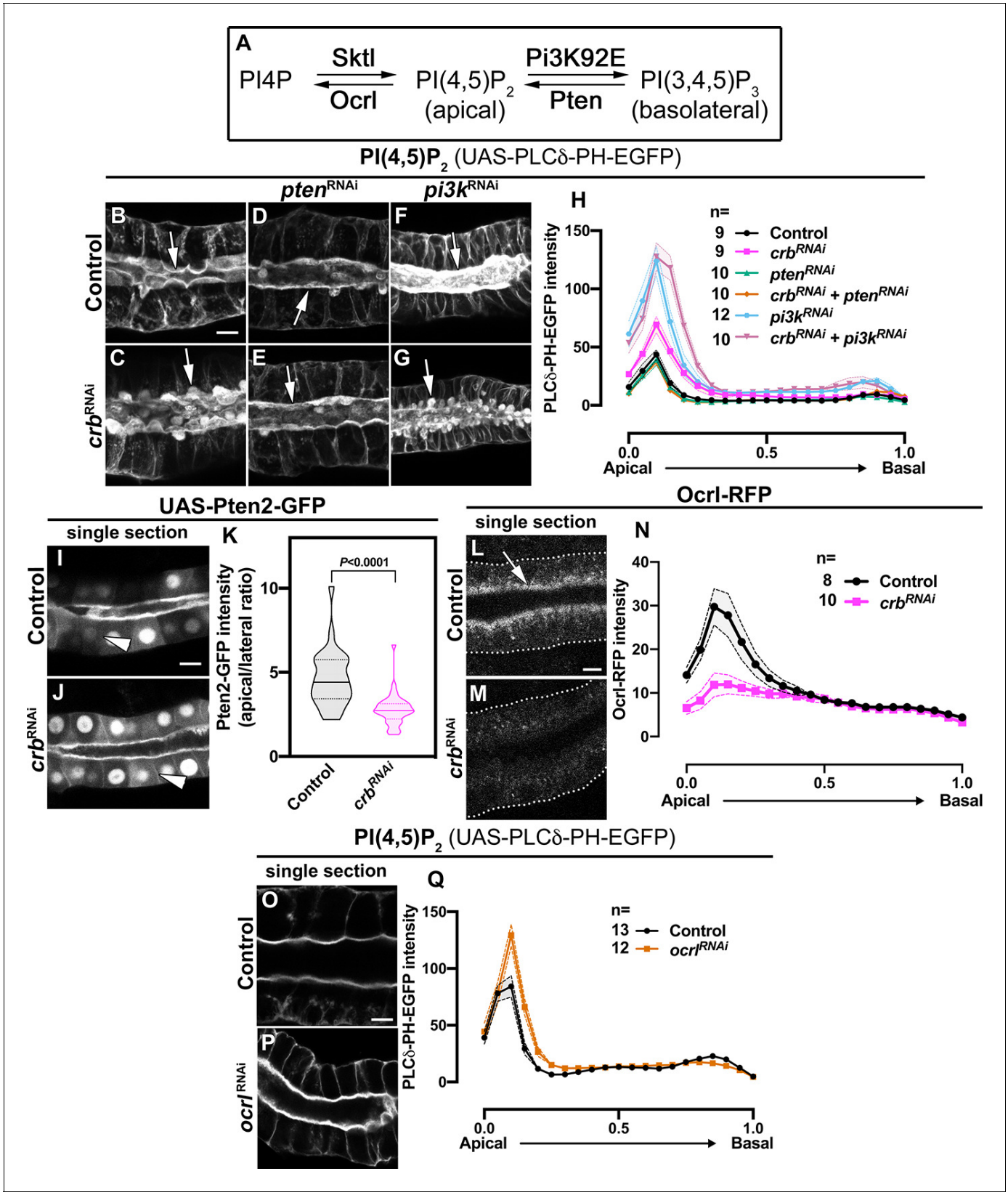

Figure 5. Crb organizes the apical secretory machinery by negatively regulating Pten A. (**A**) Simplified scheme of $PI(4,5)P_2$ biosynthesis. (**B-G**) Maximal projection of half of the z-stack (half SG-tube) showing the localization of $PI(4,5)P_2$ (PLCδ-PH-EGFP reporter) in live SGs of control (**B**, *fkh >UAS-PLCδ-PH-EGFP*), Crb KD (**C**, *fkh >UAS crb^{RNAi}; UAS-PLCδ-PH-EGFP*), Pten KD (**D**, *fkh >UAS pten^{RNAi}; UAS-PLCδ-PH-EGFP*), double KD of Crb and Pten (**E**,

Figure 5 continued on next page

Figure 5 continued

fkh >UAS crb^{RNAi}, UAS-pten^{RNAi}; UAS-PLCδ-PH-EGFP), Pi3K92E KD (**F**, *fkh >UAS-pi3k92E^{RNAi}; UAS-PLCδ-PH-EGFP*) and double KD of Crb and Pi3K92E (**G**, *fkh >UAS crb^{RNAi}, UAS-pi3k92E^{RNAi}; UAS-PLCδ-PH-EGFP*) animals. (**H, H**) Plotted is the fluorescence intensity (arbitrary units) of PLCδ-PH-EGFP along the apical-to-basal axis in live SGs of the genotypes indicated in (**B-G**), respectively. Error bars indicate the standard error of the mean, n indicates number of glands for the corresponding genotype. (**I-K**) Localization and quantification of over-expressed Pten2-GFP in SGs of control (**I**, *fkh >UAS-Pten2-GFP*) and Crb KD (**J**, *fkh >UAS crb^{RNAi}; UAS-Pten2-GFP*) animals. Violin graph (**K**) indicates the fluorescence intensity (apical vs lateral ratio) indicating the mean and quartiles (n = 28 cells for control and 36 cells for Crb KD). Statistical significance was analyzed in an unpaired two-tailed *t*-test. (**L-N**) Localization and quantification of Ocrl-RFP fluorescence intensity detected along the apical-to-basal axis in live SGs of control (black, *fkh>/+*) and Crb KD (magenta, *fkh >UAS crb^{RNAi}*) animals. Error bars indicate the standard error of the mean, n indicates number of glands of the corresponding genotypes. (**O-Q**) Localization and quantification of PLCδ-PH-EGFP fluorescence intensity detected along the apical-to-basal axis in live SGs of control (black, *fkh>/+*) and Ocrl KD (orange, *fkh >UAS ocrl^{RNAi}*) animals. Error bars indicate the standard error of the mean, n indicates the number of glands of the corresponding genotypes. Arrows point to the apical membrane domain. Arrowheads point to the lateral membrane. Dotted lines indicate the basal membrane. Scale bars in (**B,I,L,O**) indicate 10 μm.

The online version of this article includes the following source data and figure supplement(s) for figure 5:

Source data 1. Dataset for PLCδ-PH-EGFP fluorescence intensity in control glands (corresponding to panel H).
Source data 2. Dataset for PLCδ-PH-EGFP fluorescence intensity in Crb KD glands (corresponding to panel H).
Source data 3. Dataset for PLCδ-PH-EGFP fluorescence intensity in Pten KD glands (corresponding to panel H).
Source data 4. Dataset for PLCδ-PH-EGFP fluorescence intensity in glands with double KD of Crb and Pten (corresponding to panel H).
Source data 5. Dataset for PLCδ-PH-EGFP fluorescence intensity in Pi3K92E KD glands (corresponding to panel H).
Source data 6. Dataset for PLCδ-PH-EGFP fluorescence intensity in glands with double KD of Crb and Pi3K92E (corresponding to panel H).
Source data 7. Dataset for Pten2-GFP fluorescence intensity (corresponding to panel K).
Source data 8. Dataset for Ocrl-RFP fluorescence intensity in control glands (corresponding to panel N).
Source data 9. Dataset for Ocrl-RFP fluorescence intensity in Crb KD glands (corresponding to panel N).
Source data 10. Dataset for PLCδ-PH-EGFP fluorescence intensity in control glands (corresponding to panel Q).
Source data 11. Dataset for PLCδ-PH-EGFP fluorescence intensity in Ocrl KD glands (corresponding to panel Q).
Source data 12. Dataset for number of PAMS and diameter of PAMS.
Figure supplement 1. The Crb protein complex regulates apical levels of PI(4,5)P_2 and the secretory activity of SGs.
Figure supplement 1—source data 1. Dataset for apical surface quantifications.
Figure supplement 1—source data 2. Dataset for salivary gland lengths.
Figure supplement 1—source data 3. Dataset for PLCδ-PH-EGFP fluorescence intensity in control glands.
Figure supplement 1—source data 4. Dataset for PLCδ-PH-EGFP fluorescence intensity in Crb KD glands.
Figure supplement 1—source data 5. Dataset for PLCδ-PH-EGFP fluorescence intensity in Sktl KD glands.
Figure supplement 1—source data 6. Dataset for PLCδ-PH-EGFP fluorescence intensity in glands with double KD of Crb and Sktl.
Figure supplement 1—source data 7. Dataset for PLCδ-PH-EGFP fluorescence intensity in control glands incubated with vehicle.
Figure supplement 1—source data 8. Dataset for PLCδ-PH-EGFP fluorescence intensity in Crb KD glands incubated with vehicle.
Figure supplement 1—source data 9. Dataset for PLCδ-PH-EGFP fluorescence intensity in control glands incubated with VO-OHpic.
Figure supplement 1—source data 10. Dataset for PLCδ-PH-EGFP fluorescence intensity in Crb KD glands incubated with VO-OHpic.
Figure supplement 2. Pten2 over-expression induces formation of PAMS.
Figure supplement 2—source data 1. Dataset for GPR1-PH-EGFP fluorescence intensity.

Crb controls apical membrane homeostasis by regulating phosphoinositide metabolism

To understand how the loss of Crb results in accumulation of PI(4,5)P_2, we explored the involvement of Pten, Pi3K, Sktl and Ocrl, key enzymes regulating PI(4,5)P_2 levels (***Figure 5A***). Expression of *pten^{RNAi}* (***Ramachandran et al., 2009***) in Crb KD glands effectively suppresses both the accumulation of PI(4,5)P_2 as measured by PLC-PH-EGFP fluorescence, and PAMS formation (***Figure 5D,E,H***, ***Figure 5—source data 3*** and ***4***), while expression of *pi3K92E^{RNAi}* enhances the accumulation of PI(4,5)P_2 and PAMS formation (***Figure 5F,G,H***, ***Figure 5—source data 5*** and ***6***). The latter also results in smaller glands (***Figure 5—figure supplement 1H***, ***Figure 5—***

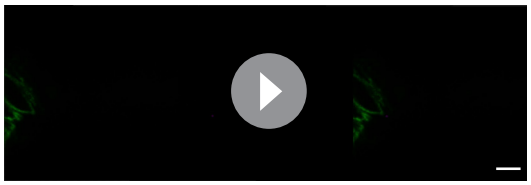

Video 8. 3D rendering of a fixed SG of a Crb KD animal expressing the PI(4,5)P_2 reporter PLCδ-PH-EGFP (green) and stained for phospho-Moesin (magenta). It is possible to appreciate the phospho-Moe and PI(4,5)P_2-enriched apical membrane sac (PAMS) below the apical membrane. Scale bar indicates 5 μm.
https://elifesciences.org/articles/50900#video8

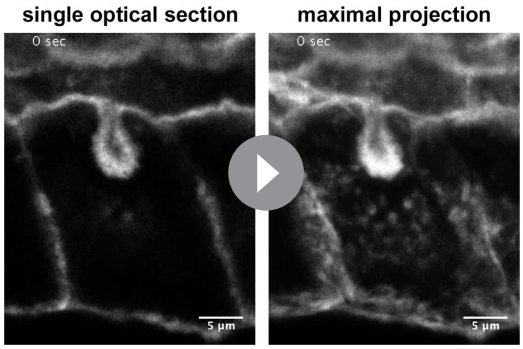

Video 9. Live imaging of a SG of a Crb KD animal expressing the PI(4,5)P_2 reporter PLCδ-PH-EGFP (*fkh >UAS crb^{RNAi}; UAS-PLCδ-PH-EGFP*). A single optical section is shown on the left. On the right, the maximal projection of the stack showing the whole PI(4,5)P_2-enriched apical membrane sac (PAMS). The arrowhead appearing at 660 s on the right panel points to an apparent opening of the sac to the lumen. It is worth noting that the PAMS are very stationary, as the movie shows 20 min recording, time lapse 20 s. Apical is up.
https://elifesciences.org/articles/50900#video9

figure supplement 1—source data 2), as expected due to the role of Pi3K in cell growth (***Huang et al., 1999***; ***Goberdhan et al., 1999***; ***Gao et al., 2000***; ***Scanga et al., 2000***). Interestingly, KD of Sktl, another enzyme producing PI(4,5)P_2, is less effective in suppressing PAMS upon Crb KD than knocking-down Pten (***Figure 5—figure supplement 1I–M***, ***Figure 5—figure supplement 1—source data 3–6***). To corroborate the importance for Pten to mediate the phenotype induced by loss of Crb, we found that over-expression of Pten2 induces accumulation of PI(4,5)P_2 and formation of PAMS (***Figure 5—figure supplement 2A,B***), while over-expression of Sktl results in strong defects in SG morphology (***Figure 5—figure supplement 2A, C***). Moreover, ex vivo incubation of SGs with VO-OHpic, a chemical inhibitor of Pten activity (***Mak et al., 2010***), eliminates the PAMS from Crb-deficient cells (***Figure 5—figure supplement 1N–R***, ***Figure 5—figure supplement 1—source data 7–10***). Thus, our findings suggest that Pten is the main source of PI(4,5)P_2 involved in the formation of the PAMS upon Crb depletion.

Since apical Pten is important for restricting PI(3,4,5)P_3 to the basolateral membrane (***Worby and Dixon, 2014***; ***Shewan et al., 2011***), we asked whether KD of Crb could affect PI(3,4,5)P_3 levels and Pten localization. We evaluated PI(3,4,5)P_3 levels using a probe containing the PH-domain of cytohesin tagged with GFP (***Pinal et al., 2006***). The signal of this probe at the plasma membrane is very weak and quantification of the fluorescence intensity revealed no significant change in the PI(3,4,5)P_3 apical-to-lateral ratio in Crb KD glands (***Figure 5—figure supplement 2D–F***, ***Figure 5—figure supplement 2—source data 1***). Immunostainings to detect endogenous Pten were unsuccessful in our hands, therefore we expressed a UAS-transgene encoding the Pten2 isoform fused to GFP, which can rescue pupal eye development of *Pten* mutants (***Pinal et al., 2006***). Pten2-GFP over-expressed in larval SGs localizes to the apical domain in addition to the nucleus (***Figure 5I,J***). Interestingly, quantification of the Pten2-GFP fluorescence intensity revealed a decrease in the apical-to-lateral ratio in Crb and Sdt KD glands (***Figure 5K*** and data not shown, ***Figure 5—source data 7***), suggesting that Crb is required to ensure Pten levels at the apical membrane (***Figure 5I,J***, arrowheads). However, it is important to note that no PAMS were found in glands overexpressing Pten2-GFP, which is in contrast to the ones overexpressing Pten2 without a GFP tag (***Figure 5—figure supplement 2A,B***). Thus, the GFP tag could partially impair the phosphatase activity or expression levels could be lower than those achieved with Pten2 over-expression.

Besides Pten, Ocrl regulates PI(4,5)P_2 levels by dephosphorylating PI(4,5)P_2 into PI4P (***Balakrishnan et al., 2015***). Live imaging of Ocrl-RFP (knock-in allele) revealed its localization at the apical aspect in SG cells (***Figure 5L***). Moreover, KD of Crb severely decreases the apical localization of Ocrl (***Figure 5M,N***, ***Figure 5—source data 8*** and ***9***). To evaluate the effect of Ocrl loss on PI(4,5)P_2 levels, we silenced the expression of Ocrl using a specific RNAi and quantified the fluorescence intensity of PLCδ-PH-EGFP. KD of Ocrl modestly increases the apical levels of PI(4,5)P_2 (***Figure 5O–Q***, ***Figure 5—source data 10*** and ***11***), yet this is not accompanied by formation of PAMS.

Together, these results show that apical accumulation of PI(4,5)P_2 and formation of PAMS induced by the loss of Crb, seem to result from a combined effect of increased Pten activity and loss of Ocrl from the apical membrane upon loss of Crb.

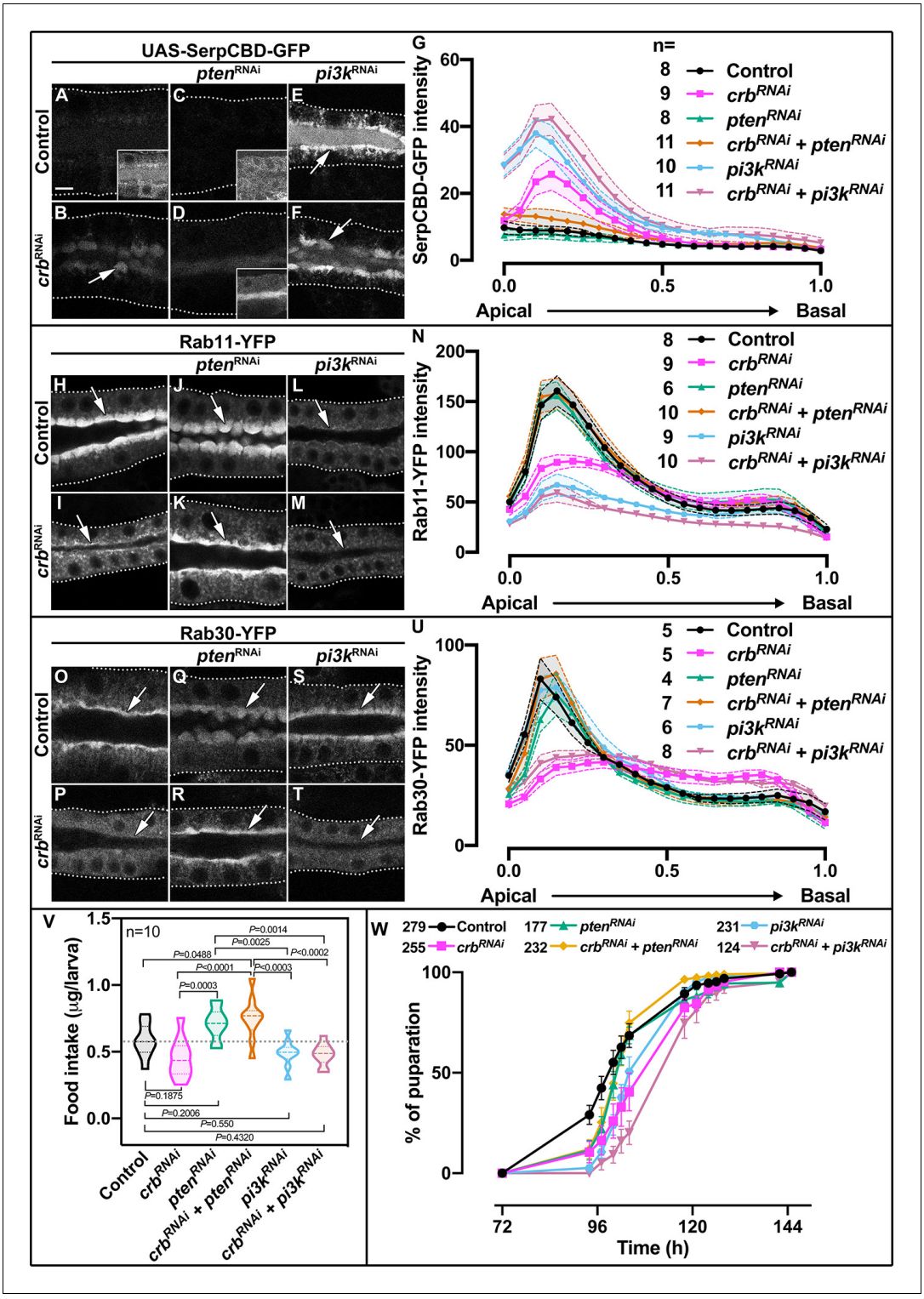

Figure 6. Control of apical secretion and localization of Rab11 and Rab30 by Crb requires Pten. (**A-F**) Maximal projection of 6.7µm through the SG lumen showing the localization of SerpCBD-GFP in live SGs of control (**A**, *fkh >UAS* SerpCBD-GFP), Crb KD (**B**, *fkh >UAS crb^{RNAi}; UAS-SerpCBD-GFP*), Pten KD (**C**, *fkh >UAS pten^{RNAi}; UAS-SerpCBD-GFP*), double KD of Crb and Pten KD (**D**, *fkh >UAS crb^{RNAi}, UAS-pten^{RNAi}; UAS-SerpCBD-GFP*), Pi3K92E KD (**E**, *fkh >UAS-pi3k92E^{RNAi}; UAS-SerpCBD-GFP*), and double KD of Crb and Pi3K92E (**F**, *fkh >UAS crb^{RNAi}, UAS-pi3k92E^{RNAi}; UAS-SerpCBD-GFP*), respectively. (**H-M**) Localization of endogenously expressed Rab11-YFP in live SGs. Shown are control (**H**, *Rab11-YFP, fkh>/+*), Crb KD (**I**, *Rab11-YFP, fkh >UAS crb^{RNAi}*), Pten KD (**J**, *Rab11-YFP, fkh >UAS pten^{RNAi}*), double KD of Crb and Pten (**K**, *Rab11-YFP, fkh >UAS crb^{RNAi}, UAS-pten^{RNAi}*), Pi3K92E KD (**L**, *Rab11-YFP, fkh >UAS-pi3k92E^{RNAi}*), and double KD of Crb and Pi3K92E (**M**, *Rab11-YFP, fkh >UAS crb^{RNAi}, UAS-pi3k92E^{RNAi}*) animals,

Figure 6 continued on next page

Figure 6 continued

respectively. (**O-T**) Localization of endogenously expressed Rab30-YFP in live SGs. Shown are control (**O**, *Rab30-YFP, fkh>/+*), Crb KD (**P**, *Rab30-YFP, fkh >UAS crb^{RNAi}*), Pten KD (**Q**, *Rab30-YFP, fkh >UAS pten^{RNAi}*), double KD of Crb and Pten (**R**, *Rab30-YFP, fkh >UAS crb^{RNAi}, UAS-pten^{RNAi}*), Pi3K92E KD (**S**, *Rab30-YFP, fkh >UAS-pi3k92E^{RNAi}*), and double KD of Crb and Pi3K92E (**T**, *Rab30-YFP, fkh >UAS crb^{RNAi}, UAS-pi3k92E^{RNAi}*) animals, respectively. Arrows point to the apical, and dotted lines to the basal membrane domain. Scale bar in (**A**) indicates 10 µm and applies to all panels. (**G,N,U**) Plotted is the fluorescence intensity (arbitrary units) of SerpCBD-GFP (**G**), Rab11-YFP (**N**) and Rab30-YFP (**U**), respectively, along the apical-to-basal axis in live SGs of the indicated genotypes. Error bars indicate the standard error of the mean, n indicates number of glands of the corresponding genotypes. (**V**) Violin graph of estimated food intake in control (first column), Crb KD (second column), Pten KD (third column), double KD of Crb and Pten (fourth column), Pi3K92E KD (fifth column), and double KD of Crb and Pi3K92E (sixth column) larvae. The dotted line indicates the mean value of the control. 60 larvae of the corresponding genotype were pooled in each biological replica. 10 biological replicas were analyzed distributed in three independent experiments. Statistical significance was tested in a one-way analysis of variance (ANOVA) followed by a Dunnett's multiple-comparison test. (**W**) Pupariation efficiency of control (black, *fkh>/+*), Crb KD (magenta, *fkh >UAS crb^{RNAi}*), Pten KD (green, *fkh >UAS pten^{RNAi}*), double KD of Crb and Pten KD (yellow, *fkh >UAS crb^{RNAi}, UAS-pten^{RNAi}*), Pi3K92E KD (blue, *fkh >UAS-pi3k92E^{RNAi}*), and double KD of Crb and Pi3K92E (, *fkh >UAS crb^{RNAi}, UAS-pi3k92E^{RNAi}*) animals. Error bars indicate the standard error of the mean, n indicates number of traced individual larvae of the corresponding genotypes in at least 15 independent experiments.

The online version of this article includes the following source data and figure supplement(s) for figure 6:

Source data 1. Dataset for SerpCBD-GFP fluorescence intensity in control glands.
Source data 2. Dataset for SerpCBD-GFP fluorescence intensity in Crb KD glands.
Source data 3. Dataset for SerpCBD-GFP fluorescence intensity in Pten KD glands.
Source data 4. Dataset for SerpCBD-GFP fluorescence intensity in glands with double KD of Crb and Pten.
Source data 5. Dataset for SerpCBD-GFP fluorescence intensity in Pi3K92E KD glands.
Source data 6. Dataset for SerpCBD-GFP fluorescence intensity in glands with double KD of Crb and Pi3K92E.
Source data 7. Dataset for Rab11-YFP fluorescence intensity in control glands.
Source data 8. Dataset for Rab11-YFP fluorescence intensity in Crb KD glands.
Source data 9. Dataset for Rab11-YFP fluorescence intensity in Pten KD glands.
Source data 10. Dataset for Rab11-YFP fluorescence intensity in glands with double KD of Crb and Pten.
Source data 11. Dataset for Rab11-YFP fluorescence intensity in Pi3K92E KD glands.
Source data 12. Dataset for Rab11-YFP fluorescence intensity in glands with double KD of Crb and Pi3K92E.
Source data 13. Dataset for Rab30-YFP fluorescence intensity in control glands.
Source data 14. Dataset for Rab30-YFP fluorescence intensity in Crb KD glands.
Source data 15. Dataset for Rab30-YFP fluorescence intensity in Pten KD glands.
Source data 16. Dataset for Rab30-YFP fluorescence intensity in glands with double KD of Crb and Pten.
Source data 17. Dataset for Rab30-YFP fluorescence intensity in Pi3K92E KD glands.
Source data 18. Dataset for Rab30-YFP fluorescence intensity in glands with double KD of Crb and Pi3K92E.
Source data 19. Dataset for food intake estimations.
Source data 20. Dataset for tracking of larval development.
Figure supplement 1. Overexpression of Pten leads to loss of Rab11 and Rab30 from the apical domain.

Efficient apical secretion requires the control of PI(4,5)P_2 metabolism by Crb

To assess whether the secretion defects are a consequence of altered phosphoinositide metabolism we analyzed the secretion of SerpCBD-GFP and the organization of the apical Rab machinery. Live imaging analysis revealed that apical secretion of SerpCBD-GFP in Crb-deficient SGs is restored upon concomitant KD of Pten (***Figure 6A–D,G***, ***Figure 6—source data 1*** to 4), while KD of Pi3K92E alone, or in combination with Crb KD, induces a stronger apical retention of SerpCBD-GFP than the one observed in Crb-deficient SGs (***Figure 6B,E–G***, ***Figure 6—source data 5*** and ***6***). Similar results were obtained using the probe for glycoproteins PNA-GFP (data not shown). Similarly, KD of Pten efficiently suppresses the loss of the apical pools of Rab11-YFP (***Figure 6H–K,N***, ***Figure 6—source data 7*** to 10) and Rab30-YFP (***Figure 6O–R,U***, ***Figure 6—source data 13*** to 16) observed upon Crb depletion. Interestingly, KD of Pi3K92E in control cells induces loss of apical Rab11-YFP (***Figure 6L, N***, ***Figure 6—source data 11*** and ***12***), but has no effect on Rab30-YFP localization (***Figure 6S,U***, ***Figure 6—source data 17*** and ***18***). Additionally, over-expression of Pten2 in the SGs induces the loss of apical pools of Rab11-YFP and Rab30-YFP (***Figure 6—figure supplement 1A–D***). This is in accordance with apical PI(4,5)P_2 levels regulating apical Rab proteins negatively. Unfortunately, the effects of Pten KD or over-expression on the apical pool of Rab6-YFP in the absence of Crb could not be studied due to lethality of the larvae. Thus, Crb function is required to organize the apical

cortex and to control the phosphoinositide metabolism, which in turn regulates the apical Rab protein machinery (Rab11-YFP, Rab30-YFP and possibly Rab6-YFP).

To assess the physiological relevance of Crb in SG secretion, we evaluated the larval food intake and tracked the pupariation time (***Deshpande et al., 2014***). We found that KD of Crb in the SGs, as well as KD of Pi3K92E, slightly reduces the amount of food intake (***Figure 6V***, ***Figure 6—source data 19***), yet this reduction is not statistically significant (one-way ANOVA followed by Tukey's multiple comparisons test). Interestingly, concomitant KD of Crb and Pten significantly increases the larval food intake when compared to controls (***Figure 6V***). Importantly, these trends are reflected in the pupariation rate (***Figure 6W***, ***Figure 6—source data 20***). Hence, while animals with SG-specific depletion of Crb take longer to pupariate than control animals (***Figure 6W***), those with additional Pten KD pupariate faster than those with Crb KD alone. Moreover, the pupariation of Pi3K92E KD animals is similar to the one of Crb-deficient animals, while concomitant KD of Crb and Pi3K92E delays the pupariation even more. Taken together, our results demonstrate that Crb is essential for apical membrane homeostasis, apical secretion and physiological function of larval SGs.

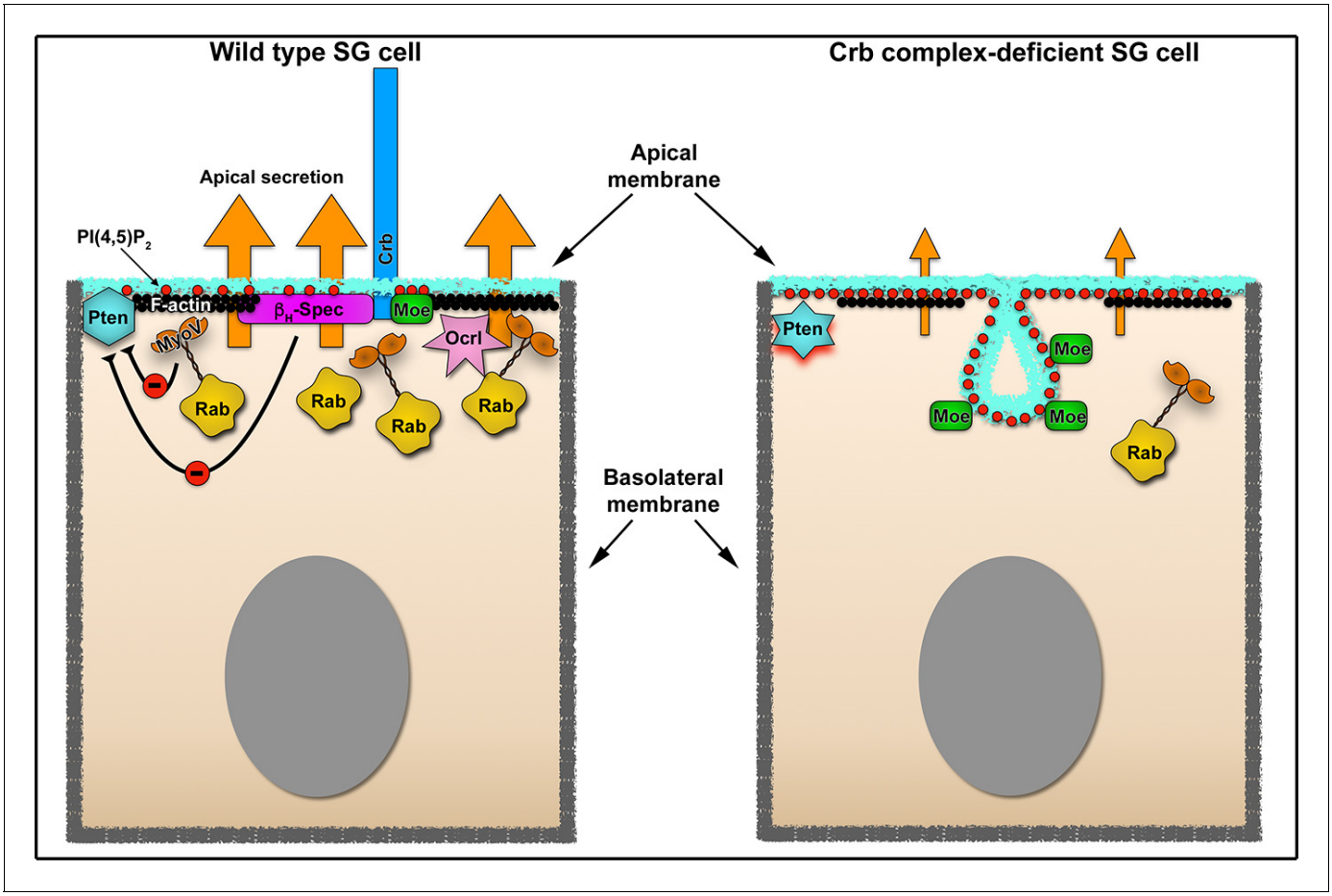

Figure 7. Crb-dependent regulation of apical secretion in SG cells Schematic representation of Crb-dependent regulation of apical secretion in SG cells. Under physiological conditions (left image), Crb mediates the apical localization of Moesin and β_H-Spec, which link the Crb protein (blue) to the apical F-actin cytoskeleton (black ribbon). This Crb-cytocortex complex is necessary for organization of the apical Rab-dependent traffic machinery (depicted as Rab vesicles in yellow). Under these conditions Crb negatively regulates the activity of Pten via β_H-Spec and MyoV. The precise molecular interactions involved in the negative regulation of Pten are not defined (see Discussion for details). The absence of Crb in the SG cells disrupts the efficient apical secretion (right image). The defects in apical secretion are a consequence of the disruption of the apical cytocortex (actin, β_H-Spec), the loss of MyoV and the excessive production of PI(4,5)P_2 (red dots) which require the activity of Pten. The loss of Ocrl form the apical membrane could also contribute to the increase in PI(4,5)P_2 apical levels. Another consequence is the formation of a novel apical membrane sac enriched in PI(4,5)P_2 (PAMS), Moe (green rectangles) and apical transmembrane proteins (not depicted).

Discussion

In this work we identified unknown roles of Crb in constitutive apical secretion of larval SGs. Defects in apical secretion upon KD of Crb are not due to an overall disruption of epithelial cell polarity. Our results point to two major components acting downstream of Crb that regulate secretion. i) We found that the Crb complex is essential for Rab6-, Rab11- and Rab30-dependent, apical membrane transport machinery by ensuring the apical pools of these Rab proteins. This suggests that Crb maintains the active pool of these Rab proteins at the apical domain, as inactive GDP-bound Rab proteins associate with chaperone-like molecules, called GDP dissociation inhibitors (GDIs), and diffuse into the cytosol (***Goody et al., 2005***; ***Grosshans et al., 2006***; ***Müller and Goody, 2018***). ii) We show that Crb restricts the levels of $PI(4,5)P_2$ on the apical membrane by regulating apical activity and apical localization of Pten and Ocrl, respectively. As a consequence, Crb controls the size and organization of the apical membrane and efficient apical secretion, processes that are mediated in part by β_H-Spec and MyoV. From this we conclude that the Crb protein complex functions as an apical hub that interconnects and regulates these cellular machineries, which, in turn, are essential to maintain the physiological activity of the SGs (***Figure 7***).

The roles of Crb in the regulation of constitutive saliva secretion

The late 3rd instar *Drosophila* SG has been extensively studied as a model for regulated exocytosis during the burst of glue granule secretion, which occurs at the onset of metamorphosis (reviewed in

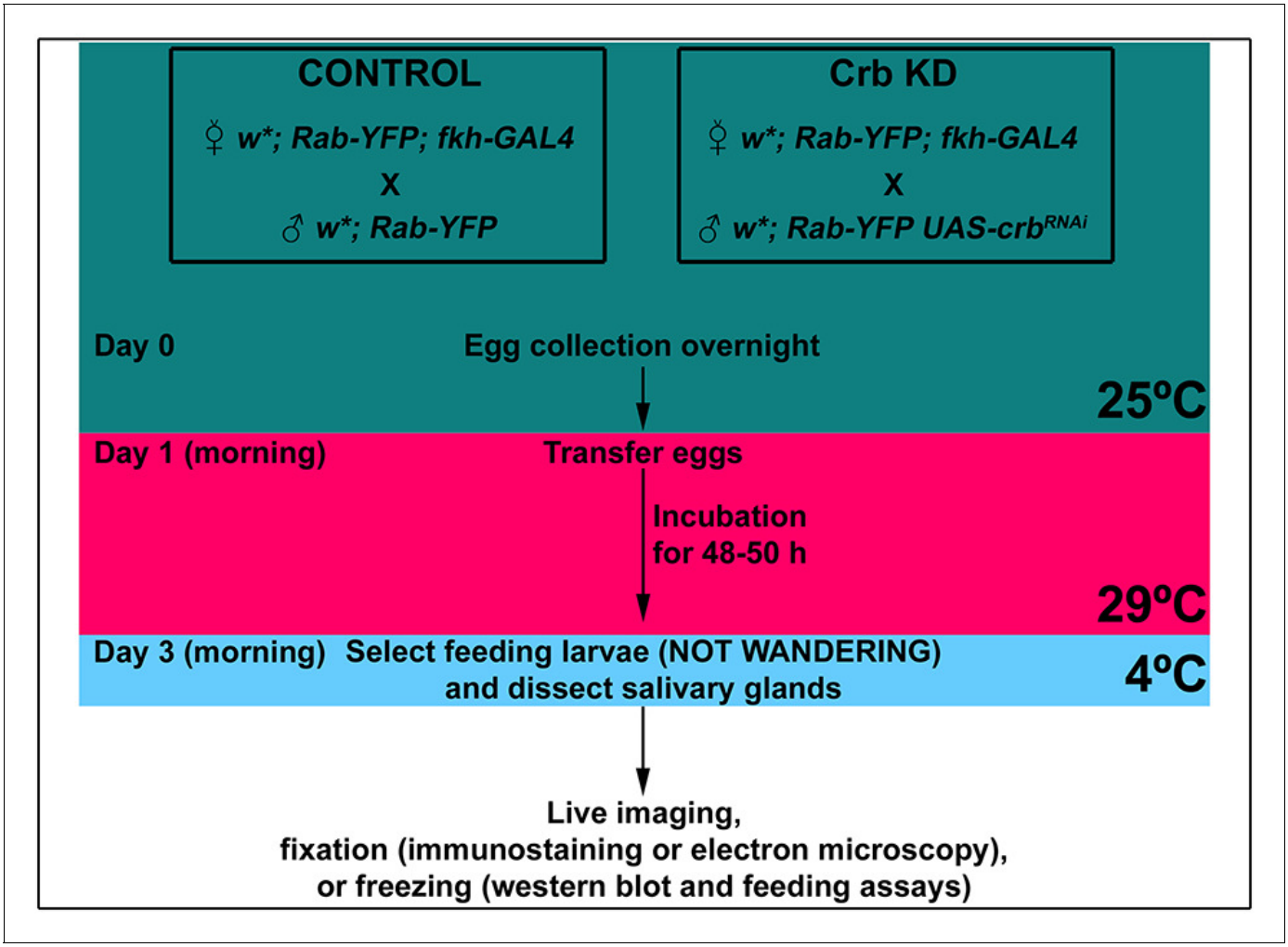

Figure 8. Schematic representation of the experimental setup. Indicated in the workflow are the times and incubation temperatures, as well as the time for dissections.

Tran and Ten Hagen, 2017). Here, we studied the roles of Crb in the regulation of constitutive saliva secretion in SGs at the beginning of the 3rd instar, while larvae are still feeding. At this stage there is a minimal synthesis of glue proteins (*Kodani, 1948*; *Rizki, 1967*; *Beckendorf and Kafatos, 1976*; *Korge, 1977*; *Zhimulev et al., 1981*), while salivary glycoproteins are actively secreted into the lumen (*Thomopoulos, 1988*; *Chung et al., 2014*; *Maruyama and Andrew, 2012*; *Csizmadia et al., 2018*; *Gregg et al., 1990*; *Fraenkel and Brookes, 1953*).

Loss of Crb or Sdt in SG cells results in hampered delivery of apical transmembrane proteins (Cad99C and CD8-RFP) as well as apical accumulation of secretion reporters (SerpCBD-GFP and PNA-GFP), which suggests at least two interpretations. Loss of Crb 1) hampers secretion, so that protein transport is jammed at the apical aspect, or 2) secretion is normal but endocytosis at the apical surface is strongly enhanced resulting in an immediate re-internalization of the secreted cargo. Loss of apical Rab6, Rab11, Rab30 and MyoV upon Crb KD supports the first interpretation. MyoV is a component of the apical secretory machinery (*Massarwa et al., 2009*; *Reck-Peterson et al., 2000*; *Li et al., 2007*) and known interactor of Crb, Rab6, Rab11 and possibly Rab30 (*Lindsay et al., 2013*; *Li et al., 2007*; *Iwanami et al., 2016*; *Pocha et al., 2011a*). Both Rab6 and Rab11 are known to facilitate apical transport and recycling (*Khanal et al., 2016*; *Iwanami et al., 2016*; *Chung and Andrew, 2014*; *Li et al., 2007*; *Satoh et al., 2005*; *Pelissier et al., 2003*), while Rab30 is suggested to be associated with the Golgi apparatus (*Kelly et al., 2012*). However, in larval SG cells Rab30 shows no co-localization with Golgi markers (*Dunst et al., 2015*) but instead localizes in a subapical pool. Interestingly, Rab30 was found as a potential MyoV-binding partner but later dismissed due to experimental threshold settings (*Lindsay et al., 2013*). Thus, although the functions of Rab30 in *Drosophila* are less clear (*Thomas et al., 2009*), our results suggest that active Rab30 contributes to MyoV-dependent transport.

A role of Crb in apical secretion rather than in apical endocytosis is further supported by our observations that the distribution of Rab proteins involved in endocytosis, namely Rab5, Rab7 and Rab21, is not affected by the loss of Crb (*Simpson et al., 2004*; *Chavrier et al., 1990*). This is also consistent with earlier observations that *crb* loss of function does not result in an overall increase in endocytosis in the eye imaginal disc epithelium (*Richardson and Pichaud, 2010*). Nevertheless, we cannot exclude the contribution of endocytosis completely, as inhibition of dynamin-dependent endocytosis seems to ameliorate the secretion phenotype of Crb-deficient glands, yet it does not block the formation of PAMS (data not shown). Moreover, by using dominant active or inactive forms of Rab5 (*Zhang et al., 2007*), we obtained inconsistent results (data not shown), probably due to pleiotropic effects of these versions of Rab5, which tend to titer effectors shared with other Rab proteins (*Pylypenko et al., 2017*; *Müller and Goody, 2018*). Although loss of β_H-Spec function has been linked to increased endocytosis in some *Drosophila* epithelia (*Williams et al., 2004*; *Pellikka et al., 2002*; *Richard et al., 2009*; *Phillips and Thomas, 2006*), or Crb mobility in the embryonic epidermis (*Bajur et al., 2019*) data presented here support the conclusion that in larval SGs Crb predominantly regulates apical membrane traffic and secretion, though we cannot completely rule out a minor contribution of endocytosis to the phenotypes observed.

We show that Crb is necessary to maintain the apical localization of MyoV. As mentioned above, MyoV is an interactor of Rab6, Rab11 and possibly Rab30 (*Lindsay et al., 2013*). This suggests that Crb can directly organize the apical secretion machinery by modulating the localization of MyoV. Additionally, our results also suggest that stabilization of β_H-Spec by Crb is important for organizing the apical Rab proteins. It is known that Crb regulates the actin cytoskeleton, and is necessary for recruitment of β_H-Spec and Moe to the apical cytocortex (*Flores-Benitez and Knust, 2015*; *Tsoumpekos et al., 2018*; *Salis et al., 2017*; *Röper, 2012*; *Sherrard and Fehon, 2015*; *Loie et al., 2015*; *Das and Knust, 2018*; *Médina et al., 2002a*; *Wei et al., 2015*; *Wodarz et al., 1995*). Unlike in other epithelia (*Wodarz et al., 1995*; *Pellikka et al., 2002*; *Médina et al., 2002b*; *Richard et al., 2009*), depletion of β_H-Spec in SGs does not result in loss of Crb or Sdt from the apical domain, but rather hampers apical secretion and induces the loss of Rab6- and Rab11-positive apical compartments. Therefore, the normal apical secretory activity of the SGs requires the Crb-dependent stabilization of β_H-Spec and MyoV at the apical cytocortex.

Crb organizes the apical trafficking machinery by controlling apical PI(4,5)P_2 levels

Our results suggest that Crb is required to maintain the apical localization of Ocrl and to negatively regulate the activity of Pten, both key regulators of PI(4,5)P_2 levels (**Worby and Dixon, 2014**; **Balakrishnan et al., 2015**). Hence, apical PI(4,5)P_2 levels increase upon loss of Crb. Concomitantly, PI(4,5)P_2 as well as phospho-Moe and apical transmembrane proteins are found in a singular apical membrane extension, dubbed PAMS. Chemical inhibition or genetic ablation of Pten in Crb-deficient glands not only suppresses the formation of PAMS, but also restores the apical pools of Rab11, Rab30, apical secretion, larval food intake and timely pupariation. The relevance of PI(4,5)P_2 levels for proper secretion is highlighted by recent results demonstrating that the activity of *Drosophila* Crag (a Rab10 GEF) and Stratum (a Rab8 GEF) is regulated by the levels of PI(4,5)P_2 (**Devergne et al., 2014**; **Devergne et al., 2017**). For example, in the follicle epithelium, reduction of PI(4,5)P_2 levels results in defective secretion of basal membrane proteins, which then accumulate at the apical membrane (**Devergne et al., 2014**; **Devergne et al., 2017**). Moreover, recent work showed that another phosphoinositide species, PI(3,4)P_2, and the enzyme producing it, SHIP1, are key determinants of apical identity in a model of lumen formation (**Román-Fernández et al., 2018**). PI(3,4)P_2 was found to be an essential component of the pre-apical membrane and of Rab11a-positive recycling endosomes containing apical proteins that cluster together during de novo formation of the lumen. Indeed, perturbing PI(3,4)P_2 levels disrupts polarization through subcortical retention of vesicles at apical membrane initiation sites (**Román-Fernández et al., 2018**). Therefore, the control of PI(4,5)P_2 levels by Crb might impact the apical secretory machinery by altering the localization of specific effectors (GEFs or GAPs) of Rab6, Rab11 and Rab30.

Crb-mediated regulation of Pten partially depends on the organization of the apical cytocortex, but the precise molecular mechanism remains to be elucidated. So far, based on co-immunoprecipitation assays (data not shown) or on previous mass-spectrometry data (**Pocha et al., 2011b**) no direct interactions between Crb and Pten could be established. Yet, since apical localization of Baz, a binding partner of Pten (**von Stein et al., 2005**), is not affected by the loss of Crb, we suggest that the Baz-Pten interaction does not depend on Crb. On the other hand, KD of MyoV or β_H-Spec induces the formation of PAMS. Therefore, we favor the hypothesis that regulation of Pten might be mediated by β_H-Spec and MyoV acting downstream of Crb. Interestingly, an interaction between β_H-Spec and Pten was found by tandem affinity purification assays (**Vinayagam et al., 2016**), but whether this interaction regulates Pten activity was not analyzed. Furthermore, inhibition of MyoV-based transport increases the cell size of neurons, which mimics the PTEN-loss of function (**van Diepen et al., 2009**). Indeed, using immunoprecipitation and FRET analysis, it was shown that mammalian PTEN can interact directly with the MyoV C-terminal cargo-binding domain, yet the consequences of this interaction on PTEN activity or its localization were not evaluated (**van Diepen et al., 2009**). Therefore, it is plausible that Pten activity in the larval SGs can be regulated by interactions with MyoV and β_H-Spec. It is well-known that Pten regulation is very complex. Mammalian PTEN, for example, has more than 20 different sites, which can be subject to post-translational modifications (**Worby and Dixon, 2014**; **Gorbenko and Stambolic, 2016**). Therefore, it is likely that Crb can impinge on Pten activity via several different mechanisms, which can even be tissue- or developmental stage-specific. Indeed, it is well established that Crb as well as other polarity proteins have tissue specific functions, regulating cell signaling, cytoskeleton dynamics, cell division and cell adhesion as well as tissue growth and morphogenesis (reviewed in **Flores-Benitez and Knust, 2016**; **Tepass, 2012**). But even in one tissue like the larval SGs, Crb may control apical trafficking via additional mechanisms independent of Pten. For example, loss of apical Rab30 upon Crb KD is independent of β_H-Spec, suggesting that Crb can organize the apical trafficking machinery by additional effectors.

PAMS – membrane entities dependent on PI(4,5)P_2 levels

It is well-known that Crb is a key determinant of the apical membrane and that over-expression of Crb in *Drosophila* embryos expands the apical membrane (**Wodarz et al., 1995**), Our findings on the functional link between Crb and Pten now provide a possible mechanism by which Crb exerts this function. In this context, the formation of the PAMS, apical membrane invaginations containing microvilli enriched in PI(4,5)P_2, phospho-Moe and apical transmembrane proteins (Sas, Crb and

CD8-RFP), offer an attractive model to study the regulation of apical membrane organization by Crb and Pten. Recently published data implicate PTEN in the regulation of apical membrane size. By using intestinal epithelial Ls174T:W4 cells in culture, Bruurs et al., showed that loss of PTEN results in formation of a larger brush border. In contrast, in mouse small intestinal organoids no change was observed (**Bruurs et al., 2018**), indicating that these effects can be tissue specific. Pten activity is necessary for the morphogenesis of rhabdomeres, a specialized apical membrane domain composed of a tightly packed stack of microvilli in *Drosophila* photoreceptors (**Pinal et al., 2006**). Indeed, Crb overexpression in *Drosophila* photoreceptor cells increases the amount of apical membrane (**Pellikka et al., 2002**; **Muschalik and Knust, 2011**). Therefore, it will be interesting to test whether this is mediated by Pten or by changes in intracellular trafficking.

It is important to note that the PAMS do not represent an expansion of the apical membrane upon loss of Crb (**Figure 5—figure supplement 1E**). On the contrary, based on our measurements of microvilli density (**Figure 2M**) and the disruption of Cad99C localization, the net effect of Crb KD is a reduction in the amount of apical membrane. Considering that one microvillus has a surface of approx. 0.55 μm^2 (roughly calculated from our EM images the height $\approx$ 2.5 µm and radius $\approx$ 35 nm), 80 microvilli are found along 10 µm of apical membrane thus 'contain' approx. 44 μm^2 of plasma membrane. Therefore, the reduction in microvilli number in Crb-deficient cells (without considering the reduction in their height) indicates that approx. 20 μm^2 of plasma membrane is found along the same length of the apical membrane, which is a loss of >50% of the apical membrane. Moreover, this loss of microvilli might be related to the defects in Cad99C localization upon loss of Crb, as Cad99C is important in maintenance of microvillar length (**Chung and Andrew, 2014**). Therefore, our results support the conclusion that Crb regulates the apical membrane architecture by maintaining the lipid homeostasis and the organization of the apical cytocortex. Upon loss of Crb, the collapse of the cytocortex together with the increase in $PI(4,5)P_2$ lead to the formation of PAMS and destabilization of the microvilli. Therefore, to understand how Crb regulates the proper proportions of apical vs. basolateral membranes, future studies need to address the biogenesis of the PAMS and whether their formation occurs at the expense of the basolateral membrane.

Possible implications in human pathology

Defects in the membrane trafficking machinery are linked to a plethora of different pathologies, including immune syndromes, deafness, neuronal degeneration and cancer (reviewed in **Seabra et al., 2002**; **Holthuis and Menon, 2014**; **Krzewski and Cullinane, 2013**; **Bronfman et al., 2007**). The PAMS in Crb-deficient SG cells have striking similarities to the inclusion bodies observed in MVID patients carrying mutations in *MYO5b* (**Müller et al., 2008**; **Ruemmele et al., 2010**) or those found in animal models of MVID, like zebrafish mutant for *myosin Vb* (**Sidhaye et al., 2016**) and mice mutant for *Rab8a* and *Rab11a* (**Feng et al., 2017**; **Sato et al., 2007**). Moreover, recent data obtained in an intestinal organoid model of microvillus inclusion formation showed that these inclusion bodies are dynamic. Within hours, these inclusions can form and detach from the plasma membrane or collapse (**Mosa et al., 2018**). Furthermore, disruption of MyoVB, Rab8a, Rab11a, Syntaxin three and Syntaxin binding protein 2, all lead to defects similar to the ones observed in MVID enterocytes (**Sidhaye et al., 2016**; **Feng et al., 2017**; **Vogel et al., 2017**; **Schneeberger et al., 2015**; **Mosa et al., 2018**). Therefore, it is tempting to speculate that up-regulation of Pten activity could contribute to the pathogenesis of MVID.

Retinal degeneration is another pathological condition often caused by compromised trafficking machinery. Mutations in human *CRB1* induce retinal degeneration (**Richard et al., 2006b**; **Bulgakova and Knust, 2009**), similar as mutations in *Drosophila crb* (**Johnson et al., 2002**; **Pocha et al., 2011a**; **Pellikka et al., 2002**; **Izaddoost et al., 2002**; **Chartier et al., 2012**; **Spannl et al., 2017**) or overexpression of dominant negative versions (**Pellikka and Tepass, 2017**). Indeed, disruption of many of the proteins regulated by Crb in the SGs, including MyoV and Pten, can affect eye development, trafficking of Rh1 and ultimately photoreceptor survival in the fly (**Pocha et al., 2011a**; **Pellikka et al., 2002**; **Richard et al., 2009**; **Karagiosis and Ready, 2004**; **Iwanami et al., 2016**; **Pinal et al., 2006**; **Satoh et al., 2016**). Thus, it will be interesting to analyze whether Crb regulates the apical trafficking machinery in photoreceptor cells by modulating the phosphoinositide metabolism and how this is related to the pathogenesis of retinal degeneration.

In conclusion, data presented here reveal a role for the Crb complex beyond its canonical function as a polarity determinant in differentiating epithelial cells and show that Crb can fine-tune the

morphology and the molecular composition of the apical domain in a mature epithelium. In the future it will be interesting to explore whether the functional interactions described here are unique to early *Drosophila* SG cells or represent a conserved module also acting in other Crb-expressing epithelia.

Materials and methods

Fly stocks

Fly stocks (see **Table 1**) were maintained at room temperature (RT) on standard food. We employed the UAS-GAL4 system (**Elliott and Brand, 2008**) to drive the expression of different UAS-transgenes specifically in the salivary gland with the *fkh*-GAL4 driver (**Henderson and Andrew, 2000**). For detailed descriptions of the genotypes used in each figure see **Table 2**. The stocks in which the UAS-RNAi lines were recombined with the *fkh*-GAL4 driver together with the temperature sensitive repressor GAL80[ts] were maintained and expanded at 18˚C. For experiments (see example in **Figure 8**), the crosses driving the different UAS-RNAi lines, and their corresponding controls, were done and maintained at 25˚C. Eggs were collected overnight and then transferred to 29˚C for approx. 48 hr. After this period, the feeding third instar larvae (not yet wandering) were collected for salivary gland dissections.

Immunostaining of salivary glands

For all experiments, and in order to always compare equal timepoints of larval development, control and experimental genotypes were collected under the same conditions (see example in **Figure 8**). After growing at 29˚C for approx. 50 hr, the salivary glands of non-wandering third instar larvae were dissected in ice cold Grace's medium (Thermo Fisher Scientific). Corresponding control and experimental glands were mounted together directly on a slide (previously coated with embryo-glue; **Figard and Sokac, 2011**) and then fixed. In this way, all staining-conditions were always identical for controls and experimental samples. Depending on the antigen (see **Table 3**), fixation was done in 100% methanol at −20˚C for 5 min or in 6% formaldehyde in Grace's medium at RT for 15 min. For microtubule staining (**Riparbelli et al., 1993**), fixation was done in 100% methanol for 10 min followed by 5 min in acetone both at −20˚C. Samples were washed at least 5 times with 0.1% Triton X-100 in 1xPBS (PBT) and blocked in 5% normal goat serum (NGS) in PBT (blocking solution) for 30 min at 4˚C. Primary antibody staining was done in blocking solution over night at 4˚C. Samples were washed at least 5 times with PBT before incubation with the appropriate secondary antibody in blocking solution for two hours at RT and washed again 5 times with PBT. The samples were covered with Vectashield (Vector Laboratories) and visualized using a Zeiss LSM 880 Airy upright single photon point scanning confocal system (ZEISS Microscopy, Jena, Germany) with a Zeiss iLCI Plan-Neofluar 63 × 1.3 Imm Korr DIC objective. In all cases, for any given marker, images were acquired under the same settings for laser power, PMT gain and offset. Maximal projections, merging and LUT-pseudocolor assignment were performed using Fiji (**Schindelin et al., 2012**). Image montage was done in Adobe Photoshop CS5 version 12.1 and when brightness, contrast and levels were adjusted, the modifications were linear and equally applied to the whole set of images. IMARIS 7.6 software was used to render the **Video 8**. Unless otherwise is stated, images are representative of at least three independent experiments, with at least three technical replicates in each experiment.

Live imaging of salivary glands

Collection of control and experimental larvae was done as described above. For live imaging, the salivary glands were dissected in ice-cold Grace's medium, mounted on the bottom of a Petri dish previously coated with embryo-glue (**Figard and Sokac, 2011**) and imaged directly using a Zeiss LSM 880 Airy upright single photon point scanning confocal system (ZEISS Microscopy, Jena, Germany) with a Zeiss W Plan-Apochromat 40 × 1.0 objective. Excitation was performed with 488 nm for GFP or YFP from an Argon Multiline Laser, and 561 nm from a Diode Pumped Solid State (DPSS) Laser for RFP, mTomato and Dextran-Rhodamine. For time-lapse imaging of Rab-YFP proteins, 10 steps (0.67 µm/step) were acquired every 5 s for 5 min. Using FIJI software, the original stack was scaled 2X with a bicubic average interpolation, filtered with a Gaussian Blur (Sigma = 1) and animation speed set of 16 fps. Final montage and rendering were made in Photoshop CC 2018. Unless

Table 1. List of fly stocks used in this study.

Designation	Genotype (as reported in FlyBase when available)	Description
Balancer	w[1118]; In(2LR)Gla, wg[Gla-1]/CyO, P{w[+mC]=GAL4 twi.G}2.2, P{w[+mC]=UAS-2xEGFP}AH2.2	Balancer for 2nd chromosome; BSC 6662
Balancer	w[1118]; Dr[Mio]/TM3, P{w[+mC]=GAL4 twi.G}2.3, P{UAS-2xEGFP}AH2.3, Sb[1] Ser [1]	Balancer for 3rd chromosome; BSC 6663
Balancer	w[*]; ry[506] Dr[1]/TM6B, P{w[+mC]=Dfd-EYFP}3, Sb[1] Tb[1] ca[1]	Balancer for 3rd chromosome; BSC 8704
crb^{RNAi}	w[1118]; P{GD14463}v39177	Expresses the RNAi against crb under the control of UAS sequences; VDRC 39177
sdt^{RNAi}	w[1118]; P{GD9163}v23822	Expresses the RNAi against sdt under the control of UAS sequences; VDRC 23822
sdt^{RNAi}	y[1] sc[*] v[1]; P{y[+t7.7] v[+t1.8]=TRiP.HMS01652}attP40	Expresses dsRNA for RNAi of sdt (FBgn0261873) under UAS control. BSC 37510
gfp^{RNAi}	y[1] sc[*] v[1]; P{y[+t7.7] v[+t1.8]=VALIUM20 EGFP.shRNA.3}attP40	Expresses small hairpin RNA under the control of UAS for RNAi of EGFP and EYFP as well as fusion proteins containing these fluors, BSC 41559
gfp^{RNAi}	y[1] sc[*] v[1]; P{y[+t7.7] v[+t1.8]=VALIUM20 EGFP.shRNA.3}attP2	Expresses small hairpin RNA under the control of UAS for RNAi of EGFP and EYFP as well as fusion proteins containing these fluors, BSC 41560
moe^{RNAi}	w[1118]; P{GD5211}v37917	Expresses the RNAi against moe under the control of UAS sequences; VDRC 37917
kst^{RNAi}	y[1] v[1]; P{y[+t7.7] v[+t1.8]=TRiP.GLC01654}attP40	Expresses dsRNA for RNAi of kst (FBgn0004167) under UAS control, BSC 50536
$ocrl^{RNAi}$	y[1] sc[*] v[1] sev[21]; P{y[+t7.7] v[+t1.8]=TRiP.HMS01201}attP2/TM3, Sb[1]	Expresses dsRNA for RNAi of Ocrl (FBgn0023508) under UAS control in the VALIUM20 vector. BSC 34722
GAL80ts	w[*]; P{w[+mC]=tubP-GAL80[ts]}7	Expresses temperature-sensitive GAL80 under the control of the alphaTub84B promoter; outcrossed from BSC 7018
Dicer	w[1118]; P{w[+mC]=UAS-Dcr-2.D}2	Expresses Dicer-2 under UAS control, BSC 24650
$myoV^{RNAi}$	y[1] sc[*] v[1]; P{y[+t7.7] v[+t1.8]=TRiP.HMC03900}attP40	Expresses dsRNA for RNAi of didum (FBgn0261397) under UAS control; BSC 55740
$pten^{RNAi}$	y[1] w[1118]; P{w[+mC]=UAS Pten.dsRNA.Exel}2	Expresses a snapback transcript for RNAi of Pten under the control of UAS. BSC 8549
$pten^{RNAi}$	w[1118]; P{w[+mC]=UAS Pten.dsRNA.Exel}3	Expresses a snapback transcript for RNAi of Pten under the control of UAS. BSC 8550
$pi3k92E^{RNAi}$	y[1] sc[*] v[1]; P{y[+t7.7] v[+t1.8]=TRiP.HMC05152}attP40	Expresses dsRNA for RNAi of Pi3K92E (FBgn0015279) under UAS control. BSC 61182
$pi3k92E^{RNAi}$	y[1] sc[*] v[1]; P{y[+t7.7] v[+t1.8]=TRiP .GL00311}attP2	Expresses dsRNA for RNAi of Pi3K92E (FBgn0015279) under UAS control. BSC 35798

Table 1 continued on next page

Table 1 continued

Designation	Genotype (as reported in FlyBase when available)	Description
sktl^{RNAi}	y[1] sc[*] v[1]; P{y[+t7.7] v[+t1.8]=TRiP .GL00072}attP2	Expresses dsRNA for RNAi of sktl (FBgn0016984) under UAS control. BSC 35198
SerpCBD-GFP	w[*];; UAS-SerpCBD-GFP	Expresses the N-terminus of Serp including the signal peptide and chitin binding domain (CBD) fused to GFP (***Luschnig et al., 2006***), kindly provided by S. Luschning
MyosinV-GFP	w[*];; UAS-didum-GFP	Expresses full length didum (amino acids 1–1792) tagged at the C-terminal end with EGFP (***Krauss et al., 2009***), kindly provided by A. Ephrussi
Sas-Venus	w[*];; tub::Sas-Venus	Stranded at Second fused with Venus under tubulin promoter on 3rd chromosome (***Firmino et al., 2013***)
PNA-GFP	w[*]; M{w[+mC]=UAS PNA.GFP}ZH-86Fb	Expresses GFP-tagged peanut agglutinin under UAS control. BSC 55247
CD8-RFP	w[*]; P{y[+t7.7] w[+mC]=10XUAS-IVS-mCD8::RFP}attP2	Expresses mCD8-tagged RFP under the control of 10 UAS sequences. BSC 32218
PI(4,5)P_2 sensor	y[1] w[*]; P{w[+mC]=UAS-PLCdelta-PH-EGFP}3	Expresses GFP-tagged pleckstrin homology domain from human PLCδ. BSC 39693
PI(3,4,5)P_3 sensor	w[*];; tub::GPR1-PH-EGFP	Expresses GFP-tagged pleckstrin homology domain from cytohesin/GRP1 (***Pinal et al., 2006***), kindly provided by F. Pichaud
Pten2-GFP	w[*]; UAS-Pten2-GFP	Expresses Pten2 isoform GFP-tagged under the control of UAS sequences (***Pinal et al., 2006***), kindly provided by F. Pichaud
Pten2	w[*]; UAS-Pten2	Expresses the Pten2 isoform under the control of UAS sequences (***von Stein et al., 2005***), kindly provided by A. Wodarz
fkhGAL4	w[*]; fkh-GAL4	On 3rd chromosome, expresses GAL4 under the control of the fkh promoter (***Henderson and Andrew, 2000***), kindly provided by K. Röpper
Fas3-GFP	w[*]; P{w[+mC]=PTT-GA}Fas3[G00258]	Fas3 fused with GFP protein trap. BSC 50841
DE-cad-GFP	w*;DE-cad::GFP	DE-cadherin fused with GFP knock-in allele; homozygous viable (***Huang et al., 2009***), kindly provided by Y. Hong
DE-cad-mTomato	w*;DE-cad::mTomato	DE-cadherin fused with mTomato knock-in allele; homozygous viable (***Huang et al., 2009***), kindly provided by Y. Hong

Table 1 continued on next page

Table 1 continued

Designation	Genotype (as reported in FlyBase when available)	Description
Crb-GFP	w*;;crb::GFP-A	Crumbs fused with GFP knock-in allele; homozygous viable (**Huang et al., 2009**), kindly provided by Y. Hong
Lac-GFP	w*; lac::GFP	Protein trap line: *lachesin* fused with GFP under endogenous promoter on 2nd chromosome; homozygous viable (kindly provided by the Klämbt Protein trap consortium)
Nrv2-GFP	w*; nrv2::GFP	Protein trap line: *nervana2* fused with GFP under endogenous promoter on 2nd chromosome; homozygous viable (kindly provided by the Klämbt Protein trap consortium)
Ocrl-RFP	TI{T-STEP.TagRFP-T}Ocrl[KI] w[*]	A T-STEP cassette was knocked into Ocrl to tag the endogenous protein with TagRFP-T. BSC 66529
Dlg-mTagRFP	Dlg-mTagRFP	On X chromosome, expresses Dlg-mTagRFP under the control of a ubiquitous promoter (**Pinheiro et al., 2017**), kindly provided by Y. Bellaïche
Rab-YFP	Rab-YFP	endogenously YFP::tagged Rab protein library generated in **Dunst et al. (2015)**

BSC - Bloomington Drosophila stock Center

VDRC - Vienna Drosophila Resource Center.

otherwise is stated, images are representative of at least three independent experiments, with at least three technical replicates in each experiment.

Image quantifications

The distribution and intensity levels of different markers were assessed using FIJI software. A flow-diagram of the analyses as well as all values obtained can be found in the accompanying Source Data. Briefly, to obtain the apical-to-basal fluorescence intensities of a particular marker, in a single-optical slice, individual straight lines (ROIs) were made from the apical membrane towards the basal membrane. The line width was set to 18 and all lines were arranged parallel to each other. Enough lines were made to cover the whole length of the salivary gland in the field of view (>70 µm) or a minimum of five cells per gland were covered (approx. 50 µm). The intensity values along the lines were obtained using the Multi Plot measurement option of FIJI. These intensity values were averaged along the length of the gland to obtain a single intensity distribution for one gland. The values for the line length were normalized to one and divided into 20 segments. The intensity values for each of the 20 segments was averaged and used to plot the final apical-to-basal fluorescence intensities.

To evaluate the apical-to-lateral ratios of a particular marker, in a single-optical slice, using the Multi-point tool of FIJI, a total of five dots (ROIs) were equally distributed along the apical membrane and five dots along the lateral membrane. The respective mean intensity values for apical and lateral membranes were obtained, averaged and the ratio was calculated. A minimum of four cells were evaluated for each gland.

For the quantification of the apical membrane (surface and volume), we analyzed the fluorescence of PLCδ-PH-EGF, to mark the plasma membrane including the PAMS, and *D*E-cadherin-mTomato, to distinguish the boundaries of the apical membrane, in Z-stacks acquired by confocal microscopy as described above. The plasma membrane was manually segmented using the Segmentation Editor

Table 2. List of detailed genotypes analyzed in each figure.

Figure 1	
B,B′	*w*; UAS-crb[RNAi]/+*
C,C′	*w*; UAS-crb[RNAi]/+; fkh-GAL4/+*
D	*w*; Rab30-YFP, UAS-crb[RNAi]/+*
E	*w*; Rab30-YFP, UAS-crb[RNAi]/+; fkh-GAL4/+*
F	*w*; UAS-crb[RNAi]/+; Rab11-YFP/+*
G	*w*; UAS-crb[RNAi]/+; Rab11-YFP/fkh-GAL4*
I	*w*;; fkhGAL4, ubiGAL80[ts]*
J	*w*; UAS-crb[RNAi]; fkhGAL4, ubiGAL80[ts]*
K	*w*;; fkhGAL4, UAS-SerpCBD-GFP-GFP/+*
L	*w*; UAS-crb[RNAi]/+; fkhGAL4, UAS-SerpCBD-GFP-GFP/+*
Figure 1—figure supplement 1	
A,C,E,G,I,K	*w*; UAS-crb[RNAi]/+*
B,D,F,H,J,L	*w*; UAS-crb[RNAi]/+; fkh-GAL4/+*
M	*w*;; UAS-CD8-RFP/fkhGAL4*
N	*w*; UAS-crb[RNAi]/+; UAS-CD8-RFP/fkhGAL4*
O	*w*;; UAS-PNA-GFP/fkhGAL4 ubiGAL80[ts]*
P	*w*;; UAS-crb[RNAi]/+; UAS-PNA-GFP/fkhGAL4 ubiGAL80[ts]*
Q: Control	*w*; UAS-crb[RNAi]/+; Rab11-YFP/+*
Q: Crb KD	*w*; UAS-crb[RNAi]/+; Rab11-YFP/fkh-GAL4*
S,U,U′,W,Y	*w*;; UAS-std[RNAi]/+*
T,V,V′,X,Z	*w*; UAS-sdt[RNAi]/fkh-GAL4*
AA	*w*;; Rab11-YFP, UAS-sdt[RNAi]/Rab11-YFP*
BB	*w*;; Rab11-YFP, UAS-sdtRNAi/Rab11-YFP, fkhGAL4*
CC	*w*;; fkhGAL4, ubiGAL80[ts]/+*
DD	*w*; UAS-sdt[RNAi]; fkhGAL4, ubiGAL80[ts]/+*
EE	*w*;; fkhGAL4, UAS-CD8-RFP/+*
FF	*w*;; fkhGAL4, UAS-CD8-RFP/UAS-sdt[RNAi]*
GG	*w*;; fkhGAL4, UAS-SerpCBD-GFP/+*
HH	*w*;; fkhGAL4, UAS-SerpCBD-GFP/UAS-sdt[RNAi]*
II	*w*;; fkhGAL4, UAS-PNA-GFP/+*
JJ	*w*;; fkhGAL4, UAS-PNA-GFP/UAS-sdt[RNAi]*
Figure 1—figure supplement 2	
A,A′,B	*w*; UAS-crb[RNAi]/+; Rab11-YFP/+*
C,C′,D′	*w*; UAS-crb[RNAi]/+; Rab11-YFP/fkh-GAL4*
E,G,I	*w*; UAS-crb[RNAi]/+*
F,H,J	*w*; UAS-crb[RNAi]/+; fkh-GAL4/+*
K,K′	*w*; Fas3-GFP/Fas3-GFP; fkhGAL4/+*
L,L′	*w*; Fas3-GFP/Fas3-GFP, UAS-crb[RNAi]; fkhGAL4/+*
M,M′	*w*; Fas3-GFP/Fas3-GFP; fkhGAL4/UAS-gfp[RNAi]*
Figure 2	
A,D	*w*; UAS-crb[RNAi]/+*
B,E	*w*; UAS-crb[RNAi]/+; fkh-GAL4/+*
G	*w*; UAS-gfp[RNAi]/+; crb-GFP-A/crb-GFP-A*

Table 2 continued on next page

Table 2 continued

Figure 1	
H	*w*; UAS-gfp[RNAi]/+; crb-GFP-A/crb-GFP-A, fkh-GAL4*
I	*w*;; fkhGAL4, ubiGAL80[ts]/tub::Sas-Venus*
J	*w*; UAS-crb[RNAi]; fkhGAL4, ubiGAL80[ts]/tub::Sas-Venus*
K,K'	*w*;; fkhGAL4, UAS-PLCdelta-PH-EGFP/+*
L,L'	*w*; UAS-crb[RNAi]/+; fkhGAL4, UAS-PLCdelta-PH-EGFP/+*
Figure 2—figure supplement 1	
A,C,E	*w*; UAS-gfp[RNAi]/+; crb-GFP-A/crb-GFP-A*
B,D,F	*w*; UAS-gfp[RNAi]/+; crb-GFP-A/crb-GFP-A, fkh-GAL4*
G,I	*w*; UAS-crb[RNAi]/+*
H,J	*w*; UAS-crb[RNAi]/+; fkh-GAL4/+*
Figure 2—figure supplement 2	
A-C'	*w*; UAS-crb[RNAi]/+; fkhGAL4, UAS-PLCdelta-PH-EGFP/+*
Figure 2—figure supplement 3	
A	*w*; UAS-crb[RNAi]/+*
B	*w*; UAS-crb[RNAi]/+; fkh-GAL4/+*
C	*w*; UAS-sdt[RNAi]/+*
D	*w*; UAS-sdt[RNAi]/+; fkh-GAL4/+*
Figure 2—figure supplement 4	
A,C,E	*w*;; fkhGAL4, ubiGAL80[ts]*
B,D,F	*w*; UAS-kst[RNAi]; fkhGAL4, ubiGAL80[ts]*
Figure 3	
A	*w*;; fkhGAL4, ubiGAL80[ts]*
B	*w*; UAS-crb[RNAi]; fkhGAL4, ubiGAL80[ts]*
C	*w*; UAS-kst[RNAi]; fkhGAL4, ubiGAL80[ts]*
E,G	*w*;; fkhGAL4, ubiGAL80[ts]/+*
F,H	*w*; UAS-didum[RNAi]/+; fkhGAL4, ubiGAL80[ts]/+*
I	*w*;; fkhGAL4, ubiGAL80[ts]/tub::Sas-Venus*
J	*w*; UAS-didum[RNAi]/+; fkhGAL4, ubiGAL80[ts]/tub::Sas-Venus*
K	*w*;; fkhGAL4, UAS-SerpCBD-GFP/+*
L	*w*; UAS-didum[RNAi]/+; fkhGAL4, UAS-SerpCBD-GFP/+*
Figure 3—figure supplement 1	
A	*w*;; fkhGAL4, ubiGAL80[ts]/UAS-MyoV-GFP*
B	*w*; UAS-crb[RNAi]/+; fkhGAL4, ubiGAL80[ts]/UAS-MyoV-GFP*
Figure 3—figure supplement 2	
A	*w*;; fkhGAL4, ubiGAL80[ts]/UAS-SerpCBD-GFP*
B	*w*; UAS-kst[RNAi]; fkhGAL4, ubiGAL80[ts]/UAS-SerpCBD-GFP*
Figure 4	
A	*w*; Rab6-YFP, UAS-crb[RNAi]/+*
B	*w*; Rab6-YFP, UAS-crb[RNAi]/+; fkh-GAL4/+*
C	*w*;; Rab11-YFP, fkhGAL4, ubiGAL80[ts]/Rab11-YFP*
D	*w*; UAS-crb[RNAi]/+; Rab11-YFP, fkhGAL4, ubiGAL80[ts]/Rab11-YFP*
E	*w*; Rab30-YFP/Rab30-YFP; fkhGAL4, ubiGAL80[ts]/+*

Table 2 continued on next page

Table 2 continued

Figure 1	
F	*w*; UAS-crb[RNAi], Rab30-YFP/Rab30-YFP; fkhGAL4, ubiGAL80[ts]/+*
G	*w*; UAS-crb[RNAi]/+; Rab1-YFP/+*
H	*w*; UAS-crb[RNAi]/+; Rab1-YFP/fkh-GAL4*
I: Rab1 Control	*w*; UAS-crb[RNAi]/+; Rab1-YFP/+*
I: Rab1 Crb KD	*w*; UAS-crb[RNAi]/+; Rab1-YFP/fkh-GAL4*
I: Rab6 Control	*w*; Rab6-YFP, UAS-crb[RNAi]/+*
I: Rab6 Crb KD	*w*; Rab6-YFP, UAS-crb[RNAi]/+; fkh-GAL4/+*
I: Rab11 Control	*w*; UAS-crb[RNAi]/+; Rab11-YFP/+*
I: Rab11 Crb KD	*w*; UAS-crb[RNAi]/+; Rab11-YFP/fkh-GAL4*
I: Rab30 Control	*w*; UAS-crb[RNAi], Rab30-YFP/+;*
I: Rab30 Crb KD	*w*; UAS-crb[RNAi], Rab30-YFP/+; fkhGAL4/+*
Figure 4—figure supplement 1	
Rab1 Control	*w*;; Rab1-YFP/fkhGAL4*
Rab1 Crb KD	*w*;UAS-crb[RNAi]/+; Rab1-YFP/fkhGAL4*
Rab2 Control	*w*; Rab2-YFP/+; fkhGAL4/+*
Rab2 Crb KD	*w*; Rab2-YFP, UAS-crb[RNAi]/+; fkhGAL4/+*
Rab4 Control	*w*; Rab4-YFP/+; fkhGAL4/+*
Rab4 Crb KD	*w*; Rab4-YFP, UAS-crb[RNAi]/+; fkhGAL4/+*
Rab5 Control	*w*; Rab5-YFP/+; fkhGAL4/+*
Rab5 Crb KD	*w*; Rab5-YFP, UAS-crb[RNAi]/+; fkhGAL4/+*
Rab6 Control	*w*; Rab6-YFP/+; fkhGAL4/+*
Rab6 Crb KD	*w*; Rab6-YFP, UAS-crb[RNAi]/+; fkhGAL4/+*
Rab7 Control	*w*;; Rab7-YFP/fkhGAL4*
Rab7 Crb KD	*w*;UAS-crb[RNAi]/+; Rab7-YFP/fkhGAL4*
Rab8 Control	*w*;; Rab8-YFP/fkhGAL4*
Rab8 Crb KD	*w*;UAS-crb[RNAi]/+; Rab8-YFP/fkhGAL4*
Rab10 Control	*w* Rab10-YFP/+;; fkhGAL4/+*
Rab10 Crb KD	*w* Rab10-YFP/+; UAS-crb[RNAi]/+; fkhGAL4/+*
Rab11 Control	*w*;; Rab11-YFP/fkhGAL4*
Rab11 Crb KD	*w*;UAS-crb[RNAi]/+; Rab11-YFP/fkhGAL4*
Rab18 Control	*w* Rab18-YFP/+;; fkhGAL4/+*
Rab18 Crb KD	*w* Rab18-YFP/+; UAS-crb[RNAi]/+; fkhGAL4/+*
Rab21 Control	*w* Rab21-YFP/+;; fkhGAL4/+*
Rab21 Crb KD	*w* Rab21-YFP/+; UAS-crb[RNAi]/+; fkhGAL4/+*
Rab35 Control	*w* Rab35-YFP/+;; fkhGAL4/+*
Rab35 Crb KD	*w* Rab35-YFP/+; UAS-crb[RNAi]/+; fkhGAL4/+*
Rab39 Control	*w* Rab39-YFP/+;; fkhGAL4/+*
Rab39 Crb KD	*w* Rab39-YFP/+; UAS-crb[RNAi]/+; fkhGAL4/+*
Rab40 Control	*w* Rab40-YFP/+;; fkhGAL4/+*
Rab40 Crb KD	*w* Rab40-YFP/+; UAS-crb[RNAi]/+; fkhGAL4/+*
Figure 4—figure supplement 2	
A	*w*; Rab6-YFP/Rab6-YFP; fhkGAL4/+*
B	*w*; Rab6-YFP, UAS-kst[RNAi]/Rab6-YFP; fhkGAL4/+*

Table 2 continued on next page

Table 2 continued

Figure 1	
C	*w*;; Rab11-YFP, fkhGAL4, ubiGAL80[ts]/Rab11-YFP*
D	*w*; UAS-kst[RNAi]/+; Rab11-YFP, fkhGAL4, ubiGAL80[ts]/Rab11-YFP*
E	*w*; Rab30-YFP/Rab30-YFP; fhkGAL4/+*
F	*w*; Rab30-YFP, UAS-kst[RNAi]/Rab30-YFP; fhkGAL4/+*
G	*w*;; Rab1-YFP/fkhGAL4, ubiGAL80[ts]*
H	*w*; UAS-kst[RNAi]/+; Rab1-YFP/fkhGAL4, ubiGAL80[ts]*
Figure 4—figure supplement 3	
A-A''	*w*; Rab6-YFP/Rab6-YFP; fhkGAL4, UAS-CD8-RFP/+*
B-B''	*w*; Rab6-YFP/Rab6-YFP, UAS-gfp[RNAi]; fhkGAL4, UAS-CD8-RFP/+*
C-C''	*w*;; Rab11-YFP, fkhGAL4, UAS-CD8-RFP/Rab11-YFP*
D-D''	*w*; UAS-gfp[RNAi]/+; Rab11-YFP, fkhGAL4, UAS-CD8-RFP/Rab11-YFP*
Figure 5	
B	*w*;; fkhGAL4, UAS-PLCdelta-PH-EGFP/+*
C	*w*; UAS-crb[RNAi]/+; fkhGAL4, UAS-PLCdelta-PH-EGFP/+*
D	*w*;; fkhGAL4, UAS-PLCdelta-PH-EGFP/UAS-pten[RNAi]*
E	*w*; UAS-crb[RNAi]/+; fkhGAL4, UAS-PLCdelta-PH-EGFP/UAS-pten[RNAi]*
F	*w*;; fkhGAL4, UAS-PLCdelta-PH-EGFP/UAS-pi3k92E[RNAi]*
G	*w*; UAS-crb[RNAi]/+; fkhGAL4, UAS-PLCdelta-PH-EGFP/UAS-pi3k92E[RNAi]*
I	*w*;; UAS-pten2-GFP/fkh-GAL4, ubiGAL80[ts]*
J	*w*; UAS-crb[RNAi]/+; UAS-pten2-GFP/fkh-GAL4, ubiGAL80[ts]*
L	*Ocrl-RFP, w*/+;; fkh-GAL4, ubiGAL80[ts]/+*
M	*Ocrl-RFP, w*; UAS-crb[RNAi]/+; fkh-GAL4, ubiGAL80[ts]/+*
O	*w*;; fkhGAL4, UAS-PLCdelta-PH-EGFP/+*
P	*w*;; fkhGAL4, UAS-PLCdelta-PH-EGFP/UAS-ocrl[RNAi]*
Figure 5—figure supplement 1	
A	*w*; DE-cad-mTomato/+; UAS-PLCdelta-PH-EGFP/fkhGAL4, ubiGAL80[ts]*
B	*w*;; fkhGAL4, UAS-PLCdelta-PH-EGFP/UAS-sdt[RNAi]*
C	*w*; UAS-kst[RNAi]/DE-cad-mTomato; fkhGAL4, ubiGAL80[ts]/UAS-PLCdelta-PH-EGFP*
D	*w*; UAS-didum[RNAi]/+; fkhGAL4 UAS-PLCdelta-PH-EGFP/+*
F	*w*;; UAS-PLCdelta-PH-EGFP/fkh-GAL4, ubiGAL80[ts]*
G	*w*; UAS-crb[RNAi]/+; UAS-PLCdelta-PH-EGFP/fkh-GAL4, ubiGAL80[ts]*
I	*w*;; fkhGAL4, UAS-PLCdelta-PH-EGFP/+*
J	*w*; UAS-crb[RNAi]/+; fkhGAL4, UAS-PLCdelta-PH-EGFP/+*
K	*w*;; fkhGAL4, UAS-PLCdelta-PH-EGFP/UAS-sktl[RNAi]*
L	*w*; UAS-crb[RNAi]/+; fkhGAL4, UAS-PLCdelta-PH-EGFP/UAS-sktl[RNAi]*
N,P	*w*;; fkhGAL4, ubiGAL80[ts]/UAS-PLCdelta-PH-EGFP*
O,Q	*w*; UAS-crb[RNAi]/+; fkhGAL4, ubiGAL80[ts]/UAS-PLCdelta-PH-EGFP*

Table 2 continued on next page

Table 2 continued

Figure 1	
Figure 5—figure supplement 2	
A	*w*;; fkhGAL4, UAS-PLCdelta-PH-EGFP/+*
B	*w*;; fkhGAL4, UAS-PLCdelta-PH-EGFP/UAS-pten2*
C	*UAS-Sktl w*/+;; fkhGAL4, UAS-PLCdelta-PH-EGFP/+*
D	*w*;; fkhGAL4, ubiGAL80[ts]/tub::GPR1-PH-EGFP*
E	*w*; UAS-crb[RNAi]/+; fkhGAL4, ubiGAL80[ts]/tub::GPR1-PH-EGFP*
Figure 6	
A	*w*;; fkhGAL4, UAS-SerpCBD-GFP/+*
B	*w*; UAS-crb[RNAi]/+; fkhGAL4, UAS-SerpCBD-GFP/+*
C	*w*;; fkhGAL4, UAS-SerpCBD-GFP/UAS-pten[RNAi]*
D	*w*; UAS-crb[RNAi]/+; fkhGAL4, UAS-SerpCBD-GFP/UAS-pten[RNAi]*
E	*w*;; fkhGAL4, UAS-SerpCBD-GFP/UAS-pi3k92E[RNAi]*
F	*w*; UAS-crb[RNAi]/+; fkhGAL4, UAS-SerpCBD-GFP/UAS-pi3k92E[RNAi]*
H	*w*;; Rab11-YFP, fkhGAL4, ubiGAL80[ts]/Rab11-YFP*
I	*w*; UAS-crb[RNAi]/+; Rab11-YFP, fkhGAL4, ubiGAL80[ts]/Rab11-YFP*
J	*w*; UAS-pten[RNAi]/+; Rab11-YFP, fkhGAL4, ubiGAL80[ts]/Rab11-YFP*
K	*w*; UAS-crb[RNAi]/UAS-pten[RNAi]; Rab11-YFP, fkhGAL4, ubiGAL80[ts]/Rab11-YFP*
L	*w*; UAS-pi3k92E[RNAi]/+; Rab11-YFP, fkhGAL4, ubiGAL80[ts]/Rab11-YFP*
M	*w*; UAS-crb[RNAi]/UAS-pi3k92E[RNAi]; Rab11-YFP, fkhGAL4, ubiGAL80[ts]/Rab11-YFP*
O	*w*; Rab30-YFP/Rab30-YFP; fkhGAL4, ubiGAL80[ts]/+*
P	*w*; UAS-crb[RNAi], Rab30-YFP/Rab30-YFP; fkhGAL4, ubiGAL80[ts]/+*
Q	*w*; Rab30-YFP/Rab30-YFP; fkhGAL4, ubiGAL80[ts]/UAS-pten[RNAi]*
R	*w*; UAS-crb[RNAi], Rab30-YFP/Rab30-YFP; fkhGAL4, ubiGAL80[ts]/UAS-pten[RNAi]*
S	*w*; Rab30-YFP/Rab30-YFP; fkhGAL4, ubiGAL80[ts]/UAS-pi3k92E[RNAi]*
T	*w*; UAS-crb[RNAi], Rab30-YFP/Rab30-YFP; fkhGAL4, ubiGAL80[ts]/UAS-pi3k92E[RNAi]*
Figure 6—figure supplement 1	
A	*w*;; Rab11-YFP, fkhGAL4, ubiGAL80[ts]/Rab11-YFP*
B	*w*;; Rab11-YFP, fkhGAL4, ubiGAL80[ts]/Rab11-YFP, UAS-pten2*
C	*w*; Rab30-YFP/Rab30-YFP; fkhGAL4, ubiGAL80[ts]/+*
D	*w*; Rab30-YFP/Rab30-YFP; fkhGAL4, ubiGAL80[ts]/UAS-pten2*

Table 3. List of antibodies and probes employed.

	Dilution	Fixation	Source
DAPI	1:200000	FA	Invitrogen Cat. D1306
Phalloidin Alexa Flour 488, 555	1:2000	FA	Invitrogen Cat. A12379, A34055
Alexa Flour 488-, 568- and 647 -conjugated	1:1000 - 1:2000		Invitrogen
Mouse antibodies			
Anti-α-Spectrin	1:100	MeOH	DSHB 3A9
Anti-Coracle	1:200	MeOH	DSHB C566.9
Anti-Disc large	1:500	MeOH	DSHB 4F3
Anti-FasIII	1:4	MeOH	DSHB 7G10
Anti-αTubulin	1:2000	MeOH/Acetone	MPI-CBG Antibody facility, P. Keller
Rabbit antibodies			
Anti-aPKC (C-20)	1:500	MeOH	Santa Cruz Biotechnology Cat. sc-216-G
Anti-Bazooka	1:200	MeOH	kindly provided by A. Wodarz (***Wodarz et al., 1999***)
Anti-Stardust	1:2000	MeOH	(***Berger et al., 2007***)
Anti-Cadherin99C	1:250	FA	kindly provided by D. Godt (***Glowinski et al., 2014***)
Anti-GFP	1:1000	FA	Invitrogen A-11122
Anti-Sinuous	1:8000	MeOH	kindly provided by G.J. Beitel (***Wu et al., 2004***)
Anti-β_HSpectrin	1:5000	MeOH	kindly provided by G. Thomas (***Thomas and Williams, 1999***)
Anti-KuneKune	1:5000	MeOH	kindly provided by M. Furuse (***Nelson et al., 2010***)
Anti-Phospho-Ezrin (Moesin)	1:500	FA	Cell Signaling Technology Cat. 3141
Anti-Moesin (Q480)	1:400	FA	Cell Signaling Technology Cat. 3150
Anti-MyosinV	1:2000	MeOH	(***Pocha et al., 2011a***)
Anti-*D*Patj	1:1000	FA	(***Richard et al., 2006a***)
Rat antibodies			
Anti-Yurt	1:500	MeOH	kindly provided by U. Tepass (***Laprise et al., 2006***)
Anti-Stardust	1:2000	FA	(***Berger et al., 2007***)
Chicken antibodies			
Anti-GFP	1:100	FA	Abcam Cat. Ab13970
Guinea pig antibodies			
Anti-Crumbs 2.8	1:500	MeOH	(***Richard et al., 2006a***)
Anti-Par6	1:500	FA	kindly provided by A. Wodarz (***Shahab et al., 2015***)
DSHB - Developmental Studies Hybridoma Bank (Iowa city, Iowa, USA)			
Invitrogen, Molecular Probes (Eugene, Oregon, USA)			
Santa Cruz Biotechnology, Inc (Dallas, Texas, USA)			
Cell Signaling Technology (Danvers, Massachusetts, USA)			
Abcam plc (Cambridge, United Kingdom)			

plugin in Fiji Software. The labeled images obtained were subsequently analyzed using the 3D Object Counter plugin to obtain the values for surface and volume.

Transmission electron microscopy (TEM) and high-pressure freezing (HPF)

Control and experimental larvae were collected as described above. Salivary glands were dissected on ice in 1xPBS and fixed with 2.5% glutaraldehyde, 2% paraformaldehyde in 1xPBS for 2 hr at RT, washed with 1xPBS, 3 times for 5 min at RT, post-fixed with 1% osmium tetroxide, 1.5% Potassium ferricyanide in water for 1 hr at 4˚C. Samples were dehydrated in serial steps (30%, 50%, 70%, 90%, and 100%) Ethanol (EtOH) 5 min/step at 4˚C, infiltrated with 1:3 EPON LX112/EtOH for 1 hr, 1:1 EPON LX112/EtOH for 1 hr, 3:1 EPON LX112/EtOH 1 hr, pure EPON LX112 overnight, and pure EPON LX112 for 2 hr. The salivary glands were embedded in rubber mold and polymerized for 24 hr at 60˚C. 70 nm cross sections were obtained using an ultramicrotome and were picked up with formvar coated copper slot grid. Grids were stained with 2% uranyl acetate in water for 10 min and lead citrate for 5 min at RT.

For HPF, salivary glands were dissected on ice in 1xPBS and frozen afterwards using a Leica ICE high pressure freezer (Leica Microsystems, Germany). Media of frozen samples was substituted with a cocktail containing 0.1% uranyl acetate and 4% water in acetone at −90˚C. Samples were transferred into ethanol at −25˚C. Then, samples were embedded into a Lowicryl HM20 resin (Polysciences, Inc, Germany) followed by UV polymerization at the same temperature. Semi-thin sections (300 nm) were cut and contrasted as described above for chemically fixed samples.

To quantify the density of microvilli, five lines, 1 µm in length each, were drawn adjacent to the apical membrane and distributed over the span of a cell. Five identical lines were drawn parallel to the first ones but at exactly 1 µm away from the first group, that is 1 µm above the apical membrane. The microvilli crossed by these lines were counted and the average per cell is presented in the ***Figure 2M***.

Image acquisition was done using a Tecnai 12 (FEI, Thermo Fisher Scientific) with a standard single tilt holder with a TVIPS TemCam F214A (TVIPS, Gauting, Germany) digital camera at 440x for an overview of the whole salivary gland cross section, and 1200x for single-cell overview and 13000x for subcellular structures. Images are representative of 3 independent experiments, at least 3–5 different salivary glands were analyzed per genotype.

Dextran-permeability assay, lysosomal activity and treatment with inhibitors

For Dextran permeability assays we adapted the method from ***Lamb et al. (1998)***. Briefly, the salivary glands were dissected as described above, and incubated 15 min at RT in Grace's medium containing 40 µg/ml Dextran-Rhodamine B 10,000 MW (Molecular Probes D1824), and immediately imaged after incubation. For lysosomal activity analysis, the salivary glands were incubated 30 min at RT in Grace's medium containing 150 nM LysoTracker Red DND-99 (Molecular Probes L7528), and immediately imaged after incubation. For the inhibition of PTEN, the salivary glands were incubated 30 min at RT with 10 µM VO-OHpic trihydrate (Santa Cruz Biotechnology sc-216061). DMSO was used as vehicle and its final concentration was 0.25 µL/mL in Grace's medium. Images are representative of 3 independent experiments, with at least three technical replicates in each experiment.

Western blot

Control and experimental larvae were collected as described above. At least 15 whole salivary glands were dissected per genotype on ice in 1xPBS, immediately frozen in liquid nitrogen and kept at −80˚C. For protein extraction, the glands were homogenized with a plastic pestle in 1% PBT lysis buffer and pelleted at 20,000 × g for 5 min at 4˚C. Protein content from recovered supernatants was measured using BCA (manufacturer protocol, Invitrogen) and equal protein amounts were loaded per lane and separated on 12.5% SDS-PAGEs. Proteins were transferred to nitrocellulose membranes, blocked with 5% milk powder in 0.1% Triton X-100 in 1xPBS and blots were probed for GFP (rabbit anti-GFP 1:2000, Molecular Probes A11122), Crb (rat anti-Crb2.8 1:1000, see supplementary ***Table 3***) and Tubulin (mouse anti-αTubulin 1:1000, see supplementary ***Table 3***).

Food intake assay and puparium formation rate

For the food intake assay we adapted a protocol reported by ***Deshpande et al. (2014)***. Briefly, eggs from the appropriate genotypes were collected overnight on apple juice agar plates and transferred into normal food containing blue bromophenol (500 mg/L). As indicated in ***Figure 8***, after 2 days of incubation at 29˚C, larvae were briefly rinsed in iced cold PBS to remove attached food. Then, for each replica, 60 larvae were manually transferred into an Eppendorf tube containing 220 µL PBS + 0.1% Triton X-100 (PBST), and frozen immediately in dry ice. The samples were thawed and homogenized with a rotor pestle, centrifuged at 10 000 x g at 4˚C for 10 min. The supernatant was diluted 1:2 into PBST for absorbance measurement at 680 nm. The standard curve was made by diluting 200 µL of liquefied bromophenol-containing food into 800 µL PBST, mixed in a ThermoMixer (Eppendorf, Germany) block at 900 rpm 80˚C for 30 min, followed by centrifugation at 10 000 x g. The supernatant was serially diluted in PBST and the serial dilutions measured at 680 nm using a FLUOstar Omega (MBG Labtech, Germany).

For the assessment of the pupariation rate, eggs from the appropriate genotypes were collected for one hour on apple juice agar plates. Afterwards, 20 eggs were transferred to a new apple juice plate containing fresh yeast paste. To score the puparium formation, the plates with the embryos were incubated at 29˚C for 72 hr and afterwards were assessed every 3 hr (excluding the overnight period). All newly appearing pupae were counted until all larvae had pupariated. To determine the puparium formation rate, the number of newly formed pupae at a given time point are divided by the total number of pupated animals. For the graphs of larval development speed (***Figure 1H***, ***Figure 1—figure supplement 1KK***, ***Figure 6W***) percentages were added up for the consecutive time points (also see source data).

Statistical analyses

All statistical analyses were performed using GraphPad Prism 8. Statistical significance was calculated in unpaired *t*-test or a one-way analysis of variance (ANOVA) followed by a Dunnett's multiple-comparison when experimental groups are specifically compared only to control conditions, or a Tukey's multiple comparison test when all groups are compared to each other. *P* values are indicated in each corresponding graph.

Acknowledgements

We thank S Eaton, A Wodarz, GJ Beitel, G Thomas, M Furuse, and U Tepass for kindly providing antibodies for our studies. We thank the MPI-CBG facilities: Patrick Keller, antibody facility, for antibody production; Light Microscopy Facility, in particular Jan Peychl and Sebastian Bundschuh, for microscopy guidance; the Electron Microscopy Facility, in particular Michaela Wilsch-Bräuninger and Tobias Fürstenhaupt, for discussions and troubleshooting. Stocks were obtained from the Bloomington *Drosophila* Stock Center (NIH P40OD018537) and from the Vienna *Drosophila* Resource Center. Antibodies were obtained from the Developmental Studies Hybridoma Bank, created by the NICHD of the NIH and maintained at The University of Iowa, Department of Biology, Iowa City, IA 52242. We thank the fly keepers Sven Ssykor, Cornelia Mass and Stefan Wernicke for excellent care of our flies. MB grants BR5490/2, BR5490/3. The work was supported by the Max-Planck Society and the Deutsche Forschungsgemeinschaft. (DFG)

Additional information

Competing interests

Elisabeth Knust: Reviewing editor, *eLife*. The other authors declare that no competing interests exist.

Funding

Funder	Grant reference number	Author
Max-Planck-Gesellschaft		Johanna Lattner Weihua Leng Elisabeth Knust David Flores-Benitez
Deutsche Forschungsgemeinschaft	BR5490/2	Marko Brankatschk
Deutsche Forschungsgemeinschaft	BR5490/3	Marko Brankatschk

The funders had no role in study design, data collection and interpretation, or the decision to submit the work for publication.

Author contributions

Johanna Lattner, Conceptualization, Formal analysis, Investigation, Visualization, Methodology, Writing—original draft, Writing—review and editing; Weihua Leng, Investigation; Elisabeth Knust, Conceptualization, Resources, Funding acquisition, Writing—review and editing; Marko Brankatschk, Conceptualization, Resources, Funding acquisition, Investigation, Methodology, Writing—original draft, Project administration, Writing—review and editing; David Flores-Benitez, Conceptualization, Data curation, Formal analysis, Supervision, Investigation, Visualization, Methodology, Writing—original draft, Project administration, Writing—review and editing

Author ORCIDs

Johanna Lattner http://orcid.org/0000-0003-3421-9134
Elisabeth Knust http://orcid.org/0000-0002-2732-9135
Marko Brankatschk https://orcid.org/0000-0001-5274-4552
David Flores-Benitez https://orcid.org/0000-0001-8244-9335

Decision letter and Author response

Decision letter https://doi.org/10.7554/eLife.50900.sa1
Author response https://doi.org/10.7554/eLife.50900.sa2

Additional files

Supplementary files

- Transparent reporting form

Data availability

We provide as source data files all the data used for statistical analyses and generation of all graphs. These files are sorted according to the figure and the corresponding figure supplements, which correspond to Figure 1 and its supplements, Figure 2, Figure 3 and its supplements, Figure 5 and its supplements, and Figure 6.

References

Antonescu CN, Aguet F, Danuser G, Schmid SL. 2011. Phosphatidylinositol-(4,5)-bisphosphate regulates clathrin-coated pit initiation, stabilization, and size. *Molecular Biology of the Cell* **22**:2588–2600. DOI: https://doi.org/10.1091/mbc.e11-04-0362, PMID: 21613550

Bachmann A, Schneider M, Theilenberg E, Grawe F, Knust E. 2001. Drosophila stardust is a partner of crumbs in the control of epithelial cell polarity. *Nature* **414**:638–643. DOI: https://doi.org/10.1038/414638a, PMID: 11740560

Baines AJ, Lu H-C, Bennett PM. 2014. The protein 4.1 family: hub proteins in animals for organizing membrane proteins. *Biochimica Et Biophysica Acta (BBA) - Biomembranes* **1838**:605–619. DOI: https://doi.org/10.1016/j.bbamem.2013.05.030

Bajur AT, Iyer KV, Knust E. 2019. Cytocortex-dependent dynamics of *Drosophila* crumbs controls junctional stability and tension during germ band retraction. *Journal of Cell Science* **132**:jcs228338. DOI: https://doi.org/10.1242/jcs.228338, PMID: 31300472

Balakrishnan SS, Basu U, Raghu P. 2015. Phosphoinositide signalling in Drosophila. *Biochimica Et Biophysica Acta (BBA) - Molecular and Cell Biology of Lipids* **1851**:770–784. DOI: https://doi.org/10.1016/j.bbalip.2014.10.010

Balla T, Varnai P, Tian Y, Smith RD. 1998. Signaling events activated by angiotensin II receptors: what Goes before and after the calcium signals. *Endocrine Research* **24**:335–344. DOI: https://doi.org/10.3109/07435809809032613, PMID: 9888505

Barroso-González J, Machado JD, García-Expósito L, Valenzuela-Fernández A. 2009. Moesin regulates the trafficking of nascent clathrin-coated vesicles. *Journal of Biological Chemistry* **284**:2419–2434. DOI: https://doi.org/10.1074/jbc.M805311200, PMID: 19047065

Bätz T, Förster D, Luschnig S. 2014. The transmembrane protein macroglobulin complement-related is essential for septate junction formation and epithelial barrier function in Drosophila. *Development* **141**:899–908. DOI: https://doi.org/10.1242/dev.102160, PMID: 24496626

Beck KA, Nelson WJ. 1998. A spectrin membrane skeleton of the golgi complex. *Biochimica Et Biophysica Acta (BBA) - Molecular Cell Research* **1404**:153–160. DOI: https://doi.org/10.1016/S0167-4889(98)00054-8

Beckendorf SK, Kafatos FC. 1976. Differentiation in the salivary glands of Drosophila Melanogaster: characterization of the glue proteins and their developmental appearance. *Cell* **9**:365–373. DOI: https://doi.org/10.1016/0092-8674(76)90081-7, PMID: 825230

Bennett V, Baines AJ. 2001. Spectrin and ankyrin-based pathways: metazoan inventions for integrating cells into tissues. *Physiological Reviews* **81**:1353–1392. DOI: https://doi.org/10.1152/physrev.2001.81.3.1353, PMID: 11427698

Bennett V, Healy J. 2009. Membrane domains based on ankyrin and spectrin associated with cell-cell interactions. *Cold Spring Harbor Perspectives in Biology* **1**:a003012. DOI: https://doi.org/10.1101/cshperspect.a003012, PMID: 20457566

Berger S, Bulgakova NA, Grawe F, Johnson K, Knust E. 2007. Unraveling the genetic complexity of Drosophila *stardust* during photoreceptor morphogenesis and prevention of light-induced degeneration. *Genetics* **176**:2189–2200. DOI: https://doi.org/10.1534/genetics.107.071449, PMID: 17603117

Blasky AJ, Mangan A, Prekeris R. 2015. Polarized protein transport and lumen formation during epithelial tissue morphogenesis. *Annual Review of Cell and Developmental Biology* **31**:575–591. DOI: https://doi.org/10.1146/annurev-cellbio-100814-125323, PMID: 26359775

Brankatschk M, Eaton S. 2010. Lipoprotein particles cross the blood-brain barrier in Drosophila. *Journal of Neuroscience* **30**:10441–10447. DOI: https://doi.org/10.1523/JNEUROSCI.5943-09.2010, PMID: 20685986

Bronfman FC, Escudero CA, Weis J, Kruttgen A. 2007. Endosomal transport of neurotrophins: roles in signaling and neurodegenerative diseases. *Developmental Neurobiology* **67**:1183–1203. DOI: https://doi.org/10.1002/dneu.20513, PMID: 17514710

Bruurs LJM, van der Net MC, Zwakenberg S, Rosendahl Huber AKM, Post A, Zwartkruis FJ, Bos JL. 2018. The phosphatase PTPL1 is required for PTEN-Mediated regulation of apical membrane size. *Molecular and Cellular Biology* **38**:e00102-18–e00118. DOI: https://doi.org/10.1128/MCB.00102-18, PMID: 29581186

Bulgakova NA, Kempkens O, Knust E. 2008. Multiple domains of stardust differentially mediate localisation of the Crumbs-Stardust complex during photoreceptor development in Drosophila. *Journal of Cell Science* **121**:2018–2026. DOI: https://doi.org/10.1242/jcs.031088, PMID: 18495840

Bulgakova NA, Knust E. 2009. The crumbs complex: from epithelial-cell polarity to retinal degeneration. *Journal of Cell Science* **122**:2587–2596. DOI: https://doi.org/10.1242/jcs.023648, PMID: 19625503

Cereijido M, Contreras RG, Shoshani L. 2004. Cell adhesion, polarity, and epithelia in the dawn of metazoans. *Physiological Reviews* **84**:1229–1262. DOI: https://doi.org/10.1152/physrev.00001.2004, PMID: 15383651

Charrier LE, Loie E, Laprise P. 2016. Mouse Crumbs3 sustains epithelial tissue morphogenesis in vivo. *Scientific Reports* **5**:17699. DOI: https://doi.org/10.1038/srep17699

Chartier FJ, Hardy ÉJ, Laprise P. 2012. Crumbs limits oxidase-dependent signaling to maintain epithelial integrity and prevent photoreceptor cell death. *The Journal of Cell Biology* **198**:991–998. DOI: https://doi.org/10.1083/jcb.201203083, PMID: 22965909

Chavrier P, Parton RG, Hauri HP, Simons K, Zerial M. 1990. Localization of low molecular weight GTP binding proteins to exocytic and endocytic compartments. *Cell* **62**:317–329. DOI: https://doi.org/10.1016/0092-8674(90)90369-P, PMID: 2115402

Chung S, Hanlon CD, Andrew DJ. 2014. Building and specializing epithelial tubular organs: the Drosophila salivary gland as a model system for revealing how epithelial organs are specified, form and specialize. *Wiley Interdisciplinary Reviews: Developmental Biology* **3**:281–300. DOI: https://doi.org/10.1002/wdev.140, PMID: 25208491

Chung S, Andrew DJ. 2014. Cadherin 99C regulates apical expansion and cell rearrangement during epithelial tube elongation. *Development* **141**:1950–1960. DOI: https://doi.org/10.1242/dev.104166

Claret S, Jouette J, Benoit B, Legent K, Guichet A. 2014. PI(4,5)P2 produced by the PI4P5K SKTL controls apical size by tethering PAR-3 in Drosophila epithelial cells. *Current Biology* **24**:1071–1079. DOI: https://doi.org/10.1016/j.cub.2014.03.056, PMID: 24768049

Croisé P, Estay-Ahumada C, Gasman S, Ory S. 2014. Rho GTPases, Phosphoinositides, and actin: a tripartite framework for efficient vesicular trafficking. *Small GTPases* **5**:e29469. DOI: https://doi.org/10.4161/sgtp.29469, PMID: 24914539

Csizmadia T, Lőrincz P, Hegedűs K, Széplaki S, Lőw P, Juhász G. 2018. Molecular mechanisms of developmentally programmed crinophagy in *Drosophila*. *The Journal of Cell Biology* **217**:361–374. DOI: https://doi.org/10.1083/jcb.201702145, PMID: 29066608

Das S, Knust E. 2018. A dual role of the extracellular domain of *Drosophila* crumbs for morphogenesis of the embryonic neuroectoderm. *Biology Open* **7**:bio031435. DOI: https://doi.org/10.1242/bio.031435, PMID: 29374056

de Renzis S, Sönnichsen B, Zerial M. 2002. Divalent rab effectors regulate the sub-compartmental organization and sorting of early endosomes. *Nature Cell Biology* **4**:124–133. DOI: https://doi.org/10.1038/ncb744, PMID: 11788822

Deshpande SA, Carvalho GB, Amador A, Phillips AM, Hoxha S, Lizotte KJ, Ja WW. 2014. Quantifying Drosophila food intake: comparative analysis of current methodology. *Nature Methods* **11**:535–540. DOI: https://doi.org/10.1038/nmeth.2899, PMID: 24681694

Devergne O, Tsung K, Barcelo G, Schüpbach T. 2014. Polarized deposition of basement membrane proteins depends on phosphatidylinositol synthase and the levels of phosphatidylinositol 4,5-bisphosphate. *PNAS* **111**:7689–7694. DOI: https://doi.org/10.1073/pnas.1407351111, PMID: 24828534

Devergne O, Sun GH, Schüpbach T. 2017. Stratum, a homolog of the human GEF Mss4, partnered with Rab8, controls the basal restriction of basement membrane proteins in epithelial cells. *Cell Reports* **18**:1831–1839. DOI: https://doi.org/10.1016/j.celrep.2017.02.002, PMID: 28228250

Di Paolo G, De Camilli P. 2006. Phosphoinositides in cell regulation and membrane dynamics. *Nature* **443**:651–657. DOI: https://doi.org/10.1038/nature05185, PMID: 17035995

Dong B, Kakihara K, Otani T, Wada H, Hayashi S. 2013. Rab9 and retromer regulate retrograde trafficking of luminal protein required for epithelial tube length control. *Nature Communications* **4**:1358. DOI: https://doi.org/10.1038/ncomms2347, PMID: 23322046

Dong B, Miao G, Hayashi S. 2014. A fat body-derived apical extracellular matrix enzyme is transported to the tracheal lumen and is required for tube morphogenesis in Drosophila. *Development* **141**:4104–4109. DOI: https://doi.org/10.1242/dev.109975, PMID: 25336738

Dunst S, Kazimiers T, von Zadow F, Jambor H, Sagner A, Brankatschk B, Mahmoud A, Spannl S, Tomancak P, Eaton S, Brankatschk M. 2015. Endogenously tagged rab proteins: a resource to study membrane trafficking in Drosophila. *Developmental Cell* **33**:351–365. DOI: https://doi.org/10.1016/j.devcel.2015.03.022, PMID: 25942626

Eaton S, Martin-Belmonte F. 2014. Cargo sorting in the endocytic pathway: a key regulator of cell polarity and tissue dynamics. *Cold Spring Harbor Perspectives in Biology* **6**:a016899. DOI: https://doi.org/10.1101/cshperspect.a016899, PMID: 25125399

Elliott DA, Brand AH. 2008. The GAL4 system : a versatile system for the expression of genes. *Methods in Molecular Biology* **420**:79–95. DOI: https://doi.org/10.1007/978-1-59745-583-1_5, PMID: 18641942

Fehon RG, McClatchey AI, Bretscher A. 2010. Organizing the cell cortex: the role of ERM proteins. *Nature Reviews Molecular Cell Biology* **11**:276–287. DOI: https://doi.org/10.1038/nrm2866, PMID: 20308985

Feng Q, Bonder EM, Engevik AC, Zhang L, Tyska MJ, Goldenring JR, Gao N. 2017. Disruption of Rab8a and Rab11a causes formation of basolateral microvilli in neonatal enteropathy. *Journal of Cell Science* **130**:2491–2505. DOI: https://doi.org/10.1242/jcs.201897, PMID: 28596241

Fiévet B, Louvard D, Arpin M. 2007. ERM proteins in epithelial cell organization and functions. *Biochimica Et Biophysica Acta (BBA) - Molecular Cell Research* **1773**:653–660. DOI: https://doi.org/10.1016/j.bbamcr.2006.06.013

Figard L, Sokac AM. 2011. Imaging cell shape change in living Drosophila embryos. *Journal of Visualized Experiments : JoVE*:2503. DOI: https://doi.org/10.3791/2503, PMID: 21490577

Firmino J, Tinevez JY, Knust E. 2013. Crumbs affects protein dynamics in anterior regions of the developing Drosophila embryo. *PLOS ONE* **8**:e58839. DOI: https://doi.org/10.1371/journal.pone.0058839, PMID: 23555600

Flores-Benitez D, Knust E. 2015. Crumbs is an essential regulator of cytoskeletal dynamics and cell-cell adhesion during dorsal closure in Drosophila. *eLife* **4**:e07398. DOI: https://doi.org/10.7554/eLife.07398, PMID: 26544546

Flores-Benitez D, Knust E. 2016. Dynamics of epithelial cell polarity in Drosophila: how to regulate the regulators? *Current Opinion in Cell Biology* **42**:13–21. DOI: https://doi.org/10.1016/j.ceb.2016.03.018, PMID: 27085003

Förster D, Armbruster K, Luschnig S. 2010. Sec24-dependent secretion drives cell-autonomous expansion of tracheal tubes in Drosophila. *Current Biology* **20**:62–68. DOI: https://doi.org/10.1016/j.cub.2009.11.062, PMID: 20045324

Fraenkel G, Brookes VJ. 1953. The process by which the puparia of many species of flies become fixed to a substrate. *The Biological Bulletin* **105**:442–449. DOI: https://doi.org/10.2307/1538461

Gao X, Neufeld TP, Pan D. 2000. Drosophila PTEN regulates cell growth and proliferation through PI3K-dependent and -independent pathways. *Developmental Biology* **221**:404–418. DOI: https://doi.org/10.1006/dbio.2000.9680, PMID: 10790335

Gassama-Diagne A, Yu W, ter Beest M, Martin-Belmonte F, Kierbel A, Engel J, Mostov K. 2006. Phosphatidylinositol-3,4,5-trisphosphate regulates the formation of the basolateral plasma membrane in epithelial cells. *Nature Cell Biology* **8**:963–970. DOI: https://doi.org/10.1038/ncb1461, PMID: 16921364

Genevet A, Tapon N. 2011. The hippo pathway and apico-basal cell polarity. *Biochemical Journal* **436**:213–224. DOI: https://doi.org/10.1042/BJ20110217, PMID: 21568941

Gervais L, Claret S, Januschke J, Roth S, Guichet A. 2008. PIP5K-dependent production of PIP2 sustains microtubule organization to establish polarized transport in the Drosophila oocyte. *Development* **135**:3829–3838. DOI: https://doi.org/10.1242/dev.029009, PMID: 18948416

Glowinski C, Liu R-HS, Chen X, Darabie A, Godt D. 2014. Myosin VIIA regulates microvillus morphogenesis and interacts with cadherin Cad99C in Drosophila oogenesis. *Journal of Cell Science* **127**:4821–4832. DOI: https://doi.org/10.1242/jcs.099242

Goberdhan DC, Paricio N, Goodman EC, Mlodzik M, Wilson C. 1999. Drosophila tumor suppressor PTEN controls cell size and number by antagonizing the chico/PI3-kinase signaling pathway. *Genes & Development* **13**:3244–3258. DOI: https://doi.org/10.1101/gad.13.24.3244, PMID: 10617573

Gong L-W, Di Paolo G, Diaz E, Cestra G, Diaz M-E, Lindau M, De Camilli P, Toomre D. 2005. Phosphatidylinositol phosphate kinase type I regulates dynamics of large dense-core vesicle fusion. *PNAS* **102**:5204–5209. DOI: https://doi.org/10.1073/pnas.0501412102

Goody RS, Rak A, Alexandrov K. 2005. The structural and mechanistic basis for recycling of rab proteins between membrane compartments. *Cellular and Molecular Life Sciences* **62**:1657–1670. DOI: https://doi.org/10.1007/s00018-005-4486-8, PMID: 15924270

Gorbenko O, Stambolic V. 2016. PTEN at 18: still growing. *Methods in Molecular Biology* **1388**:13–19. DOI: https://doi.org/10.1007/978-1-4939-3299-3_2, PMID: 27033067

Grawe F, Wodarz A, Lee B, Knust E, Skaer H. 1996. The Drosophila genes crumbs and stardust are involved in the biogenesis of adherens junctions. *Development* **122**:951–959. PMID: 8631272

Gregg TG, McCrate A, Reveal G, Hall S, Rypstra AL. 1990. Insectivory and social digestion in Drosophila. *Biochemical Genetics* **28**:197–207. DOI: https://doi.org/10.1007/BF00561337, PMID: 2383246

Grosshans BL, Ortiz D, Novick P. 2006. Rabs and their effectors: achieving specificity in membrane traffic. *PNAS* **103**:11821–11827. DOI: https://doi.org/10.1073/pnas.0601617103, PMID: 16882731

Harlan JE, Yoon HS, Hajduk PJ, Fesik SW. 1995. Structural characterization of the interaction between a pleckstrin homology domain and phosphatidylinositol 4,5-bisphosphate. *Biochemistry* **34**:9859–9864. DOI: https://doi.org/10.1021/bi00031a006, PMID: 7632686

Henderson KD, Andrew DJ. 2000. Regulation and function of scr, exd, and hth in the Drosophila salivary gland. *Developmental Biology* **217**:362–374. DOI: https://doi.org/10.1006/dbio.1999.9560, PMID: 10625560

Herranz H, Stamataki E, Feiguin F, Milán M. 2006. Self-refinement of notch activity through the transmembrane protein crumbs: modulation of gamma-secretase activity. *EMBO Reports* **7**:297–302. DOI: https://doi.org/10.1038/sj.embor.7400617, PMID: 16440003

Holleran EA, Holzbaur EL. 1998. Speculating about spectrin: new insights into the Golgi-associated cytoskeleton. *Trends in Cell Biology* **8**:26–29. DOI: https://doi.org/10.1016/S0962-8924(97)01195-1, PMID: 9695804

Holthuis JC, Menon AK. 2014. Lipid landscapes and pipelines in membrane homeostasis. *Nature* **510**:48–57. DOI: https://doi.org/10.1038/nature13474, PMID: 24899304

Homma Y, Kinoshita R, Kuchitsu Y, Wawro PS, Marubashi S, Oguchi ME, Ishida M, Fujita N, Fukuda M. 2019. Comprehensive knockout analysis of the rab family GTPases in epithelial cells. *The Journal of Cell Biology* **218**:2035–2050. DOI: https://doi.org/10.1083/jcb.201810134

Hong Y, Stronach B, Perrimon N, Jan LY, Jan YN. 2001. Drosophila stardust interacts with crumbs to control polarity of epithelia but not neuroblasts. *Nature* **414**:634–638. DOI: https://doi.org/10.1038/414634a, PMID: 11740559

Huang H, Potter CJ, Tao W, Li DM, Brogiolo W, Hafen E, Sun H, Xu T. 1999. PTEN affects cell size, cell proliferation and apoptosis during Drosophila eye development. *Development* **126**:5365–5372. PMID: 10556061

Huang J, Zhou W, Dong W, Watson AM, Hong Y. 2009. From the cover: directed, efficient, and versatile modifications of the Drosophila genome by genomic engineering. *PNAS* **106**:8284–8289. DOI: https://doi.org/10.1073/pnas.0900641106, PMID: 19429710

Iruela-Arispe ML, Beitel GJ. 2013. Tubulogenesis. *Development* **140**:2851–2855. DOI: https://doi.org/10.1242/dev.070680, PMID: 23821032

Ivanova ME, Fletcher GC, O'Reilly N, Purkiss AG, Thompson BJ, McDonald NQ. 2015. Structures of the human Pals1 PDZ domain with and without ligand suggest gated access of crb to the PDZ peptide-binding groove. *Acta Crystallographica Section D Biological Crystallography* **71**:555–564. DOI: https://doi.org/10.1107/S139900471402776X, PMID: 25760605

Iwanami N, Nakamura Y, Satoh T, Liu Z, Satoh AK. 2016. Rab6 is required for multiple apical transport pathways but not the basolateral transport pathway in Drosophila photoreceptors. *PLOS Genetics* **12**:e1005828. DOI: https://doi.org/10.1371/journal.pgen.1005828, PMID: 26890939

Izaddoost S, Nam SC, Bhat MA, Bellen HJ, Choi KW. 2002. Drosophila crumbs is a positional cue in photoreceptor adherens junctions and rhabdomeres. *Nature* **416**:178–183. DOI: https://doi.org/10.1038/nature720, PMID: 11850624

Jaźwińska A, Ribeiro C, Affolter M. 2003. Epithelial tube morphogenesis during Drosophila tracheal development requires piopio, a luminal ZP protein. *Nature Cell Biology* **5**:895–901. DOI: https://doi.org/10.1038/ncb1049, PMID: 12973360

Johnson K, Grawe F, Grzeschik N, Knust E. 2002. Drosophila crumbs is required to inhibit light-induced photoreceptor degeneration. *Current Biology* **12**:1675–1680. DOI: https://doi.org/10.1016/S0960-9822(02)01180-6, PMID: 12361571

Jost M, Simpson F, Kavran JM, Lemmon MA, Schmid SL. 1998. Phosphatidylinositol-4,5-bisphosphate is required for endocytic coated vesicle formation. *Current Biology* **8**:1399–1404. DOI: https://doi.org/10.1016/S0960-9822(98)00022-0, PMID: 9889104

Kakihara K, Shinmyozu K, Kato K, Wada H, Hayashi S. 2008. Conversion of plasma membrane topology during epithelial tube connection requires Arf-like 3 small GTPase in Drosophila. *Mechanisms of Development* **125**: 325–336. DOI: https://doi.org/10.1016/j.mod.2007.10.012, PMID: 18083504

Kang Q, Wang T, Zhang H, Mohandas N, An X. 2009. A Golgi-associated protein 4.1B variant is required for assimilation of proteins in the membrane. *Journal of Cell Science* **122**:1091–1099. DOI: https://doi.org/10.1242/jcs.039644

Karagiosis SA, Ready DF. 2004. Moesin contributes an essential structural role in Drosophila photoreceptor morphogenesis. *Development* **131**:725–732. DOI: https://doi.org/10.1242/dev.00976, PMID: 14724125

Kelly EE, Giordano F, Horgan CP, Jollivet F, Raposo G, McCaffrey MW. 2012. Rab30 is required for the morphological integrity of the golgi apparatus. *Biology of the Cell* **104**:84–101. DOI: https://doi.org/10.1111/boc.201100080, PMID: 22188167

Kempkens O, Médina E, Fernandez-Ballester G, Ozüyaman S, Le Bivic A, Serrano L, Knust E. 2006. Computer modelling in combination with in vitro studies reveals similar binding affinities of Drosophila Crumbs for the PDZ domains of Stardust and DmPar-6. *European Journal of Cell Biology* **85**:753–767. DOI: https://doi.org/10.1016/j.ejcb.2006.03.003

Kerman BE, Cheshire AM, Myat MM, Andrew DJ. 2008. Ribbon modulates apical membrane during tube elongation through crumbs and moesin. *Developmental Biology* **320**:278–288. DOI: https://doi.org/10.1016/j.ydbio.2008.05.541, PMID: 18585700

Khanal I, Elbediwy A, Diaz de la Loza MC, Fletcher GC, Thompson BJ. 2016. Shot and patronin polarise microtubules to direct membrane traffic and biogenesis of microvilli in epithelia. *Journal of Cell Science* **129**: 2651–2659. DOI: https://doi.org/10.1242/jcs.189076, PMID: 27231092

Klebes A, Knust E. 2000. A conserved motif in crumbs is required for E-cadherin localisation and zonula adherens formation in Drosophila. *Current Biology* **10**:76–85. DOI: https://doi.org/10.1016/S0960-9822(99)00277-8, PMID: 10662667

Knirr S, Santel A, Renkawitz-Pohl R. 1997. Expression of the PI4P 5-kinase Drosophila homologue skittles in the germline suggests a role in spermatogenesis and oogenesis. *Development Genes and Evolution* **207**:127–130. DOI: https://doi.org/10.1007/s004270050099, PMID: 27747405

Knowles BC, Roland JT, Krishnan M, Tyska MJ, Lapierre LA, Dickman PS, Goldenring JR, Shub MD. 2014. Myosin vb uncoupling from RAB8A and RAB11A elicits microvillus inclusion disease. *Journal of Clinical Investigation* **124**:2947–2962. DOI: https://doi.org/10.1172/JCI71651, PMID: 24892806

Knowles BC, Weis VG, Yu S, Roland JT, Williams JA, Alvarado GS, Lapierre LA, Shub MD, Gao N, Goldenring JR. 2015. Rab11a regulates syntaxin 3 localization and microvillus assembly in enterocytes. *Journal of Cell Science* **128**:1617–1626. DOI: https://doi.org/10.1242/jcs.163303, PMID: 25673875

Knust E, Bossinger O. 2002. Composition and formation of intercellular junctions in epithelial cells. *Science* **298**: 1955–1959. DOI: https://doi.org/10.1126/science.1072161, PMID: 12471248

Kodani M. 1948. The protein of the salivary gland secretion in Drosophila. *PNAS* **34**:131–135. DOI: https://doi.org/10.1073/pnas.34.4.131, PMID: 16588792

Korayem AM, Fabbri M, Takahashi K, Scherfer C, Lindgren M, Schmidt O, Ueda R, Dushay MS, Theopold U. 2004. A Drosophila salivary gland mucin is also expressed in immune tissues: evidence for a function in coagulation and the entrapment of Bacteria. *Insect Biochemistry and Molecular Biology* **34**:1297–1304. DOI: https://doi.org/10.1016/j.ibmb.2004.09.001, PMID: 15544943

Korge G. 1977. Larval saliva in Drosophila Melanogaster: production, composition, and relationship to chromosome puffs. *Developmental Biology* **58**:339–355. DOI: https://doi.org/10.1016/0012-1606(77)90096-3, PMID: 407116

Krauss J, López de Quinto S, Nüsslein-Volhard C, Ephrussi A. 2009. Myosin-V regulates oskar mRNA localization in the Drosophila oocyte. *Current Biology* **19**:1058–1063. DOI: https://doi.org/10.1016/j.cub.2009.04.062, PMID: 19481457

Krzewski K, Cullinane AR. 2013. Evidence for defective rab GTPase-dependent cargo traffic in immune disorders. *Experimental Cell Research* **319**:2360–2367. DOI: https://doi.org/10.1016/j.yexcr.2013.06.012, PMID: 23810987

Lamb RS, Ward RE, Schweizer L, Fehon RG. 1998. *Drosophila coracle*, a member of the protein 4.1 superfamily, has essential structural functions in the septate junctions and developmental functions in embryonic and adult epithelial cells. *Molecular Biology of the Cell* **9**:3505–3519. DOI: https://doi.org/10.1091/mbc.9.12.3505, PMID: 9843584

Laprise P, Beronja S, Silva-Gagliardi NF, Pellikka M, Jensen AM, McGlade CJ, Tepass U. 2006. The FERM protein yurt is a negative regulatory component of the crumbs complex that controls epithelial polarity and apical membrane size. *Developmental Cell* **11**:363–374. DOI: https://doi.org/10.1016/j.devcel.2006.06.001, PMID: 16950127

Laprise P, Paul SM, Boulanger J, Robbins RM, Beitel GJ, Tepass U. 2010. Epithelial polarity proteins regulate Drosophila tracheal tube size in parallel to the luminal matrix pathway. *Current Biology* **20**:55–61. DOI: https://doi.org/10.1016/j.cub.2009.11.017, PMID: 20022244

Lee H-G, Zarnescu DC, MacIver B, Thomas GH. 2010. The cell adhesion molecule roughest depends on Heavy-spectrin during eye morphogenesis in Drosophila. *Journal of Cell Science* **123**:277–285. DOI: https://doi.org/10.1242/jcs.056853

Lee T, Luo L. 1999. Mosaic analysis with a repressible cell marker for studies of gene function in neuronal morphogenesis. *Neuron* **22**:451–461. DOI: https://doi.org/10.1016/S0896-6273(00)80701-1, PMID: 10197526

Lee SK, Thomas GH. 2011. Rac1 modulation of the apical domain is negatively regulated by β (Heavy)-spectrin. *Mechanisms of Development* **128**:116–128. DOI: https://doi.org/10.1016/j.mod.2010.11.004, PMID: 21111816
Lemaitre B, Miguel-Aliaga I. 2013. The digestive tract of *Drosophila* Melanogaster. *Annual Review of Genetics* **47**:377–404. DOI: https://doi.org/10.1146/annurev-genet-111212-133343, PMID: 24016187
Lemmon MA, Ferguson KM, Abrams CS. 2002. Pleckstrin homology domains and the cytoskeleton. *FEBS Letters* **513**:71–76. DOI: https://doi.org/10.1016/S0014-5793(01)03243-4, PMID: 11911883
Li BX, Satoh AK, Ready DF. 2007. Myosin V, Rab11, and dRip11 direct apical secretion and cellular morphogenesis in developing *Drosophila* photoreceptors. *The Journal of Cell Biology* **177**:659–669. DOI: https://doi.org/10.1083/jcb.200610157, PMID: 17517962
Li Y, Wei Z, Yan Y, Wan Q, Du Q, Zhang M. 2014. Structure of crumbs tail in complex with the PALS1 PDZ-SH3-GK tandem reveals a highly specific assembly mechanism for the apical crumbs complex. *PNAS* **111**:17444–17449. DOI: https://doi.org/10.1073/pnas.1416515111, PMID: 25385611
Liem RK. 2016. Cytoskeletal integrators: the spectrin superfamily. *Cold Spring Harbor Perspectives in Biology* **8**: a018259. DOI: https://doi.org/10.1101/cshperspect.a018259, PMID: 27698030
Lindsay AJ, Jollivet F, Horgan CP, Khan AR, Raposo G, McCaffrey MW, Goud B. 2013. Identification and characterization of multiple novel Rab-myosin va interactions. *Molecular Biology of the Cell* **24**:3420–3434. DOI: https://doi.org/10.1091/mbc.e13-05-0236, PMID: 24006491
Ling C, Zheng Y, Yin F, Yu J, Huang J, Hong Y, Wu S, Pan D. 2010. The apical transmembrane protein crumbs functions as a tumor suppressor that regulates hippo signaling by binding to expanded. *PNAS* **107**:10532–10537. DOI: https://doi.org/10.1073/pnas.1004279107, PMID: 20498073
Loie E, Charrier LE, Sollier K, Masson JY, Laprise P. 2015. CRB3A controls the morphology and cohesion of Cancer cells through Ehm2/p114RhoGEF-Dependent signaling. *Molecular and Cellular Biology* **35**:3423–3435. DOI: https://doi.org/10.1128/MCB.00673-15, PMID: 26217016
Luschnig S, Bätz T, Armbruster K, Krasnow MA. 2006. Serpentine and vermiform encode matrix proteins with chitin binding and deacetylation domains that limit tracheal tube length in Drosophila. *Current Biology* **16**:186–194. DOI: https://doi.org/10.1016/j.cub.2005.11.072, PMID: 16431371
Maehama T, Kosaka N, Okahara F, Takeuchi K, Umeda M, Dixon JE, Kanaho Y. 2004. Suppression of a phosphatidylinositol 3-kinase signal by a specific spliced variant of Drosophila PTEN. *FEBS Letters* **565**:43–47. DOI: https://doi.org/10.1016/j.febslet.2004.03.074, PMID: 15135050
Mak LH, Vilar R, Woscholski R. 2010. Characterisation of the PTEN inhibitor VO-OHpic. *Journal of Chemical Biology* **3**:157–163. DOI: https://doi.org/10.1007/s12154-010-0041-7, PMID: 21643420
Martin-Belmonte F, Mostov K. 2007. Phosphoinositides control epithelial development. *Cell Cycle* **6**:1957–1961. DOI: https://doi.org/10.4161/cc.6.16.4583, PMID: 17712229
Maruyama R, Andrew DJ. 2012. Drosophila as a model for epithelial tube formation. *Developmental Dynamics* **241**:119–135. DOI: https://doi.org/10.1002/dvdy.22775, PMID: 22083894
Massarwa R, Schejter ED, Shilo BZ. 2009. Apical secretion in epithelial tubes of the Drosophila embryo is directed by the Formin-Family protein diaphanous. *Developmental Cell* **16**:877–888. DOI: https://doi.org/10.1016/j.devcel.2009.04.010, PMID: 19531358
Mayinger P. 2012. Phosphoinositides and vesicular membrane traffic. *Biochimica Et Biophysica Acta (BBA) - Molecular and Cell Biology of Lipids* **1821**:1104–1113. DOI: https://doi.org/10.1016/j.bbalip.2012.01.002
McClatchey AI. 2014. ERM proteins at a glance. *Journal of Cell Science* **127**:3199–3204. DOI: https://doi.org/10.1242/jcs.098343, PMID: 24951115
Médina E, Lemmers C, Lane-Guermonprez L, Le Bivic A. 2002a. Role of the crumbs complex in the regulation of junction formation in Drosophila and mammalian epithelial cells. *Biology of the Cell* **94**:305–313. DOI: https://doi.org/10.1016/S0248-4900(02)00004-7, PMID: 12500938
Médina E, Williams J, Klipfell E, Zarnescu D, Thomas G, Le Bivic A. 2002b. Crumbs interacts with moesin and beta(Heavy)-spectrin in the apical membrane skeleton of *Drosophila*. *The Journal of Cell Biology* **158**:941–951. DOI: https://doi.org/10.1083/jcb.200203080, PMID: 12213838
Miguel-Aliaga I, Jasper H, Lemaitre B. 2018. Anatomy and physiology of the digestive tract of *Drosophila melanogaster*. *Genetics* **210**:357–396. DOI: https://doi.org/10.1534/genetics.118.300224, PMID: 30287514
Milosevic I, Sørensen JB, Lang T, Krauss M, Nagy G, Haucke V, Jahn R, Neher E. 2005. Plasmalemmal phosphatidylinositol-4,5-bisphosphate level regulates the releasable vesicle pool size in chromaffin cells. *Journal of Neuroscience* **25**:2557–2565. DOI: https://doi.org/10.1523/JNEUROSCI.3761-04.2005, PMID: 15758165
Mosa MH, Nicolle O, Maschalidi S, Sepulveda FE, Bidaud-Meynard A, Menche C, Michels BE, Michaux G, de Saint Basile G, Farin HF. 2018. Dynamic formation of microvillus inclusions during enterocyte differentiation in *Munc18-2*-Deficient Intestinal Organoids. *Cellular and Molecular Gastroenterology and Hepatology* **6**:477–493. DOI: https://doi.org/10.1016/j.jcmgh.2018.08.001, PMID: 30364784
Müller T, Hess MW, Schiefermeier N, Pfaller K, Ebner HL, Heinz-Erian P, Ponstingl H, Partsch J, Röllinghoff B, Köhler H, Berger T, Lenhartz H, Schlenck B, Houwen RJ, Taylor CJ, Zoller H, Lechner S, Goulet O, Utermann G, Ruemmele FM, et al. 2008. MYO5B mutations cause microvillus inclusion disease and disrupt epithelial cell polarity. *Nature Genetics* **40**:1163–1165. DOI: https://doi.org/10.1038/ng.225, PMID: 18724368
Müller MP, Goody RS. 2018. Molecular control of rab activity by GEFs, GAPs and GDI. *Small GTPases* **9**:5–21. DOI: https://doi.org/10.1080/21541248.2016.1276999, PMID: 28055292
Muschalik N, Knust E. 2011. Increased levels of the cytoplasmic domain of crumbs repolarise developing Drosophila photoreceptors. *Journal of Cell Science* **124**:3715–3725. DOI: https://doi.org/10.1242/jcs.091223, PMID: 22025631

Nelson KS, Furuse M, Beitel GJ. 2010. The Drosophila claudin Kune-kune is required for septate junction organization and tracheal tube size control. *Genetics* **185**:831–839. DOI: https://doi.org/10.1534/genetics.110.114959, PMID: 20407131

Nemetschke L, Knust E. 2016. *Drosophila* crumbs prevents ectopic notch activation in developing wings by inhibiting ligand-independent endocytosis. *Development* **143**:4543–4553. DOI: https://doi.org/10.1242/dev.141762, PMID: 27899511

Pelissier A, Chauvin JP, Lecuit T. 2003. Trafficking through Rab11 endosomes is required for cellularization during Drosophila embryogenesis. *Current Biology* **13**:1848–1857. DOI: https://doi.org/10.1016/j.cub.2003.10.023, PMID: 14588240

Pellikka M, Tanentzapf G, Pinto M, Smith C, McGlade CJ, Ready DF, Tepass U. 2002. Crumbs, the Drosophila homologue of human CRB1/RP12, is essential for photoreceptor morphogenesis. *Nature* **416**:143–149. DOI: https://doi.org/10.1038/nature721, PMID: 11850625

Pellikka M, Tepass U. 2017. Unique cell biological profiles of retinal disease-causing missense mutations in the polarity protein crumbs. *Journal of Cell Science* **130**:2147–2158. DOI: https://doi.org/10.1242/jcs.197178, PMID: 28515229

Peng J, Awad A, Sar S, Komaiha OH, Moyano R, Rayal A, Samuel D, Shewan A, Vanhaesebroeck B, Mostov K, Gassama-Diagne A. 2015. Phosphoinositide 3-kinase p110δ promotes lumen formation through the enhancement of apico-basal polarity and basal membrane organization. *Nature Communications* **6**:5937. DOI: https://doi.org/10.1038/ncomms6937, PMID: 25583025

Perez-Mockus G, Roca V, Mazouni K, Schweisguth F. 2017. Neuralized regulates crumbs endocytosis and epithelium morphogenesis via specific stardust isoforms. *The Journal of Cell Biology* **216**:1405–1420. DOI: https://doi.org/10.1083/jcb.201611196, PMID: 28400441

Petkau G, Wingen C, Jussen LC, Radtke T, Behr M. 2012. Obstructor-A is required for epithelial extracellular matrix dynamics, exoskeleton function, and tubulogenesis. *Journal of Biological Chemistry* **287**:21396–21405. DOI: https://doi.org/10.1074/jbc.M112.359984, PMID: 22544743

Pfeffer SR. 2013. Rab GTPase regulation of membrane identity. *Current Opinion in Cell Biology* **25**:414–419. DOI: https://doi.org/10.1016/j.ceb.2013.04.002

Phillips MD, Thomas GH. 2006. Brush border spectrin is required for early endosome recycling in Drosophila. *Journal of Cell Science* **119**:1361–1370. DOI: https://doi.org/10.1242/jcs.02839, PMID: 16537648

Pinal N, Goberdhan DC, Collinson L, Fujita Y, Cox IM, Wilson C, Pichaud F. 2006. Regulated and polarized PtdIns (3,4,5)P3 accumulation is essential for apical membrane morphogenesis in photoreceptor epithelial cells. *Current Biology* **16**:140–149. DOI: https://doi.org/10.1016/j.cub.2005.11.068, PMID: 16431366

Pinheiro D, Hannezo E, Herszterg S, Bosveld F, Gaugue I, Balakireva M, Wang Z, Cristo I, Rigaud SU, Markova O, Bellaïche Y. 2017. Transmission of cytokinesis forces via E-cadherin dilution and actomyosin flows. *Nature* **545**:103–107. DOI: https://doi.org/10.1038/nature22041, PMID: 28296858

Pocha SM, Shevchenko A, Knust E. 2011a. Crumbs regulates rhodopsin transport by interacting with and stabilizing myosin V. *The Journal of Cell Biology* **195**:827–838. DOI: https://doi.org/10.1083/jcb.201105144, PMID: 22105348

Pocha SM, Wassmer T, Niehage C, Hoflack B, Knust E. 2011b. Retromer controls epithelial cell polarity by trafficking the apical determinant crumbs. *Current Biology* **21**:1111–1117. DOI: https://doi.org/10.1016/j.cub.2011.05.007, PMID: 21700461

Pocha SM, Knust E. 2013. Complexities of crumbs function and regulation in tissue morphogenesis. *Current Biology* **23**:R289–R293. DOI: https://doi.org/10.1016/j.cub.2013.03.001, PMID: 23578880

Pylypenko O, Hammich H, Houdusse A. 2017. Rab GTPases and their interacting protein partners: structural insights into rab functional diversity. *Small GTPases* **27**:22–48. DOI: https://doi.org/10.1080/21541248.2017.1336191

Ramachandran P, Barria R, Ashley J, Budnik V. 2009. A critical step for postsynaptic F-actin organization: regulation of baz/Par-3 localization by aPKC and PTEN. *Developmental Neurobiology* **69**:583–602. DOI: https://doi.org/10.1002/dneu.20728, PMID: 19472188

Ramel D, Wang X, Laflamme C, Montell DJ, Emery G. 2013. Rab11 regulates cell-cell communication during collective cell movements. *Nature Cell Biology* **15**:317–324. DOI: https://doi.org/10.1038/ncb2681, PMID: 23376974

Ramkumar N, Omelchenko T, Silva-Gagliardi NF, McGlade CJ, Wijnholds J, Anderson KV. 2016. Crumbs2 promotes cell ingression during the epithelial-to-mesenchymal transition at Gastrulation. *Nature Cell Biology* **18**:1281–1291. DOI: https://doi.org/10.1038/ncb3442, PMID: 27870829

Reck-Peterson SL, Provance DW, Mooseker MS, Mercer JA. 2000. Class V myosins. *Biochimica Et Biophysica Acta (BBA) - Molecular Cell Research* **1496**:36–51. DOI: https://doi.org/10.1016/S0167-4889(00)00007-0

Rescher U, Ruhe D, Ludwig C, Zobiack N, Gerke V. 2004. Annexin 2 is a phosphatidylinositol (4,5)-bisphosphate binding protein recruited to actin assembly sites at cellular membranes. *Journal of Cell Science* **117**:3473–3480. DOI: https://doi.org/10.1242/jcs.01208, PMID: 15226372

Richard M, Grawe F, Knust E. 2006a. DPATJ plays a role in retinal morphogenesis and protects against light-dependent degeneration of photoreceptor cells in the Drosophila eye. *Developmental Dynamics* **235**:895–907. DOI: https://doi.org/10.1002/dvdy.20595, PMID: 16245332

Richard M, Roepman R, Aartsen WM, van Rossum AG, den Hollander AI, Knust E, Wijnholds J, Cremers FP. 2006b. Towards understanding CRUMBS function in retinal dystrophies. *Human Molecular Genetics* **15**:R235–R243. DOI: https://doi.org/10.1093/hmg/ddl195, PMID: 16987889

Richard M, Muschalik N, Grawe F, Ozüyaman S, Knust E. 2009. A role for the extracellular domain of crumbs in morphogenesis of Drosophila photoreceptor cells. *European Journal of Cell Biology* **88**:765–777. DOI: https://doi.org/10.1016/j.ejcb.2009.07.006, PMID: 19717208

Richardson EC, Pichaud F. 2010. Crumbs is required to achieve proper organ size control during Drosophila head development. *Development* **137**:641–650. DOI: https://doi.org/10.1242/dev.041913, PMID: 20110329

Riparbelli MG, Callaini G, Dallai R. 1993. Spatial organization of microtubules and microfilaments in larval and adult salivary glands of Drosophila Melanogaster. *Tissue and Cell* **25**:751–762. DOI: https://doi.org/10.1016/0040-8166(93)90056-Q, PMID: 8296309

Rizki TM. 1967. Ultrastructure of the secretory inclusions of the salivary gland cell in Drosophila. *The Journal of Cell Biology* **32**:531–534. DOI: https://doi.org/10.1083/jcb.32.2.531, PMID: 10976239

Roch F, Polesello C, Roubinet C, Martin M, Roy C, Valenti P, Carreno S, Mangeat P, Payre F. 2010. Differential roles of PtdIns(4,5)P2 and phosphorylation in moesin activation during Drosophila development. *Journal of Cell Science* **123**:2058–2067. DOI: https://doi.org/10.1242/jcs.064550, PMID: 20519583

Rodriguez-Boulan E, Kreitzer G, Müsch A. 2005. Organization of vesicular trafficking in epithelia. *Nature Reviews Molecular Cell Biology* **6**:233–247. DOI: https://doi.org/10.1038/nrm1593, PMID: 15738988

Rodriguez-Boulan E, Macara IG. 2014. Organization and execution of the epithelial polarity programme. *Nature Reviews Molecular Cell Biology* **15**:225–242. DOI: https://doi.org/10.1038/nrm3775, PMID: 24651541

Roh MH, Makarova O, Liu CJ, Shin K, Lee S, Laurinec S, Goyal M, Wiggins R, Margolis B. 2002. The Maguk Protein, Pals1, functions as an adapter, linking mammalian homologues of crumbs and discs lost. *The Journal of Cell Biology* **157**:161–172. DOI: https://doi.org/10.1083/jcb.200109010, PMID: 11927608

Román-Fernández Á, Roignot J, Sandilands E, Nacke M, Mansour MA, McGarry L, Shanks E, Mostov KE, Bryant DM. 2018. The phospholipid PI(3,4)P2 is an apical identity determinant. *Nature Communications* **9**:5041. DOI: https://doi.org/10.1038/s41467-018-07464-8, PMID: 30487552

Román-Fernández A, Bryant DM. 2016. Complex polarity: building multicellular tissues through apical membrane traffic. *Traffic* **17**:1244–1261. DOI: https://doi.org/10.1111/tra.12417, PMID: 27281121

Röper K. 2012. Anisotropy of crumbs and aPKC drives myosin cable assembly during tube formation. *Developmental Cell* **23**:939–953. DOI: https://doi.org/10.1016/j.devcel.2012.09.013, PMID: 23153493

Rousso T, Shewan AM, Mostov KE, Schejter ED, Shilo BZ. 2013. Apical targeting of the formin diaphanous in Drosophila tubular epithelia. *eLife* **2**:e00666. DOI: https://doi.org/10.7554/eLife.00666, PMID: 23853710

Ruemmele FM, Müller T, Schiefermeier N, Ebner HL, Lechner S, Pfaller K, Thöni CE, Goulet O, Lacaille F, Schmitz J, Colomb V, Sauvat F, Revillon Y, Canioni D, Brousse N, de Saint-Basile G, Lefebvre J, Heinz-Erian P, Enninger A, Utermann G, et al. 2010. Loss-of-function of MYO5B is the main cause of microvillus inclusion disease: 15 novel mutations and a CaCo-2 RNAi cell model. *Human Mutation* **31**:544–551. DOI: https://doi.org/10.1002/humu.21224, PMID: 20186687

Salis P, Payre F, Valenti P, Bazellieres E, Le Bivic A, Mottola G. 2017. Crumbs, moesin and yurt regulate junctional stability and dynamics for a proper morphogenesis of the Drosophila pupal wing epithelium. *Scientific Reports* **7**:16778. DOI: https://doi.org/10.1038/s41598-017-15272-1, PMID: 29196707

Sato T, Mushiake S, Kato Y, Sato K, Sato M, Takeda N, Ozono K, Miki K, Kubo Y, Tsuji A, Harada R, Harada A. 2007. The Rab8 GTPase regulates apical protein localization in intestinal cells. *Nature* **448**:366–369. DOI: https://doi.org/10.1038/nature05929, PMID: 17597763

Satoh AK, O'Tousa JE, Ozaki K, Ready DF. 2005. Rab11 mediates post-Golgi trafficking of rhodopsin to the photosensitive apical membrane of Drosophila photoreceptors. *Development* **132**:1487–1497. DOI: https://doi.org/10.1242/dev.01704

Satoh T, Nakamura Y, Satoh AK. 2016. Rab6 functions in polarized transport in Drosophila photoreceptors. *Fly* **5**:123–127. DOI: https://doi.org/10.1080/19336934.2016.1182273

Sauvanet C, Wayt J, Pelaseyed T, Bretscher A. 2015. Structure, regulation, and functional diversity of microvilli on the apical domain of epithelial cells. *Annual Review of Cell and Developmental Biology* **31**:593–621. DOI: https://doi.org/10.1146/annurev-cellbio-100814-125234, PMID: 26566117

Scanga SE, Ruel L, Binari RC, Snow B, Stambolic V, Bouchard D, Peters M, Calvieri B, Mak TW, Woodgett JR, Manoukian AS. 2000. The conserved PI3'K/PTEN/Akt signaling pathway regulates both cell size and survival in Drosophila. *Oncogene* **19**:3971–3977. DOI: https://doi.org/10.1038/sj.onc.1203739, PMID: 10962553

Schindelin J, Arganda-Carreras I, Frise E, Kaynig V, Longair M, Pietzsch T, Preibisch S, Rueden C, Saalfeld S, Schmid B, Tinevez J-Y, White DJ, Hartenstein V, Eliceiri K, Tomancak P, Cardona A. 2012. Fiji: an open-source platform for biological-image analysis. *Nature Methods* **9**:676–682. DOI: https://doi.org/10.1038/nmeth.2019

Schneeberger K, Vogel GF, Teunissen H, van Ommen DD, Begthel H, El Bouazzaoui L, van Vugt AH, Beekman JM, Klumperman J, Müller T, Janecke A, Gerner P, Huber LA, Hess MW, Clevers H, van Es JH, Nieuwenhuis EE, Middendorp S. 2015. An inducible mouse model for microvillus inclusion disease reveals a role for myosin vb in apical and basolateral trafficking. *PNAS* **112**:12408–12413. DOI: https://doi.org/10.1073/pnas.1516672112, PMID: 26392529

Seabra MC, Mules EH, Hume AN. 2002. Rab GTPases, intracellular traffic and disease. *Trends in Molecular Medicine* **8**:23–30. DOI: https://doi.org/10.1016/S1471-4914(01)02227-4, PMID: 11796263

Shahab J, Tiwari MD, Honemann-Capito M, Krahn MP, Wodarz A. 2015. Bazooka/PAR3 is dispensable for polarity in Drosophila follicular epithelial cells. *Biology Open* **4**:528–541. DOI: https://doi.org/10.1242/bio.201410934, PMID: 25770183

Sherrard KM, Fehon RG. 2015. The transmembrane protein crumbs displays complex dynamics during follicular morphogenesis and is regulated competitively by moesin and aPKC. *Development* **142**:1869–1878. DOI: https://doi.org/10.1242/dev.115329, PMID: 25926360

Shewan A, Eastburn DJ, Mostov K. 2011. Phosphoinositides in cell architecture. *Cold Spring Harbor Perspectives in Biology* **3**:a004796. DOI: https://doi.org/10.1101/cshperspect.a004796, PMID: 21576256

Sidhaye J, Pinto CS, Dharap S, Jacob T, Bhargava S, Sonawane M. 2016. The zebrafish goosepimples/myosin vb mutant exhibits cellular attributes of human microvillus inclusion disease. *Mechanisms of Development* **142**:62–74. DOI: https://doi.org/10.1016/j.mod.2016.08.001, PMID: 27497746

Simpson JC, Griffiths G, Wessling-Resnick M, Fransen JA, Bennett H, Jones AT. 2004. A role for the small GTPase Rab21 in the early endocytic pathway. *Journal of Cell Science* **117**:6297–6311. DOI: https://doi.org/10.1242/jcs.01560, PMID: 15561770

Spannl S, Kumichel A, Hebbar S, Kapp K, Gonzalez-Gaitan M, Winkler S, Blawid R, Jessberger G, Knust E. 2017. The Crumbs_C isoform of *Drosophila* shows tissue- and stage-specific expression and prevents light-dependent retinal degeneration. *Biology Open* **6**:165–175. DOI: https://doi.org/10.1242/bio.020040, PMID: 28202468

Studer D, Humbel BM, Chiquet M. 2008. Electron microscopy of high pressure frozen samples: bridging the gap between cellular ultrastructure and atomic resolution. *Histochemistry and Cell Biology* **130**:877–889. DOI: https://doi.org/10.1007/s00418-008-0500-1, PMID: 18795316

Szymaniak AD, Mahoney JE, Cardoso WV, Varelas X. 2015. Crumbs3-Mediated polarity directs airway epithelial cell fate through the hippo pathway effector yap. *Developmental Cell* **34**:283–296. DOI: https://doi.org/10.1016/j.devcel.2015.06.020, PMID: 26235047

Tan X, Thapa N, Choi S, Anderson RA. 2015. Emerging roles of PtdIns(4,5)P2–beyond the plasma membrane. *Journal of Cell Science* **128**:4047–4056. DOI: https://doi.org/10.1242/jcs.175208, PMID: 26574506

Tepaß U, Knust E. 1990. Phenotypic and developmental analysis of mutations at Thecrumbs Locus, a gene required for the development of epithelia inDrosophila Melanogaster. *Roux's Archives of Developmental Biology* **199**:189–206. DOI: https://doi.org/10.1007/BF01682078, PMID: 28306104

Tepass U, Theres C, Knust E. 1990. Crumbs encodes an EGF-like protein expressed on apical membranes of Drosophila epithelial cells and required for organization of epithelia. *Cell* **61**:787–799. DOI: https://doi.org/10.1016/0092-8674(90)90189-L, PMID: 2344615

Tepass U. 2012. The apical polarity protein network in *Drosophila* epithelial cells: regulation of polarity, junctions, Morphogenesis, cell growth, and survival. *Annual Review of Cell and Developmental Biology* **28**:655–685. DOI: https://doi.org/10.1146/annurev-cellbio-092910-154033, PMID: 22881460

Tepass U, Knust E. 1993. Crumbs and stardust act in a genetic pathway that controls the organization of epithelia in Drosophila Melanogaster. *Developmental Biology* **159**:311–326. DOI: https://doi.org/10.1006/dbio.1993.1243, PMID: 8365569

Theopold U, Dorian C, Schmidt O. 2001. Changes in glycosylation during Drosophila development. The influence of ecdysone on hemomucin isoforms. *Insect Biochemistry and Molecular Biology* **31**:189–197. DOI: https://doi.org/10.1016/S0965-1748(00)00117-X, PMID: 11164341

Thomas C, Rousset R, Noselli S. 2009. JNK signalling influences intracellular trafficking during Drosophila morphogenesis through regulation of the novel target gene Rab30. *Developmental Biology* **331**:250–260. DOI: https://doi.org/10.1016/j.ydbio.2009.05.001, PMID: 19427848

Thomas GH, Williams JA. 1999. Dynamic rearrangement of the spectrin membrane skeleton during the generation of epithelial polarity in Drosophila. *Journal of Cell Science* **112 (Pt 17**:2843–2852. PMID: 10444379

Thomopoulos GN. 1988. Ultrastructure of the Drosophila larval salivary gland cells during the early developmental stages. I. morphological studies. *Journal of Morphology* **198**:83–93. DOI: https://doi.org/10.1002/jmor.1051980109, PMID: 29898570

Tian E, Ten Hagen KG. 2007. O-linked glycan expression during Drosophila development. *Glycobiology* **17**:820–827. DOI: https://doi.org/10.1093/glycob/cwm056, PMID: 17522109

Tran DT, Masedunskas A, Weigert R, Ten Hagen KG. 2015. Arp2/3-mediated F-actin formation controls regulated exocytosis in vivo. *Nature Communications* **6**:10098. DOI: https://doi.org/10.1038/ncomms10098, PMID: 26639106

Tran DT, Ten Hagen KG. 2017. Real-time insights into regulated exocytosis. *Journal of Cell Science* **130**:1355–1363. DOI: https://doi.org/10.1242/jcs.193425

Tsoumpekos G, Nemetschke L, Knust E. 2018. *Drosophila* big bang regulates the apical cytocortex and wing growth through junctional tension. *The Journal of Cell Biology* **217**:1033–1045. DOI: https://doi.org/10.1083/jcb.201705104, PMID: 29326288

van Diepen MT, Parsons M, Downes CP, Leslie NR, Hindges R, Eickholt BJ. 2009. MyosinV controls PTEN function and neuronal cell size. *Nature Cell Biology* **11**:1191–1196. DOI: https://doi.org/10.1038/ncb1961, PMID: 19767745

Várnai P, Balla T. 1998. Visualization of phosphoinositides that bind pleckstrin homology domains: calcium- and agonist-induced dynamic changes and relationship to myo-[3H]inositol-labeled phosphoinositide pools. *The Journal of Cell Biology* **143**:501–510. DOI: https://doi.org/10.1083/jcb.143.2.501, PMID: 9786958

Vinayagam A, Kulkarni MM, Sopko R, Sun X, Hu Y, Nand A, Villalta C, Moghimi A, Yang X, Mohr SE, Hong P, Asara JM, Perrimon N. 2016. An Integrative Analysis of the InR/PI3K/Akt Network Identifies the Dynamic Response to Insulin Signaling. *Cell Reports* **16**:3062–3074. DOI: https://doi.org/10.1016/j.celrep.2016.08.029

Vogel GF, Janecke AR, Krainer IM, Gutleben K, Witting B, Mitton SG, Mansour S, Ballauff A, Roland JT, Engevik AC, Cutz E, Müller T, Goldenring JR, Huber LA, Hess MW. 2017. Abnormal Rab11-Rab8-vesicles cluster in enterocytes of patients with microvillus inclusion disease. *Traffic* **18**:453–464. DOI: https://doi.org/10.1111/tra.12486

von Stein W, Ramrath A, Grimm A, Müller-Borg M, Wodarz A. 2005. Direct association of bazooka/PAR-3 with the lipid phosphatase PTEN reveals a link between the PAR/aPKC complex and phosphoinositide signaling. *Development* **132**:1675–1686. DOI: https://doi.org/10.1242/dev.01720, PMID: 15743877

Wandinger-Ness A, Zerial M. 2014. Rab proteins and the compartmentalization of the endosomal system. *Cold Spring Harbor Perspectives in Biology* **6**:a022616. DOI: https://doi.org/10.1101/cshperspect.a022616, PMID: 25341920

Wang S, Jayaram SA, Hemphälä J, Senti KA, Tsarouhas V, Jin H, Samakovlis C. 2006. Septate-junction-dependent luminal deposition of chitin deacetylases restricts tube elongation in the Drosophila Trachea. *Current Biology* **16**:180–185. DOI: https://doi.org/10.1016/j.cub.2005.11.074, PMID: 16431370

Wei Z, Li Y, Ye F, Zhang M. 2015. Structural basis for the phosphorylation-regulated interaction between the cytoplasmic tail of cell polarity protein crumbs and the actin-binding protein moesin. *Journal of Biological Chemistry* **290**:11384–11392. DOI: https://doi.org/10.1074/jbc.M115.643791, PMID: 25792740

Weisz OA, Rodriguez-Boulan E. 2009. Apical trafficking in epithelial cells: signals, clusters and motors. *Journal of Cell Science* **122**:4253–4266. DOI: https://doi.org/10.1242/jcs.032615, PMID: 19923269

Weixel KM, Blumental-Perry A, Watkins SC, Aridor M, Weisz OA. 2005. Distinct golgi populations of phosphatidylinositol 4-phosphate regulated by phosphatidylinositol 4-kinases. *Journal of Biological Chemistry* **280**:10501–10508. DOI: https://doi.org/10.1074/jbc.M414304200, PMID: 15634669

Whiteman EL, Fan S, Harder JL, Walton KD, Liu CJ, Soofi A, Fogg VC, Hershenson MB, Dressler GR, Deutsch GH, Gumucio DL, Margolis B. 2014. Crumbs3 is essential for proper epithelial development and viability. *Molecular and Cellular Biology* **34**:43–56. DOI: https://doi.org/10.1128/MCB.00999-13, PMID: 24164893

Williams JA, MacIver B, Klipfell EA, Thomas GH. 2004. The C-terminal domain of Drosophila (beta) heavy-spectrin exhibits autonomous membrane association and modulates membrane area. *Journal of Cell Science* **117**:771–782. DOI: https://doi.org/10.1242/jcs.00922, PMID: 14734656

Wodarz A, Grawe F, Knust E. 1993. CRUMBS is involved in the control of apical protein targeting during Drosophila epithelial development. *Mechanisms of Development* **44**:175–187. DOI: https://doi.org/10.1016/0925-4773(93)90066-7, PMID: 8155580

Wodarz A, Hinz U, Engelbert M, Knust E. 1995. Expression of crumbs confers apical character on plasma membrane domains of ectodermal epithelia of drosophila. *Cell* **82**:67–76. DOI: https://doi.org/10.1016/0092-8674(95)90053-5

Wodarz A, Ramrath A, Kuchinke U, Knust E. 1999. Bazooka provides an apical cue for Inscuteable localization in Drosophila neuroblasts. *Nature* **402**:544–547. DOI: https://doi.org/10.1038/990128

Worby CA, Dixon JE. 2014. PTEN. *Annual Review of Biochemistry* **83**:641–669. DOI: https://doi.org/10.1146/annurev-biochem-082411-113907, PMID: 24905788

Wu VM, Schulte J, Hirschi A, Tepass U, Beitel GJ. 2004. Sinuous is a *Drosophila* claudin required for septate junction organization and epithelial tube size control. *The Journal of Cell Biology* **164**:313–323. DOI: https://doi.org/10.1083/jcb.200309134, PMID: 14734539

Xiao Z, Patrakka J, Nukui M, Chi L, Niu D, Betsholtz C, Pikkarainen T, Pikkarainan T, Vainio S, Tryggvason K. 2011. Deficiency in crumbs homolog 2 (Crb2) affects gastrulation and results in embryonic lethality in mice. *Developmental Dynamics* **240**:2646–2656. DOI: https://doi.org/10.1002/dvdy.22778, PMID: 22072575

Xu H, Brill JA, Hsien J, McBride R, Boulianne GL, Trimble WS. 2002. Syntaxin 5 is required for cytokinesis and spermatid differentiation in Drosophila. *Developmental Biology* **251**:294–306. DOI: https://doi.org/10.1006/dbio.2002.0830, PMID: 12435359

Yonemura S, Matsui T, Tsukita S, Tsukita S. 2002. Rho-dependent and -independentactivation mechanisms of ezrin/radixin/moesin proteins: an essential role forpolyphosphoinositides in vivo. *Journal of Cell Science* **115**:2569–2580. PMID: 12045227

Yoon HS, Hajduk PJ, Petros AM, Olejniczak ET, Meadows RP, Fesik SW. 1994. Solution structure of a pleckstrin-homology domain. *Nature* **369**:672–675. DOI: https://doi.org/10.1038/369672a0, PMID: 8208296

Zhang J, Schulze KL, Hiesinger PR, Suyama K, Wang S, Fish M, Acar M, Hoskins RA, Bellen HJ, Scott MP. 2007. Thirty-one flavors of Drosophila rab proteins. *Genetics* **176**:1307–1322. DOI: https://doi.org/10.1534/genetics.106.066761, PMID: 17409086

Zhimulev IF, Izquierdo ML, Lewis M, Ashburner M. 1981. Patterns of protein synthesis in salivary glands ofDrosophila Melanogaster during larval and prepupal development. *Wilhelm Roux's Archives of Developmental Biology* **190**:351–357. DOI: https://doi.org/10.1007/BF00863272, PMID: 28305294

Zhou B, Bagri A, Beckendorf SK. 2001. Salivary gland determination in Drosophila: a salivary-specific, fork head enhancer integrates spatial pattern and allows fork head autoregulation. *Developmental Biology* **237**:54–67. DOI: https://doi.org/10.1006/dbio.2001.0367, PMID: 11518505